Online power management with embedded optimization for a multi-source hybrid with real time applications

Von der Fakultät für Ingenieurwissenschaften,
Abteilung Maschinenbau und Verfahrenstechnik
der
Universität Duisburg-Essen
zur Erlangung des akademischen Grades
einer
Doktorin der Ingenieurwissenschaften
Dr.-Ing.
genehmigte Dissertation

von

Bedatri Moulik
aus
Kalkutta, Indien

Gutachter: Univ.-Prof. Dr.-Ing. Dirk Söffker
Univ.-Prof. Dr.-Ing. Dirk Abel

Tag der mündlichen Prüfung: 11. April 2016

Acknowledgment

I would like to thank my supervisor Univ.-Prof. Dr.-Ing. Dirk Söffker for his constant support and valuable guidance which helped me achieve my goals. I also thank him for giving me an opportunity to pursue my research in Germany. It is because of this chance that he gave me, I could develop my academic and professional skills. I am grateful to him for helping me gain an insight on both scientific and as well as on other aspects of life.

I am also grateful to Univ.-Prof. Dr.-Ing. Dirk Abel for being the second supervisor for my thesis. Without his keen scientific questions and helpful advice towards the thesis, I could not have improved my work.

I also wish to convey thanks to my committee members in the Chair of Dynamics and Control at University of Duisburg-Essen for their both academical and personal support. It is these friends and co-workers both present and previous, who made my stay in Germany so memorable.

Last but not the least, I would like to thank my parents who made all this possible, who stood by me whenever I needed them.

Duisburg, April 2016 Bedatri Moulik

Kurzfassung

Der Schwerpunkt dieser Arbeit beinhaltet die Entwicklung einer Power-Management-Optimierungsstrategie für ein Drei-Quellen-Hybridfahrzeug. Diese Strategie berücksi -chtigt die Integration von optimierten Parametern, die eine dynamische Strombegrenzung von Batterie und Brennstoffzelle umsetzen. Hierbei wird ein Supercapacitor als dritte Stromquelle verwendet. Das Ziel ist die Entwicklung eine modulare Struktur mit entkoppelten Online- und Offline-Teilen, so dass die Umsetzung bei realen Fahrzyklen möglich ist. Von der Literatur kann geschlossen werden, dass die Online Optimierung mehrerer Ziele eine Schwierigkeit darstellt. Ein weiteres Problem ist die Anpassung einer optimierten Powermanagement Strategie auf reale Farzyklen. Die entwickelte Strategie/Methode verwendet online ein regelbasiertes Power management mit offline integriert optimierten Parametern. Die Parameter werden in Bezug auf mehrere widerspüchliche Zeile optimiert, z.B. in Bezug auf den maximalen Kraftstoffverbrauch im Widerspruch zur minimalen Abweichung des State-of-Charge. Durch eine geeignete Wahl der Parameter ist unter Berücksichtigung der Lastanforderung der Betrieb aller drei Quellen innerhalb der gewünschten Arbeitsbereiche möglich. Einem oder mehreren Optimierungszielen kann durch Variation der Gewichtungen der Ziele mehr Priorität als anderen Zielen zuordnet werden. Die Anwendung dieses Konzepts auf einen Brennstoffzellen-Batterie-Supercapacitor Hybrid wird in dieser Arbeit diskutiert. Eine detaillierte Modellbildung aller Komponenten sowie Verifizierung und Plausibilitätsbewertung wird berücksichtigt/durchgeführt. Zum Zweck der experimentellen Validierung werden die eigentlichen Antriebskomponenten durch regelbare Stromquellen und -senken ersetzt, die die Dynamik der reellen Komponenten nachbilden. Schließlich wird ein Konzept zur Integration der entwickelten Powermanagement-Optimierung in reale Fahrszenarien vorgestellt. Zur Validierung/Verifikation wird eine Fahrsimulatorumgebung mit dem experimentellen Hybrid-Elektrofahrzeug verbunden. Mit Hilfe eines erklärenden Beispiels werden die gewünschten optimalen Werte berechnet und dem menschlichen Fahrer über eine geeignete Schnittstelle angezeigt.

Abstract

The focus of this thesis is to develop a suitable power management optimization strategy for a three-source hybrid vehicle powertrain. This strategy takes into account the integration of optimized parameters that limit the battery and fuel cell current by utilizing a third power source, namely supercapacitor. The goal is to develop a modular structure with decoupled online and offline parts such that implementation in case of real driving conditions is feasible. Based on the literature review it can be concluded that providing optimal solutions in terms of multiple objectives online is an issue. Adaption of optimized control strategy to real driving data is another concern. The developed strategy employs an online rule-based control with embedded offline-optimized parameters. The parameters are optimized with respect to multiple and conflicting objectives such as fuel consumption and state-of-charge deviation minimization. By a suitable selection of parameters, operation of all three sources within desired working ranges is possible, keeping in mind the load demand. By varying the weights between the objectives, one or more objectives can be given more priority than others. The application of this concept to fuel cell-battery-supercapacitor hybrid is discussed in this thesis. Detailed modeling of all components along with verification and plausibility assessment is done. For the purpose of experimental validation, the real powertrain components are replaced by controllable power sources and sinks that emulate the dynamics of real components. Finally, a brief concept is presented to integrate the developed power management optimization in real driving scenarios. For validation/verification purposes, a driving simulator environment is connected to the experimental hybrid electric vehicle set-up and with the help of an illustrative example, the desired predicted optimal values are calculated online and displayed to the human driver by a suitable interface. The absence of online tuning of controller parameters in this example is counteracted by developing a concept based on literature. With the help of this concept, the adaption of the power management control concept, developed in this thesis, can be realized.

Contents

List of Figures **VI**

Nomenclature **VIII**

1 Introduction **2**
1.1 Hybrid powertrains: applications and scope 2
1.2 Contribution of the thesis 3

2 Literature review **4**
2.1 Introduction 4
2.2 Rule-based power management and optimization 8
2.3 Power management optimization with battery lifetime management . 11
2.4 Power management optimization with unknown velocity input 12
2.5 Need for a Generalized Optimal Rule-Based Control 14
2.6 Conclusions 15

3 Hybrid vehicle: Components and configurations **16**
3.1 Types of modeling 16
3.1.1 Forward-backward modeling 16
3.1.2 Quasistatic-dynamic modeling 17
3.2 Possible topologies and considered configuration 18
3.3 Modeling and plausibility assessment of components 20
3.3.1 Drive cycles 20
3.3.2 Backward/quasi-static models 21
3.3.3 Fuel cell 25
3.3.4 Battery 27
3.3.5 Supercapacitor 30
3.3.6 DC/DC converter 33
3.3.7 Theoretical sizing of components 36
3.3.8 Model verification based on literature 39
3.3.9 Comparison of simulated powertrain dynamics with simplified and complex DC/DC converter models 42
3.4 Emulation of powertrain components 43
3.4.1 Powertrain configuration with emulated components 45
3.4.2 Comparison of simulation and emulation results 46

4 Power management and optimization 49

4.1 Introduction 49

4.1.1 Classification and comparison of power management strategies 49

4.1.2 Concept of power management with embedded optimization . 51

4.2 Details of supervisory controller 53

4.2.1 Mode selection block 54

4.2.2 Look-up tables LUT block 54

4.2.3 PM controller block 56

4.2.4 Simulation results and discussion 58

4.3 Optimization as a decoupled process 60

4.3.1 Optimization goals and constraints 62

4.3.2 Simulation results and discussion 63

4.4 Experimental results and discussion 69

5 Scope of developed rule-based power management controller 72

5.0.1 Illustrative example: drive cycle prediction and optimization . 73

5.1 Adaptive power management for dynamic/variable driving behavior . 81

5.1.1 Driving condition recognition 82

5.1.2 Modified concept 86

6 Summary, Conclusion, and Outlook 89

6.1 Conclusion 89

6.2 Contributions 90

6.3 Outlook 90

Bibliography 92

List of Figures

2.1	Rule-based controller for mode selection [TGGL14][MS15b]]	10
2.2	Optimization of battery charge patterns [BMFF11][MS15b]	12
2.3	Driving pattern recognition and control [LJPML04][MS15b]	14
3.1	Typical topologies in ICE-based powertrains	19
3.2	Typical topologies in electrical powertrains	19
3.3	Chosen configuration for HEV	20
3.4	New European Drive Cycle (NEDC)	21
3.5	Representation of motor/generator	22
3.6	Circuit diagram of motor model	23
3.7	Power demand for NEDC drive cycle	25
3.8	Look-up table for V-I characteristics	26
3.9	Look-up table for power-efficiency characteristics	26
3.10	Circuit diagram of battery model	28
3.11	Relation between SoC and voltage	28
3.12	Circuit diagram of supercapacitor model	29
3.13	Relationship between capacitance and voltage	30
3.14	Circuit diagram of DC/DC converter	31
3.15	Average fuel cell power	35
3.16	Battery voltage variation during charging and discharging	37
3.17	Battery SoC and energy during charging	38
3.18	Capacitor voltage during charging and discharging	38
3.19	Bus voltage during charging and discharging	39
3.20	Source current during charging and discharging	40
3.21	Comparison of battery current for both models	41
3.22	Comparison of fuel cell current for both models	41
3.23	Comparison of supercapacitor current for both models	42
3.24	Comparison of SoC for both models	42
3.25	Emulation experimental set-up	44
3.26	Emulation hardware configuration	44
3.27	Emulation of motor/generator behavior	45
3.28	Simulated and emulated load current	45
4.1	Classification of power management strategies	47

4.2	Power management optimization concept [MS16a]	49
4.3	Details of mode selection block	52
4.4	Details of look-up table block	53
4.5	Details of PM controller block	5
4.6	Working of PM controller block	55
4.7	Power demand and actual power	56
4.8	Power from the three sources	57
4.9	Variation between t=670s-770s	57
4.10	Bus voltage	57
4.11	NSGA II and model interaction [MKS13]	57
4.12	Objective function convergence for a) Reference supercapacitor b) Double of reference supercapacitor c) Half of reference supercapacitor d) One-fourth of reference supercapacitor [MS16a]	61
4.13	Confliction of objectives [MS16a]	62
4.14	Effect of optimization parameters at different supercapacitor sizes (Simulated) [MS16a]	65
4.15	Effect of varying priorities between optimization goals (Simulated) [MS16a]	66
4.16	Comparison of all results in terms of energy consumption	67
4.17	a) Simulated source and load current b) Emulated batttery and supercapacitor current c) Emulated load current [MS16a]	68
5.1	Optimization concept for HEV-driving simulator coupling [MS16b]	71
5.2	Topology of HEV powertrain according to [ÖWMS13]	73
5.3	Displaying optimal velocity to the human driver [MWS15]	75
5.4	Displaying SOCs and velocity change suggestion to the human driver [MWS15]	75
5.5	Actual velocity and SoC variations [MWS15]	76
5.6	Actual and predicted velocities	77
5.7	Velocities between 25-60 s zoomed [MWS15]	77
5.8	Velocities between 90-130 s zoomed [MWS15]	77
5.9	Predicted velocity and SoC variations [MWS15]	78
5.10	Predicted and actual SoCs [MWS15]	78
5.11	State-of-Charge variations zoomed [MWS15]	79
5.12	Implementation possibilities of adaptive control (according to [FYR$^+$14]) [MS16b]	80
5.13	Driving condition recognition [MS16b]	81
5.14	Creation of representative drive patterns (according to [LJPML04]) [MS16b]	82
5.15	Driving condition recognition (modified from [LJPML04]) [MS16b]	85

Nomenclature

Symbol	Parameter	Unit
v	Vehicle velocity	[km/hr]
F_t	Traction Force	[Newton]
F_a	Aerodynamic friction	[Newton]
F_r	Rolling friction	[Newton]
F_g	Gravitational force	[Newton]
F_d	Disturbance force	[Newton]
F_t	Traction Force	[Newton]
P_{Motor}	Motor input power	[Watt]
T_m	Torque generated at the rotor shaft	[Nm]
φ_{Motor}	mutual flux linkage	[-]
T_2	Load torque	[Nm]
U_d, U_q and I_d, I_q	d-q axes components for stator voltage and current	[Volts and Amperes]
$\cos\varphi$	Power factor [-]	
E_{SW} and f_{SW}	Switching losses and switching frequency of inverter	[-]
U_{fc}	Fuel cell voltage	[Volts]
U_{oc}	Open circuit voltage of battery	[V]
I_{bat}	Battery current	[A]
I_{SC}	Supercapacitor current	[A]
U_{SC}	Supercapacitor voltage	[V]
U_L and U_C	Voltages over DC/DC converter inductor and capacitor elements	[V]
I_L and I_C	Currents over DC/DC converter inductor and capacitor elements	[A]
J	Performance index of optimization	[-]
P_{FC}	Fuel cell power	[W]
ΔSoC	SoC deviation	[Pa]

Abbreviations

EV	Electric Vehicle
HEV	Hybrid Electric Vehicle
ICE	Internal Combustion Engine
FCEV	Fuel Cell Electric Vehicle
ESS	Energy Storage Systems
DP	Dynamic Programming
GA	Genetic algorithm
ECMS	Equivalent Consumption Minimization Strategy
NSGA II	Non-dominated Sorting Genetic Algorithm II
SoC	State of Charge
LUT	Look-Up Table
NEDC	New European Drive Cycle
HiL	Hardware-in-the-Loop
PM	Power Management

1 Introduction

The increasing problems of environmental pollution and fast depletion of fossil fuel reserves is a global issue that requires immediate attention. The transportation sector being one of the major consumers of fossil fuels and producers of pollutants and greenhouse gases, makes a thorough retrospect of the existing technologies important. A radical solution to lower fuel consumption and emissions is an alternative powertrain, of which continuously variable transmission (CVT), electric vehicle (EV), fuel cell electric vehicle (FCEV), hybrid electric vehicle (HEV), and advanced power net control are mentioned in [KKDJ+05]. A hybrid electric vehicle generally combines two or more power sources such as an internal combustion engine (ICE), generator/motor or both, and a storage element such as a battery. An all-electric vehicle can be a battery electric vehicle (BEV) or a FCEV. A comparison of the characteristics of BEVs, HEVs, and FCEVs is given in [BGT10]. In this work, a FCEV is considered with two storage elements: battery and supercapacitor and is named as a multi-source HEV. The problem of controlling the power flows and other parameters between different power sources such that desired behavior is achieved is considered as power management problem. Desired behavior in [KKDJ+05] is expressed in terms of fuel consumption, emissions, component wear, and comfort with operating points and storage levels of components within bounds. In this work, a suitable power management optimization strategy is developed for the considered hybrid powertrain configuration. This newly developed concept of power management optimization addresses some of the open issues of existing methods namely, integration of multiple objectives of power management in online, real-time control of hybrid powertrains. Adaption of the power management control strategy to real driving behavior is another issue which is considered in this work.

1.1 Hybrid powertrains: applications and scope

The history of hybrid electric vehicles dates back to the 1900s when the first hybrid vehicle was developed by Ferdinand Porsche in 1901 [Wik15]. Their popularity increased with the release of Toyota Prius in 1997 followed by Honda Insight in 1999 [Wik15]. The more recent releases include Ford C-Max Hybrid, Toyota Prius C, Honda Accord, BMW i8, Porsche Panamera E-Hybrid, etc. in 2015. The technological innovations at the automobile industries are progressing at a fast pace. Toyota proposes the use of electric motor powered by batteries at start-up to give a smooth start, battery's stored energy to run the car at low speed ranges, engine as the primary source with energy-efficiency driving capacity [Glo15b]. It also boasts of the new fuel cell car: Mirai [Glo15a]. Mercedes-Benz has also launched passenger cars and city buses based on fuel cell technology [Dai15]. Keeping the industrial demands in mind, the research on hybrid vehicle technology has also escalated in the past

few years. Use of different alternative sources of energy are being considered along with power management strategies to ensure desired operation. However, one of the major challenges faced by the ongoing research of hybrid powertrains is to develop real-time implementable power management that can provide solutions in unknown driving situations.

1.2 Contribution of the thesis

In this thesis, an optimal power management strategy is developed which is based on rules. The strategy is online implementable and is capable of providing intantaneous optimal solutions based on multiple objectives. The strategy is implemented on a multi-source hybrid electric vehicle model, subject to a particular drive cycle. The application of the developed strategy in case the drive cycle is not given is also discussed. Parts of this thesis are published/submitted as journal papers [MS16a],[MS16b],[MS15b] and presented in international conferences [MS15a],[MWS15],[MS14],[MKS13].

In chapter 2 [MS15b], a review of previous works is presented with focus on rule-based power management, its optimization methods, and its applications in real-time systems. The alternatives of rule-based power management is also discussed. The advantages of combining storage elements commonly used in HEVs is given with relevance to the chosen power management optimization strategy.

In chapter 3 , the configurations and modeling options in hybrid powertrains is discussed and the reasons for choosing the considered topology is emphasized. Then the detailed dynamical modeling of each component of the considered HEV is given followed by a plausibility check where the behavior of each component is verified with literature. Finally, a simplified version of the detailed dynamical model is presented and compared.

In chapter 4 [MS16b], first a classification and comparison of different power management strategies is given followed by the concept of the developed strategy. Next, each part of the power management control module is described followed by the working of the controller. Next, the optimization of the controller parameters as a decoupled process is detailed emphasizing, the presence of multiple and conflicting goals and therefore, the choice of an appropriate algorithm. Both simulation and emulation results for the optimized control strategy is presented.

In chapter 5 [MS16a], an application of the proposed power management optimization concept is given. An adaption/modification of the developed strategy to work with real driver velocities is given based on concepts from literature. For the purpose of validation/verfication, an example is presented by using a driving simulator-hybrid vehicle coupled experimental set-up.

In the last chapter a conclusion and summary of the thesis is given.

2 Literature review

2.1 Introduction

This chapter is published in the form of a scientific paper [MS15b]. For the past several years, hybrid electric vehicles (HEVs) have mostly implied two power sources with power management approaches responsible for distributing power between these two sources. However, the presence of multiple power sources with a suitable power distribution between components makes further reduction in fuel consumption possible. In hybrid powertrains, two different sources of power are considered. As an example, in [KL10], the drivetrain output mechanically driven by an internal combustion engine (ICE) is supplemented by an electric motor. However, due to the growing trend of all-electric powertrains [BGT10], the efficiency assessment of such powertrains becomes important. According to [KL10], the efficiency of all-electric hybrid vehicles depends on the capability of the energy storage systems (ESSs), where batteries and supercapacitors are considered as the most common options for vehicular ESSs. As stated in [KL10], a hybrid drive composed of batteries, supercapacitors and fuel cells could be considered as an appropriate option for advanced hybrid vehicular drives. According to [AK12], Li-ion batteries possess high energy density, but have relatively poor power density, whereas supercapacitors possess high power density, but lower energy density, along with high charging/discharging efficiency compared to batteries. As a result, hybridization of Li-ion batteries and supercapacitors is considered in [AK12] to lead to a high performance storage unit. According to [AK12], the desired operation is when a nearly constant load current is supplied by the battery. This reduces its I^2R losses and prevents terminal voltage drops. The dynamic current with zero average is supplied by the supercapacitor in order to match the battery to the load. A fuel cell-battery-supercapacitor combination was also chosen in [PDRL07], stating the advantage of this combination. The advantage of the battery-supercapacitor combination has also been stated in [KBK10], where the constraint for the control strategy was to remain charge depleting. Due to the battery-supercapacitor combination, the supercapacitor can take over more dynamic power fluctuations, while the battery takes a low pass filtered profile. According to [KBK10], this can extend the battery life. The advantage of fuel the cell-battery-supercapacitor combination has also been discussed in [LCL$^+$12], where fuzzy logic control was used to design energy management strategy for the hybrid powertrain. Along with primary energy sources (such as fuel cells) and ESSs, DC/DC converters are also integral parts of HEVs. The current flow into the DC bus can be controlled with the help of DC/DC converters. The power split ratio between the battery and the fuel cell is obtained by sending the fuel cell net current required to the DC/DC converter. In [BMFF07], a supervisory controller is considered along with a combined power management and design optimization for a fuel cell hybrid vehicle. This controller sends the current request to DC/DC converters. Here,

the aim was to minimize the fuel consumption by maintaining the battery State of Charge (SoC). by sending the appropriate current request command to the DC/DC converter. The DC/DC converter, which plays a central role in power management, has also been considered in [NGK10] with fuel cell hybrids. However, an integration of three DC/DC converters for all three sources in a fuel cell-battery-supercapacitor powertrain, with at least two bi-directional DC/DC converters, provides more degrees of freedom, as detailed in [AK12, CE12]. Power management with DC/DC converter control can be realized with real hardware components, of which emulator hardware [GBS+09] has been considered as a less expensive and more compact substitute for complex real hardware. The emulator test-rig developed and implemented in [ÖWMS13] is capable of accurately replicating the vehicle dynamics and can also be used for validating power flow algorithms. This was extended and modified to emulate an entire hybrid powertrain in [MS14].

An important criteria in HEV design is to achieve an efficient conversion of energy on the powertrain [BGT10], where the effectiveness of the results can be checked with standard drive cycles. In order to achieve this purpose, in [BGT10], the need to design a suitable controller and control strategies is emphasized. Therefore, the control strategies can satisfy a number of goals, such as maximum fuel economy, good driving performance, etc. Amongst these power management control strategies, the effectiveness of rule-based power management in real-time supervisory control has been stated in [Sal07]. According to [Sal07], under rule-based power management, deterministic rule-based power management, as an easy to realize method, relies on heuristics to design rules that are generally implemented via look-up tables. An adaptive rule-based power management for optimization of both energy use and emissions is also mentioned. In the case of hybrid vehicles, which involve multi-variables and/or multi-objectives, rules that cover all important trade-offs among different optimization objectives are difficult to design, and therefore, in [LFL+04], dynamic programming (DP) is used to understand the deficiency of rules and to serve as a reference to construct improved rules in terms of a fuel economy-emissions optimization problem. In [MPP13], a two-mode, low and high level controller design is considered, which is subjected to an offline control variables' optimization in terms of fuel consumption minimization. Similarly, in [TGGL14], a rule-based energy management controller was developed that includes off-line calculation relative to the optimization problem. State-of-charge was the key variable that determined the selection between modes. Some of the earliest works in rule-based control include [JKS97], where optimal energy management deals with power split in series hybrid electric vehicles. A sub-categorization of rule-based control is considered in [BGT10].

Apart from online rule-based power management techniques, various offline optimization algorithms are also available, such as DP [BGR00, BLGP09, PBMG06] and GA [PIGV01, JDW09]. These methods are capable of producing globally-optimal solutions, and some more sophisticated ones, such as the Non-dominated Sorting Genetic Algorithm II (NSGA II) [DPAM02], are also capable of tackling multiple

and conflicting objectives, such as the problem of fuel consumption and emissions minimization in [ZCMM09], fuel consumption and component sizing in [BLM+10] and fuel cost and battery health degradation minimization in [BMFF11]. The other category of power management optimization techniques includes those that can be implemented in real-time, such as [PRS05], where along with a real-time controller, two optimization goals of fuel consumption and battery SoC deviation minimization were considered. Model predictive control (MPC) has also been widely used for real-time control. For instance, in [KMS09], a non-linear MPC was considered to carry out the task of fuel efficiency maximization with battery SoC, vehicle relative position and performance as constraints. Equivalent consumption minimization strategies (ECMS) [PDG+02, GS07], on the other hand, are instantaneous power management strategies that can be implemented online, offline, as well as in real time. A detailed classification of power management optimization methods has been given in [KS14]. An interesting procedure to evaluate the performance of online power management strategies in terms of fuel consumption and computational cost was carried out in [SSD+14]. Here, nine participating teams were provided with a hybrid vehicle model. Each of the power management solutions presented by participants were tested for two realistic driving cycles not known to the participants. The comparison results were obtained for rule-based vs. ECMS. The best solution obtained was compared with global, offline optimization.

The non-optimality resulting from conventional rule-based power management with respect to off-line techniques [KS14] leads to the consideration of improvement methods in [MF08]. Here, a parameter optimization using genetic algorithms (GA) was considered to determine the optimal control variables for fixed parameters. Using this as the baseline, an equivalent consumption management strategy (ECMS) to dynamically control the controller parameters and a route-based strategy to dynamically control the parameters for current and predicted future routes were developed. The combination of rule-based control strategies with optimal power management strategies has also been considered in [SRA11]. Here, the performance of the rule-based strategy was assessed by comparing with GA, and the suitability of using GA was established by comparing with dynamic programming (DP). Additionally, power delivered by primary source and SoC deviation are defined as functions of traction power. These functional dependencies were integrated as look-up tables (LUTs) for an online implementation. The values in the LUT were defined by optimizing in terms of fuel efficiency. Battery SoC was taken as the state variable. Similarly, rule-based strategies were also considered in combination with ECMS, where optimization is carried out offline with DP in [HS07] and with more sophisticated multi-objective techniques, such as NSGA II in [BLM+10].

Optimization in HEVs often involves multi-objectives [LFL+04], and for a multi-objective optimization problem where the objectives are conflicting, multi-objective genetic algorithms are considered suitable [BLM+10], as they search for a Pareto optimal set. In [BLM+10], the two conflicting objectives of fuel consumption min-

imization and sizing were considered. When the configuration was evaluated, the parameters of the control strategy were optimized, whereas while evaluating the control strategy, it was manually tuned for minimum fuel consumption for one combination of drivetrain components. In [PDRL07], on the other hand, the best hybrid vehicle configuration and control strategy to reduce fuel consumption were identified at first. The control strategy was comprised of a set of rules based on both required power and battery and supercapacitor SoCs. Optimization goals included finding parameters that minimized fuel consumption and sustained battery SoC at the same time. The optimization results gave rise to a group of design parameters, indicating a compromise between fuel consumption and battery SoC.

Hybrid vehicles are often equipped with batteries as secondary storage elements. The battery aging process and its integration as a power management objective has already been discussed in [BMS15]. The following material and text is based on [BMS15]. In [SOS$^+$11], an optimal control problem is formulated to minimize fuel consumption, as well as battery aging. With regards to battery lifetime, State of Health (SoH) estimation, commonly related to the battery capacity fade [EBV14], is important. The maximum peak of the battery current is one of the factors influencing SoH and has to be limited. The number of battery recharge cycles during an interval have to be decreased as detailed in [HS06], but as mentioned in [HS06], this leads to more power generation from the primary source and, simultaneously, to higher fuel consumption. Thus, an inclusion of a second objective function as an optimization goal is necessary for extending the system's longevity without disregarding functionality. The two goals, fuel efficiency and battery aging, are conflicting objectives, as stated in [BMFF11]. Here, the requirement of high SoC for the minimization of total energy cost and the requirement of limited charging/discharging of the battery are the two conflicting objectives. In [BMFF11], two such conflicting objectives are evaluated for a plug-in hybrid electric vehicle charge pattern optimization. The optimal parameters corresponding to the objectives can be generated by optimization algorithms suitable for dealing with more than one objective.

In [BMFF11], these objectives are traded off using NSGA II. Here, the time, the maximum amount and the rate at which the HEV charges before each trip are taken as optimization variables. The consideration of both SoC and SoH is considered in [RBBP11], where, to carry out the task of optimal power management, a supervisor is presented. In [WY06a, WY06b], a genetic algorithm (GA) was used to fine-tune the parameters of a fuzzy logic controller. Three aspects of battery management were considered: minimization of resistive losses, yet supplying peak power demands, balanced battery energy in the entire duty cycle and controlling of the depth of charge/discharge for preserving the battery life.

In the field of hybrid electric vehicles (HEVs), power management and optimization strategies are not just restricted to those cases where the entire driving pattern is considered. In [PIGV01, BGR00, LJPML04], for example, the optimal division of

output torque is based on a specific driving pattern, and in [PL00], DP is considered for the optimization of several respective driving patterns. On the other hand, in [IYD+04], a prediction of the future driving pattern is considered based on past data. Use of human-in-the-loop in order to analyze driver requirements and the corresponding dynamic response of the vehicle is also not uncommon [VIPn+09]. In [HS06], a fuzzy rule-based control was considered along with the prediction of the future path of the vehicle. Use of GPS for the knowledge of obstacles to come and the assumption of drive cycle being provided as a reference were one of the key aspects here. Apart from GPS, track-based prediction [CB11] and dynamic recurrent neural networks (DRNN) [MSS12] have also been applied. Without the information available from telemetry, prediction strategies based on neural networks and stochastic Markov chain have been considered in [SHMS15] within an MPC framework. Past trajectories have been used for prediction, as considered in [MS12, MSS12, SWS+13]. Here, a prediction algorithm considers certain features of the past trajectory measured over predefined time horizons. The adaption of horizon length (the number of past measurements) depending on the prediction performance is a key aspect here. The task of control optimization in [MS12] is carried out using MPC, and the results are compared to globally-optimal solutions determined by dynamic programming. In [Mur08], an intelligent control, both with and without knowledge of the unknown, is considered; whereas in [WL11], control based on both the driving cycle, as well as driving style is elaborated. Within driving cycle-based control, methods to recognize present and to predict future driving conditions are detailed followed by methods for data analyses. In [PCM10], an intelligent strategy based on the prediction of both the driving environment, as well as driving trends is considered. It consists of three major neural network systems: the first one for predicting road type and traffic congestion; the second one for predicting driving trend; the third one as a suite of intelligent networks, trained for all roadway types. In driving style-based control, methods to recognize drivers' driving styles, such as mild driving style, normal driving style, aggressive driving style, etc., are mentioned. The use of a driving simulator as an experimental platform is stated. In [WMS15], a driving simulator has been used for improving driving efficiency and safety.

2.2 Rule-based power management and optimization

According to [MF08], the available power management optimization strategies can be categorized into three broad classes, namely global, static real time and dynamic real time. The rule-based control strategy is a basic control strategy that involves several modes of operation [MF08]. As detailed in [MF08], four operation modes are considered, namely motor and engine-only modes, hybrid braking mode and hybrid propelling mode. In these modes, an average constant charge is maintained in the storage component. Hence, SoC of the storage component is a constraint or determining factor for the switching between modes. Another factor is the desired torque.

Three methods to improve rule-based control are discussed. The goal to be achieved is to optimize the vehicle's efficiency. In the first method, the modes are individually optimized on the basis of three criteria: optimal internal combustion engine (ICE) operation point, when to switch to electric-only mode and SoC maintenance, done by modifying/adding rules based on the three criteria. However, in [MF08], this is considered as not a very effective optimization method. The next optimization method for rule-based strategies is discussed: parameter optimization using genetic algorithms is termed as a static method suitable for determining globally-optimal values of a set of fixed parameters, such as upper and lower SoC bounds, etc. However, the inability of this optimization to dynamically control the parameters leads to the consideration of a third improvement method in [MF08], namely ECMS. Here, the storage efficiency or fuel to electric energy and the electric to motor efficiencies are determined in order to calculate the future savings in terms of the 'cost' of energy. An important advantage of combining with the ECMS approach is its real-time applicability in combination with prediction algorithms [GS07]. Finally, a real-time route-based optimization strategy is developed, capable of dynamically controlling the upper and lower bounds of SoC and the desired torque from the primary source based on pre-calculated optimal set points for the present and future. In [TGGL14], the controller not only has to assure the vehicles's power requirements, but also to minimize the energy consumption while maximizing the vehicle's autonomy. Here, offline calculation of optimal parameters for a rule-based controller is considered. Three machines, namely an electric motor, a generator and a battery, are considered, and modes are defined for a control strategy that will be able to manage the three different machines involved. Each mode has its own optimization problem definition, and the corresponding parameters can be offline optimized. This is detailed in Figure 1. Mode 1 is a full-electric mode, where the torque provided by the motor comes from the battery, and therefore, there are no degrees of freedom. Mode 2 is also an electric mode, but here, the generator assists the motor to propel the vehicle. This mode has one degree of freedom, and hence, the optimization problem concerns the efficiency maximization of both machines. Mode 3 is a range-extended mode, and here, both the engine and generator are used to produce power. The related optimization problem has two objectives: first, maximal production of electric energy by the generator and, second, minimal fuel consumption. Mode 4 is the power split mode, where all three machines are connected. As it is a combination of Modes 2 and 3, the optimal values calculated in the modes before can be used. The function of the controller is to select the most appropriate mode. The task of selecting modes is divided into first and second decision layers. In the first decision layer, SoC is the determining variable that decides whether to avoid battery use completely (safety reasons) or to switch between Modes 1, 2 (charge depleting) and 3, 4 (charge sustaining). The selection between Modes 1, 2, 3 and 4 is carried out in the second decision layer that incorporates the offline optimized values of the parameters, calculated for each mode. In [BLM$^+$10], the rule-based controller is based on five operating modes. The driver torque request, speed of the

crankshaft and SoC determine which mode is active. The optimization problem is divided into two sub-problems: optimization of the control strategy with the objective being fuel consumption minimization and optimization of component sizing. According to [BLM+10], only with the help of an appropriate control strategy, the fuel economy can be improved. This control strategy has to be adapted when the drivetrain configuration is evaluated. The evaluation of the configuration is done based on the hybridization factor (HF), which, in turn, affects the fuel economy and dynamic performance of the vehicle. This inter-dependence between goals is formulated in [BLM+10] as a multi-objective optimization problem. The solution is obtained in two steps: first, the optimization of the control strategy is carried out for different HF with fuel consumption minimization as the objective, leading to a set of parameters that are suitable for different HF; second, all of the following optimizations are carried out with a combined measure for fuel efficiency. In the optimization results, three kinds of solutions are marked: a good compromise of fuel consumption and performance, a bad compromise where the hybridization factor and fuel consumption are slightly lower, but with an increased acceleration time, and the best fuel consumption region, but with the worst acceleration.

2.3 Power management optimization with battery lifetime management

This section discusses topics that have already been elaborated in [BMS15] and repeats the material. In terms of power management and optimization, fuel consumption minimization is the commonly known and accepted design goal. Rule-based power management often takes the battery SoC into account while designing the rules. In [Con06], based on battery SoC and SoH, as well as other relevant parameters, the battery management system is able to deduce the electrical management. The results are communicated via controller area network (CAN bus) to the vehicle power management, which determines the power split between components while keeping the currents and voltages within the limits to safeguard the battery. According to [Con06, KR99], overcharging, over-discharging, mechanical stress and high temperature are some of the factors that lead to safety issues. The consideration of both SoC and SoH is also considered in [RBBP11]. The battery aging and degradation is limited by using SoC and SoH as constraints. The proposed supervisor consists of forecasting, predictive optimization and the local command stage. The forecast of inputs is sent from the forecasting stage to the optimization stage, which gives current commands to the DC/DC converter connected to the batteries at the local command stage. The physical parameters interacting at the local command stage are battery current and battery SoC and SoH. The battery model considered estimates SoC, taking into account charge variation as a function of current and temperature, SoH as a representation of capacity losses according to the battery depth of discharge and voltage as a function of SoC. The power management and optimization developed in [RBBP11] considers battery aging in the optimization process for a grid-connected PV system with batteries. The results show the reduction in grid power fluctuations, so that it is balanced to the power exchanged with the batteries.

At first, a non-optimal rule-based algorithm was developed taking into account the above-mentioned constraints. According to [RBBP11], the results obtained can be used as a reference for dynamic programming (DP). In [LSWZ11], a fuzzy logic management system was tested in a real-time test-bench. A new quantity, called the battery working state (BWS), based on both battery terminal voltage and SoC, was used to make a decision on the power split. The control strategies were classified into rule-based and optimization-based. The advantages and disadvantages of both were stated, and the need to optimize rule-based strategies was emphasized. In [BMFF11], the conflicting objectives of fuel efficiency and battery aging are solved using a multi-objective solver, as shown in Figure 2. During charging, constant current and constant voltage cycles are applied on the battery model based on the optimized variables: time, maximum amount and the rate at which the HEV charges before each trip. During discharging, first, the drive cycle is given as the input to the vehicle model with available battery charge. Next, the current absorbed by

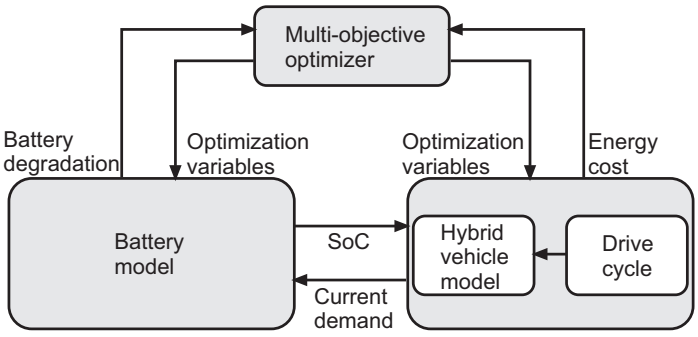

Figure 2.2: Optimization of battery charge patterns (according to [BMFF11]) [MS15b]

the powertrain during the trip is recorded and sent to the electrochemical battery model. According to [BMFF11], this can help in evaluating the battery degradation while driving. During standstill conditions, battery degradation is calculated from the battery model alone. The two objectives are calculated at the end of the drive cycle and sent back to the optimizer, as shown in Figure 2.2.

2.4 Power management optimization with unknown velocity input

Apart from battery lifetime management, another issue with hybrid vehicles is the real-time applicability of power management optimization strategies. Under real driving conditions, no pre-defined drive cycle is followed, and optimal future driving behavior needs to be predicted. In [HS06], both predictive and protective algorithms are considered, where in the first part, the energy management based on the predicted future has fuel economy, performance and emission minimization as objectives; and in the second part, the modified energy management has battery SoH improvement as an additional objective. The controller based on fuzzy rules has two inputs, that is the differences between future and present speeds and positions. It has one output that manipulates the charge and discharge of the battery. Here, GPS has been used to acquire knowledge of the obstacles in the future, but in the absence of GPS, use of human-in-the-loop to analyze driver requirements and corresponding dynamic responses of the vehicle is also not uncommon [VIPn$^+$09]. In [VIPn$^+$09], a hardware test-bench used for HiL simulations of HEV powertrain was coupled with an advanced virtual driving simulator. First, a forward facing model was selected. This kind of model requires controllers and a driver who can either track a given drive cycle or drive over a virtual scenario. The aim of using this model is to calculate vehicle speed and dynamic variables, such as forces in a forward direction along the powertrain. A real driver is asked to drive over a virtual scenario of 3 km, and some dynamic variables were saved in order to analyze and re-design the

powertrain control system later. Next, the backward facing model is tested. Here, the driving cycle information is also integrated, while the driver is driving over the same virtual scenario. Driving over the same driving scenario can be compared to a real case of a vehicle driven over the same commuting route every day, as given in [IYD+04]. According to [IYD+04], the future driving pattern can then be predicted based on past databases and a pattern matching system, where the database is used for storing past data and the pattern matching system for comparing current and past driving patterns and predicting the most likely future driving pattern. Since the driving patterns over a specific route are not unique, in [IYD+04], with the help of a clustering method, dividing driving patterns into certain classes is considered. Clustering is also considered in [WL11], where the task of collecting historical and current driving cycle data in order to analyze the previous driving pattern and to predict future driving conditions is elaborated. The importance of selecting a suitable length of time window is also stated. The methods for data analysis are detailed in [WL11]. In [LJPML04], an adaptive power management based on driving pattern recognition is presented. The driving pattern recognition algorithm classifies the given representative drive cycles (RDPs) based on low, medium and high power demands and creates driving patterns satisfying the characteristic parameters obtained from the driver velocity. The procedure followed is capable of executing an optimal online power management, along with driver velocity classification and prediction without using complicated algorithms stated in [WL11]. Here, two separate offline processes are considered: first is the RDP, where representative drive cycles are used to create six driving patterns satisfying certain criteria. These patterns are classified according to power demand and stored in a look-up table for online implementation; second is the driving pattern recognition (DPR), where the same six representative drive cycles are analyzed for determining the optimal power split that minimizes fuel consumption. Based on this, six control rules are formulated for a sub-optimal rule-based controller. This controller can now be implemented online. In the online process, the driver velocity is saved as historical data, and prediction is based on the assumption that the driving condition within a finite history will continue in the near future. The data in the most recent time frame from the historical data buffer can be used for characteristic parameter extraction. The classification of the driver velocity into six patterns is carried out based on the look-up table values from the first offline process (RDP). The corresponding control rule can also be determined based on the data from the second offline process (DPR). As shown in Figure 2.3, vehicle input signals are measured and control actions generated with sampling time “T”. The duration of historical data sent from the buffer to the DPR process is “pT”; the duration of the RDP process is “fT”; and the duration of the control horizon is “NT”.

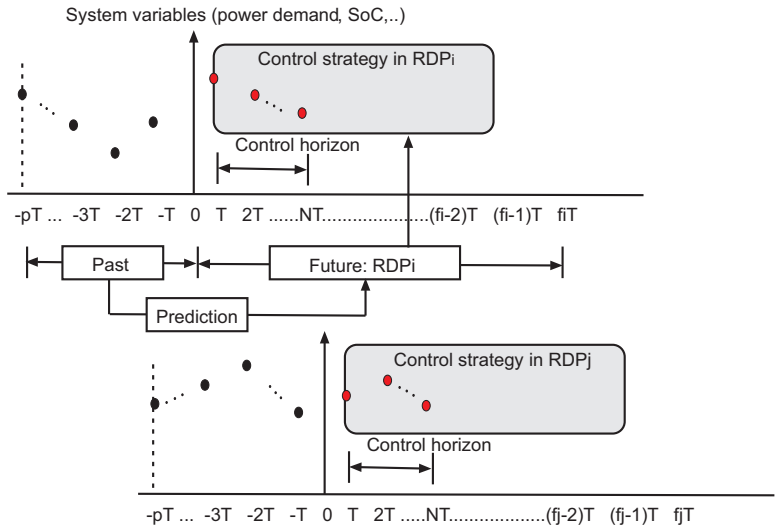

Figure 2.3: Driving pattern recognition and control (according to [LJPML04]) [MS15b]

2.5 Need for a Generalized Optimal Rule-Based Control

From the review of the published results, it can be stated that rule-based power management strategies are implementable in online, real-time control of hybrid electric vehicles. Their shortcomings in terms of non-optimality can be rectified by combining with global optimization methods, such as DP, GA, etc., to optimize various objectives, such as fuel consumption, etc. Rule-based strategies can also be combined with prediction algorithms and real-time control methods, such as ECMS, to provide route-based optimal control. Rule-based strategies often have rules formulated based on battery state-of-charge values, but since the rules are based on heuristics, they can also be modified to include state-of-health aspects with respect to the control of the aging of batteries. Maximum battery current being one of the factors affecting the state of health can lead to the development of a power management controller that can set limits to the rate of current increase, thereby minimizing the aging effects. The possibilities of individually optimizing the power management rules offline have already been considered in the literature. The results from optimization, stored in look-up tables, can be used to tune controller parameters online. Thus, depending on the particular optimization objective considered—minimization of fuel consumption, finding optimal current limits to minimize battery aging, or reducing the state-of-charge deviation, or a combination of these objectives—a suitable optimization can be carried out. Offline optimization with respect to these objectives makes the use of multi-objective optimization techniques plausible. Due to the flexibility of this rule-based controller, its application to a multi-source hybrid powertrain can be considered. For this, rules can be modified to include state-of-charge values of all of the storage components present. According to the literature,

amongst multi-source hybrids, the use of a battery-supercapacitor combination can prove particularly beneficial. The main purpose of this literature research was to evaluate the potentials and application prospects of rule-based power management and to lay the foundations for the development of an appropriate optimal power management controller that takes into account multiple optimization objectives, in the presence of multiple sources.

2.6 Conclusions

In this chapter, an elaborate view of rule-based power management, its alternatives, optimization potentials and applications are given. First, an overview of HEVs and the advantages of selecting a suitable combination of components is given, followed by the details of optimizing rule-based power management. Then, optimization in the presence of multiple, complex and conflicting goals is discussed. Finally, the extent of rule-based power management in solving the issues of battery aging and dealing with real driving scenarios is reported with the help of relevant literature.

3 Hybrid vehicle: Components and configurations

Mathematical models of hybrid vehicle components are often required for detailed analysis of powertrain performance and power management strategies. Simulation of these models is the first step for realizing their behavior in experimental set-ups and real-time systems. In this chapter, a three-source hybrid vehicle comprising of a fuel cell, battery, and supercapacitor is considered. The different modeling approaches are discussed along with topologies available followed by reasons for choosing the considered configuration. Mathematical models of the considered powertrain are given, with complex dynamic models for battery, supercapacitor, and DC/DC converter. Dynamic modeling is followed by plausibility assessment of component dynamics. Finally, a simplified modeling approach is discussed, suitable for use with the optimization toolbox. The comparison of results from complex and simplified modeling approaches is also given. Parts from this section are based on the text and material from [MS16b].

3.1 Types of modeling

In order to investigate the behavior of hybrid vehicles and evaluate the dynamic response of the system to varying load profiles, building a mathematical model is often considered as a pre-requisite. Modeling can be done based on a given drive cycle where the vehicle energy losses and its performance can be calculated backwards [GS07] or based on an unknown velocity pattern where forward modeling becomes necessary. The individual components can also be modeled in two ways: quasi-static and dynamic depending on the control objectives considered.

3.1.1 Forward-backward modeling

Backward modeling is an important method to calculate energy consumption, efficiency, emissions, etc based on a pre-defined drive cycle. Simulating such models require vehicle speed and acceleration values from drive cycle in order to calculate the required torques and speeds backwards through the drive train [VIPn$^+$09]. The model may be based on static equations and efficiency maps of components as detailed in [VIPn$^+$09]. The drivability that is the ability of the system to follow a particular drive cycle can be determined using a backward model. In [GS07], the dynamics of the longitudinal motion of a general road vehicle are analyzed with the help of a backward model where, vehicle energy losses and performance calculations are elaborated. The drivability can be defined as the ability of the system to follow the given drive cycle. It can be expressed in terms of power as follows

$$Drivability = \frac{\int_{t_0}^{t_{end}} |P_{ref} - P_{act}| dt}{\int_{t_0}^{t_{end}} |P_{ref}| dt}, \tag{3.1}$$

where P_{ref} denotes the reference power or the power demand that the given drive cycle requires and P_{act} represents the actual power available. This drivability term is particularly useful in evaluating power management strategies. The error between the power required by the backward modeled powertrain components and the actual power available from the sources as defined by the power management can be kept as low as possible. This error is termed as drivability error.

A forward model is one which calculates the available power from the sources depending on the power demand. It is possible to combine a backward model with a forward model in order to measure the drivability error or to model an entire vehicle in a forward manner to investigate real time systems where the drive cycle is not given. In [VIPn$^+$09], a forward model is considered for cases where a driver model or real driver is present. Here, differential equations of longitudinal and lateral vehicle dynamics are solved using throttle, brake, and steering wheel positions as inputs, and vehicle speed and position as outputs. The advantage of backward modeling its lower computational time as compared to forward modeling where appropriate vehicle component models are required resulting in longer simulation times [GS07, VIPn$^+$09].

3.1.2 Quasistatic-dynamic modeling

Depending on whether the HEV powertrain is forward or backward modeled, the individual components have to be modeled accordingly. According to [GS07], the quasi-static models which generally take speed, acceleration, and road angle as inputs can be useful in determining the fuel consumption. Together with a backward modeling approach, the speed and acceleration that the vehicle is required to follow can be calculated with the assumption that these values remain constant in a very small interval of the given drive cycle time. A dynamic model on the other hand, can be used to represent the dynamics of the mathematical model more correctly and also be used in combination with forward simulation [GS07]. Here, the powertrain model is expressed with sets of ordinary differential equations in state-space form. In [DCC$^+$10], both quasi-static and dynamic models are considered where, the reason for considering a dynamic model of battery is stated. Therefore, components like batteries and supercapacitors where the state-of-charge is an unknown result of power management and optimization algorithms need to be modeled dynamically. A fuel cell on the other hand can be modeled based on experimentally determined parameters as detailed in [OIQ05]. Thus, instead of a complex dynamical model as developed in [ÖWMS13], a quasi-static model can be used based on look-up table values of experimentally determined parameters in [ÖWMS13], namely, voltage-current and power-efficiency characteristics. A DC/DC converter which an essential component in pure-electric powertrains can also be dynamically modeled like the battery and supercapacitor. The main elements in DC/DC converters are

inductances and capacitances. The switching between states to enable energy exchange between these elements make DC/DC converters highly dynamic systems. The modeling of the entire powertrain in this work is a combination of forward-backward simulation as shown in Figure 3.3, comprising of both dynamically and quasi-statically modeled components. A suitable power management is designed for the chosen configuration of fuel cell-battery-supercapacitor hybrid. The role of the forward part is to calculate, based on the available power from the three sources, and the desired power requirements from the power management, the total available power. The backward part on the other hand, calculates the power demand based on the pre-defined drive cycle. If the drive cycle is unknown, then this part must also be forward modeled. The battery, supercapacitor, and DC/DC converters are modeled dynamically whereas the fuel cell along with the backward part is modeled quasi-statically. A simplified version of the model which will be described in the later sections can also be developed. The DC/DC converters in this simplified model can be modeled quasi-statically along with fuel cell and the backward part in order to reduce the computational time. This is particularly suitable for use with the optimization toolbox.

3.2 Possible topologies and considered configuration

Among the commonly known topologies in HEV powertrains, a brief overview on topologies with ICE-based and fuel cell-based powertrains is given in [ERWL05]. In series topology, there is no mechanical connection between the source and wheels whereas in parallel topology, the sources are mechanically connected to the transmission. The series-parallel topology is a combination of both series and parallel topologies. The series, parallel, and series-parallel topologies are shown in Figure 3.1. The advantages and disadvantages of each of these topologies is given in [BGT10]. However, in case of an electrical powertrain, there is no mechanical link and therefore no mechanical transmission system is required. The HEV powertrain considered in this work is an all-electric powertrain and employs DC/DC converters for controlling the power distribution. Apart from DC/DC converters, the configuration also comprises of fuel cell as primary energy source and a battery-supercapacitor combination as storage unit. In order to overcome the problems faced by batteries, the concept of hybrid storage systems (HESS) previously proposed in [LCB+08, LWR+06, BE04], and later elaborated in [CE12] has been introduced. The idea is to combine batteries and supercapacitors to improve overall performance. This is possible due to the higher power density of supercapacitors and better energy density of batteries. Thus, the supercapacitor acts as a support to the batteries and is much more robust in handling surge current. The advantages of HESS is mentioned in [KL10, AK12, CE12]. The topologies resulting from hybridization of the storage unit are classified as passive, semi-active, and active hybrids [AK12] as shown in Figure 3.2. This classification is based on the presence/absence/position of DC/DC

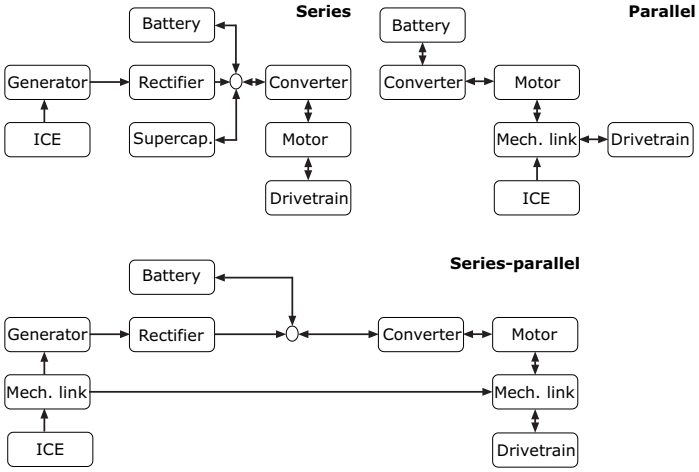

Figure 3.1: Typical topologies in ICE-based powertrains

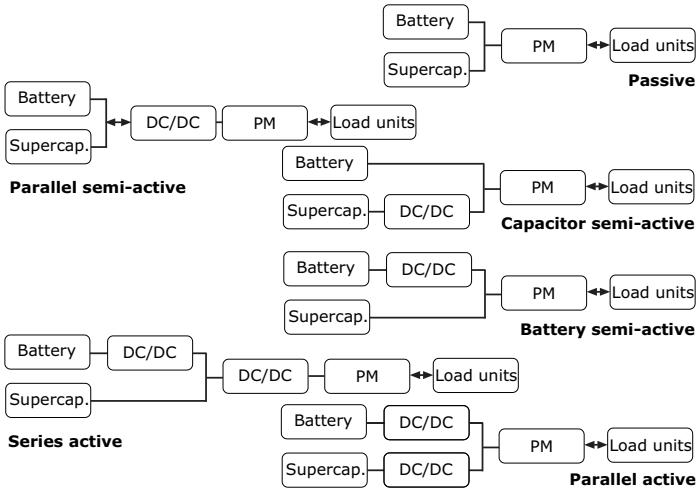

Figure 3.2: Typical topologies in electrical powertrains

converters. Of the three topologies, the parallel active topology is considered as the best option in [AK12], and has therefore been chosen in this work. The considered HEV powertrain consists of three sources namely, fuel cell, battery, and supercapacitor, each accompanied by a DC/DC converter. This part is modeled in a forward manner. The vehicle together with motor and AC/DC converter is modeled in a backward manner. The NEDC drive cycle is given as input. The link between the forward and backward parts is the power management controller. This controller checks the power demand and requests the power from sources by sending control signals to DC/DC converters. The considered configuration is shown in Figure 3.3. The control output from the supervisory controller can be fed to the backward part with the help of a driver model which can be a simple PI-controller [EHr00] or an imitation of a real human driver [VIPn$^+$09]. As a first step, the driver model is not

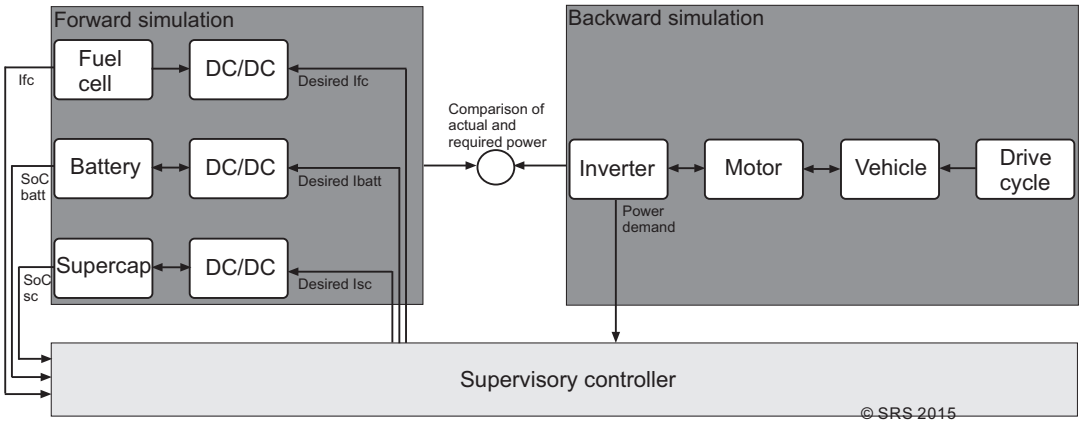

Figure 3.3: Chosen configuration for HEV

considered, but the difference between the power demand from the backward part and the power available from the forward part is compared to analyze the working of the supervisory controller. According to [GS07], the electrical coupling of quasi-static backward part and the dynamic forward part by a common bus is possible. The bus power in that case will simply be the sum of all three output power from the three DC/DC converters such that the required or demanded power is always satisfied.

3.3 Modeling and plausibility assessment of components

In this section, the powertrain models of vehicle, motor, AC/DC converter, fuel cell, battery, supercapacitor, and DC/DC converter will be briefly discussed followed by the verification of their dynamic behavior based on literature. Details of modeling and verification are given in [Rau15]. The backward modeling of components is quasi-static and their detailed dynamics will not be discussed. Since SoC is a key dynamic state, so both battery and supercapacitor are forward modeled. In this work, specific modeling approaches are chosen from literature where the models have been experimentally validated. Since the focus is on power management optimization so a detailed analysis of different experiment-based modeling approaches is not considered. However, the correctness of these easy-to-realize models is verified by comparing dynamic behaviors of real components as reported in literature.

3.3.1 Drive cycles

Drive cycles are usually represented in the form of velocity time profiles and can be considered as inputs to backward-facing models. The use of such pre-defined drive cycles is useful in designing power management strategies. The velocity-time profile

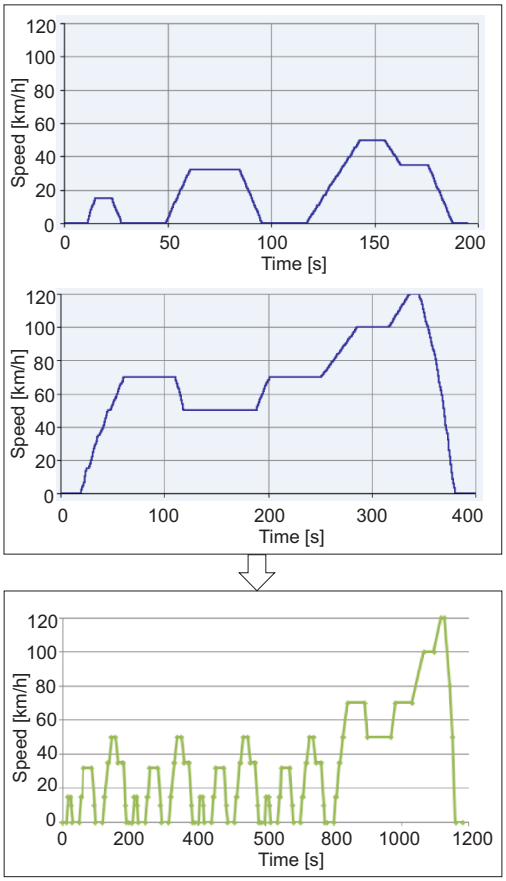

Figure 3.4: New European Drive Cycle (NEDC)

can be used to deduce expression for torque in mechanical powertrains [KVNS00] or current in electrical powertrains. The drive cycle chosen in this work is the New European Drive Cycle (NEDC) which is a combination of Urban Drive cycle (UDC/ECE 15) and Extra Urban Drive cycle (EUDC) as shown in Figure 3.4. The simulation results are based on the drive cycle chosen but power management strategies designed based on one particular drive cycle can be adapted to other drive cycles.

3.3.2 Backward/quasi-static models

The vehicle model takes drive cycle as input and generates a load profile as the output. The amount of energy required by the vehicle which is following a pre-defined drive cycle can be represented as the sum of the force required to accelerate the vehicle and the losses incurred due to the external forces acting on the vehicle as given in [GS07].From the equations of longitudinal dynamics of a road vehicle

namely [GS07]

$$m_v \frac{dv}{dt} = F_t(t) - (F_a(t) + F_r(t) + F_g(t) + F_d(t)), \tag{3.2}$$

the vehicle speed v can be calculated as a function of the traction force F_t. Here, the aerodynamic friction is represented by $F_a(t)$, the rolling friction be $F_r(t)$, gravitational force by $F_g(t)$, and disturbance force by $F_d(t)$. Therefore, the required force is the traction force (generated by the power sources in the vehicle) minus the losses.

Electric motors have the capability to act in motor mode when power is required to propel the vehicle and to act in generator mode when the vehicle is in braking mode (regeneration). With the help of power electronic devices, it is possible to operate AC motors supplied with DC current or vice versa. In [ÖWMS13], a four-quadrant drive motor controller is is used in order to recuperate braking energy back to the supply source. This converts the supplied DC current to three-phase AC to drive the load motor. The load motor used in the test-rig developed in [ÖWMS13] is a synchronous three-phase motor whereas the drive motor is a brushless DC motor. Here, the load motor is supplied from the grid and can recuperate power back to the grid. The drive motor is capable of realizing any pre-defined drive cycle and the load motor can apply the calculated load based on the vehicle model on the drive motor. In this work, the motor is modeled according to [GS07, HEMF10]. The detailed dynamics described in [GS07] is repeated and discussed in brief in the following text.

Induction AC motor generally have 3-phase stator windings, fed by an AC source and 3-phase rotor windings with no external connections. Brushless DC motors, which have been considered in this work, also have their stator windings supplied by 3-phase AC voltage as induction motors. In order to simplify the analysis of 3-phase circuits, direct-quadrature (d-q) analysis is carried out. Here, 3-phase systems are modeled using 2-phase reference and in each reference frame, electrical quantities are described by their d-q component. Considering a synchronous reference frame, the components can be treated as DC quantities. The motor input power is given by

$$P_{Motor} = P_{transmission} + P_{losses}. \tag{3.3}$$

where, $P_{transmission}$ or P_2 is the input from the vehicle model and is known; P_{losses} is calculated with the help of inputs: torque T and angular speed ω. The power $P_{transmission}$ is given by $P_1 = U_1 \cdot I_1$ is the output power at the DC link. It is considered as positive when power is absorbed by the machine acting as motor and negative when power is delivered as generator. Since the brushless DC motor does not have internal commutation, it needs an inverter to convert the DC voltage U_1 to 3-phase AC as shown in Figure 3.5. For this purpose, an inverter is needed. The relationship between P_1 and P_2 can be calculated by stationary maps where efficiency

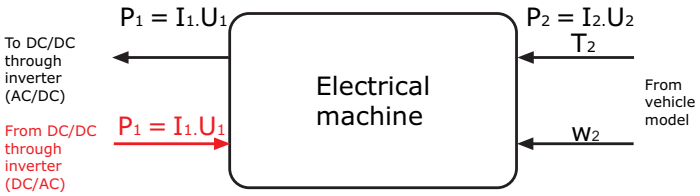

Figure 3.5: Representation of motor/generator

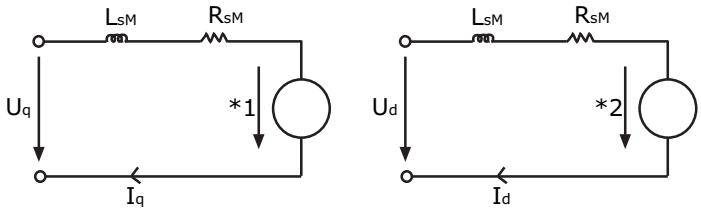

Figure 3.6: Circuit diagram of motor model

η is a function of T and ω [GS07]. The dependency between armature current and voltage, and input current and voltage is determined by motor controller. DC/DC converters apply a switching control mechanism and chop the supply DC voltage into segments. The average value of the voltage is determined by the duty cycle.

According to [GS07], torque generated at the rotor shaft is given by

$$T_m(t) = \frac{3}{2} \cdot pol \cdot \varphi_{Motor}(t) \cdot I_q(t), \tag{3.4}$$

and,

$$\frac{d}{dt}\omega_2(t) = \frac{T_m(t) - T_2(t)}{\Theta_{Motor}}, \tag{3.5}$$

where pol is the number of pole pairs and φ_{Motor} is the mutual flux linkage, I_q is the q axis component for stator current, T_2 is the load torque, and Θ_{Motor} is the moment of inertia. Since a quasi-static model is considered, therefore,

$$\frac{d}{dt}\omega_2(t) = 0 \tag{3.6}$$

According to [GS07], from Figure 3.6 the kirschhoff's voltage law, as applied to the stator (d-q axes) yields,

$$U_q = R_{sM} \cdot I_q + L_{sM} \cdot \frac{d}{dt} I_q + pol \cdot \omega_2 \cdot \varphi_{Motor} + L_{sM} \cdot pol \cdot \omega_2 \cdot I_d, \tag{3.7}$$

$$U_d = R_{sM} \cdot I_d + L_{sM} \cdot \frac{d}{dt} I_d - L_{sM} \cdot pol \cdot \omega_2 \cdot I_q, \tag{3.8}$$

where, L_{sM} and R_{sM} are inductance and resistance of the stator, U_d, U_q and I_d, I_q are the d-q axes components for stator voltage and current. The relationship between T_2 and ω_2 as derived from equations 3.4-3.8 is given by

$$T_2 = \frac{3}{2} \cdot pol \cdot \varphi_{Motor} \cdot \frac{R_{sM} \cdot U_q - pol \cdot \omega_2 \cdot R_{sM} \cdot \varphi_{Motor} - pol \cdot \omega_2 \cdot L_s \cdot U_d}{R_s^2 \cdot + pole^2 \cdot \omega_2^2 \cdot L_s^2}. \quad (3.9)$$

Considering L_s^2 to be negligible, T_2 can be represented as an affine function of ω_2 as explained in [GS07]. Thus, the expression for U_q is given by

$$U_q = \frac{2 \cdot R_{sM} \cdot T_2}{3 \cdot pol \cdot \varphi_{Motor}} + \frac{2 \cdot L_s^2 \cdot pol \cdot \omega_2 \cdot T_2}{3 \cdot R_{sM} \cdot \varphi_{Motor}} + pol \cdot \omega_2 \cdot \varphi_{Motor}. \quad (3.10)$$

The generation and waveform of stator phase voltages is determined by the sequence of switch operation of the inverter connected to the motor. The power balance at the two sides of the inverter is given as [GS07]

$$P_1 = \frac{3}{2} \cdot (U_q \cdot I_q + U_d \cdot I_d) + P_{losses} \quad (3.11)$$

where P_{losses} is calculated in [GS07] as

$$P_{losses} = \frac{2}{3} \frac{T_2^2}{\varphi_{Motor}^2} \cdot \left(\frac{R_{sM}}{pol^2} + \frac{L_{sM}^2 \cdot \omega_2^2}{R_{sM}} \right) + P_{inverterloss}. \quad (3.12)$$

In order to calculate the inverter losses, phase voltage (U_{eff} or $\hat{U}$) and current (I_{eff}) are calculated as

$$I_{eff} = \frac{P_{Motor}}{U_{eff} \cdot \sqrt{3} \cdot \cos\varphi} = \frac{P_{Motor} \cdot \sqrt{2}}{\hat{U} \cdot \sqrt{3} \cdot \cos\varphi}, \quad (3.13)$$

where $\cos\varphi$ is the power factor.

The inverter circuit mainly consists of IGBTs and diodes. It is an important task of the inverter to ensure both motor and generator operations of the brushless DC motor. The chosen approach in this work as according to [HEMF10], is to calculate the switching and conduction losses of the inverter. The 3-phase motor current is reduced to a single phase. Again, considering a quasi-static modeling approach, the switching losses can be calculated as [HEMF10]

$$P_{SW} = \frac{f_{SW} \cdot E_{SW} \cdot \hat{I} \cdot U_{Bus}}{\pi \cdot \hat{I}_0 \cdot U_0}, \quad (3.14)$$

where the switching losses E_{SW} lie in the operating point U_0, I_0 and are proportional to the switching frequency f_{SW}, bus voltage U_{Bus}, and switching current $\hat{I}_0$. the calculation of conduction losses (at the diodes and IGBTs) is as follows

$$P_{DC-IGBT} = V_{CE0} \cdot \hat{I} \cdot \left(\frac{1}{2\pi} + \frac{m_{ACDC} \cdot \cos\varphi}{8} \right) + r_I \cdot \hat{I}^2 \cdot \left(\frac{1}{8} + \frac{m_{ACDC} \cdot \cos\varphi}{3\pi} \right), \quad (3.15)$$

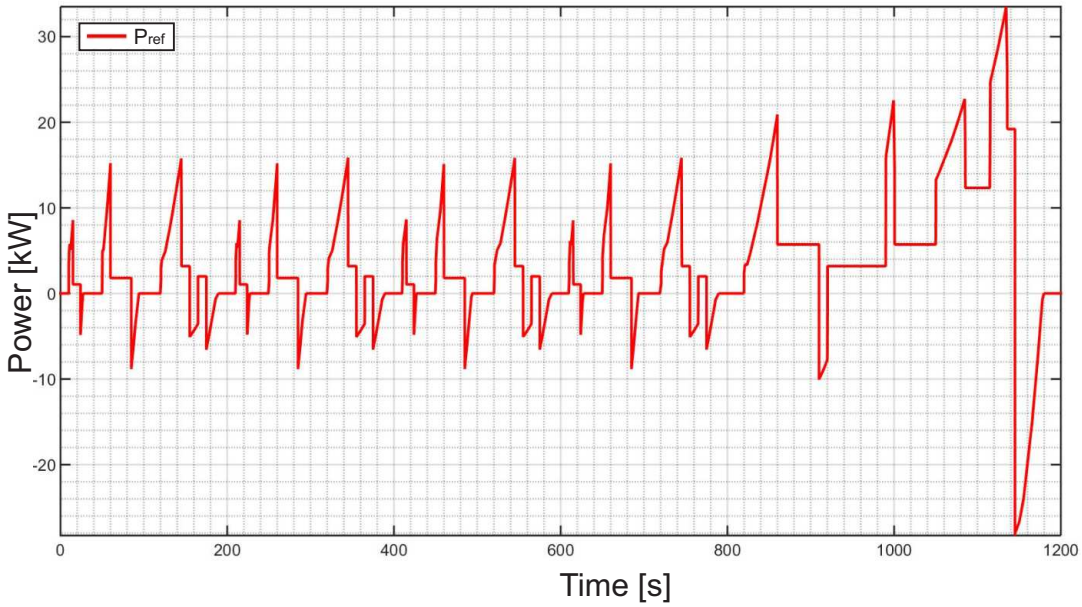

Figure 3.7: HEV power demand according NEDC drive cycle

$$P_{DC-D} = V_{F0} \cdot \hat{I} \cdot \left(\frac{1}{2\pi} + \frac{m_{ACDC} \cdot \cos\varphi}{8} \right) + r_D \cdot \hat{I}^2 \cdot \left(\frac{1}{8} - \frac{m_{ACDC} \cdot \cos\varphi}{3\pi} \right), \quad (3.16)$$

with

$$m_{ACDC} = \frac{\hat{U}}{U_{Bus}}, \ \hat{I} = \frac{\sqrt{2}}{3} \cdot I_{eff}, \quad (3.17)$$

where $\hat{U}$ and $\hat{I}$ are the peak values of motor voltage and current and m_{ACDC} gives the relation between motor peak voltage and bus voltage. The voltage and resistance V_{CE0} and r_I for the IGBTs and V_{F0} and r_D for the diodes are responsible for the conduction losses. The parameters chosen in this work are according to [HEMF10]. The total inverter loss is given by

$$P_{inverterloss} = 6 \cdot [P_{SW} + P_{DC-IGBT} + P_{DC-D}], \quad (3.18)$$

The power at the bus can now be calculated as

$$P_{bus} = P_{Motor} + P_{inverterloss}, \quad (3.19)$$

The load profile corresponding to the velocity-time profile of the input drive cycle is calculated as shown in Figure 3.7. This load profile corresponds to the bus power P_{bus}. This variation of power with time is termed as power demand in this work.

3.3.3 Fuel cell

Fuel cells are electrochemical devices that convert chemical energy to electrical energy. Unlike internal combustion engines, they deliver pure electrical energy. Fuel

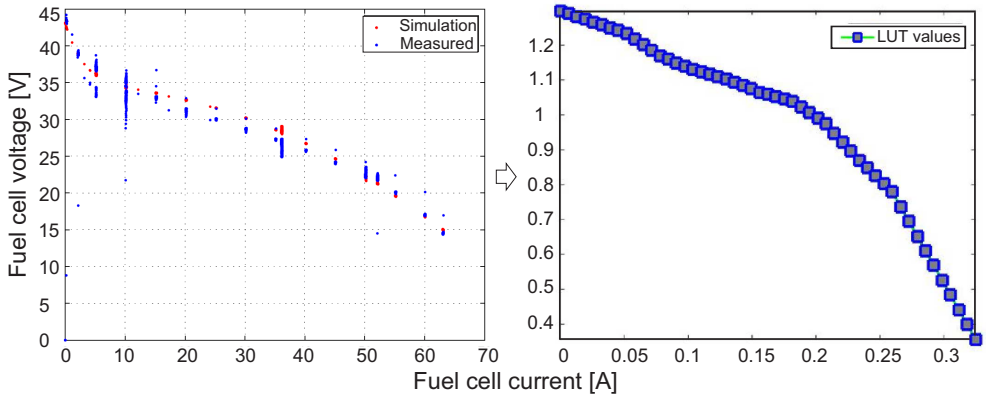

Figure 3.8: Look-up table for V-I characteristics [MS16b]

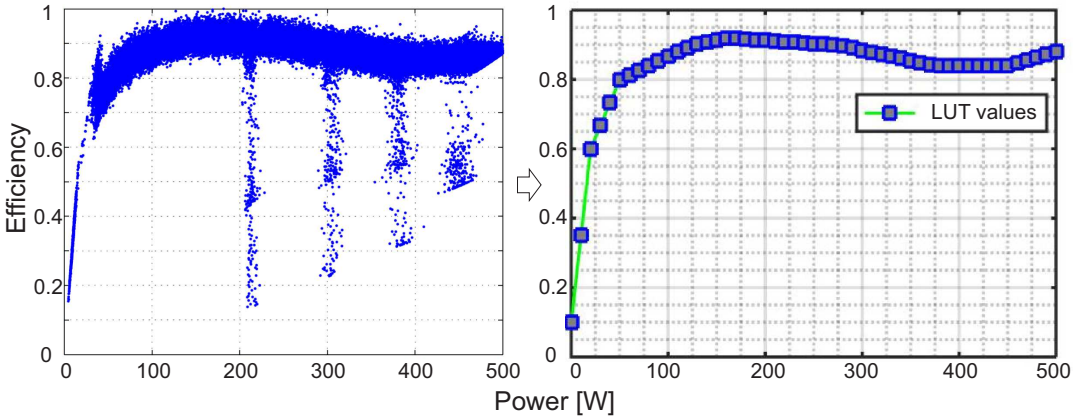

Figure 3.9: Look-up table for power-efficiency characteristics [MS16b]

cells are more efficient as compared to internal combustion engines [OAK97]. A detailed model of a PEM fuel cell has been considered in [ÖWMS13]. The model used in [ÖWMS13] has also been validated with hardware. Therefore, based on the results obtained in [ÖWMS13], a fuel cell model based on look-up tables (LUTs) has been considered in this work. The used LUTs represent the fuel cell voltage-current and efficiency-power relations are are shown in Figures 3.8 and 3.9 respectively. According to [GS07, ÖWMS13], the behavior of a single cell is given in terms of cell voltage U_{fc} and current density i_{fc}, defined as follows

$$i_{fc} = \frac{I_{fc}}{A_{fc}}, \tag{3.20}$$

where A_{fc} represents total cell area of the fuel cell. The stack voltage is given by

$$U = U_{fc} \cdot N, \tag{3.21}$$

where U_{fc} represents the cell voltage and N the number of number of single cells in series. The maximum value of U_{fc} is considered in [ÖWMS13] to be 1.299 volts.

The output power of the fuel cell is given by

$$P_{fc} = U_{fc} \cdot I_{fc} \cdot \mu_{fc}. \tag{3.22}$$

The efficiency can be determined based on the LUT as shown in Figure 3.9.

Fuel cells are clean and environmental friendly power sources but the long time constant limits their performance in HEVs [KL10]. According to [KL10], the efficiency and range of HEVs depend on the capability of the energy storage unit. A possible option is to combine a fuel cell with battery, but due to the disadvantages posed by batteries, supercapacitors can be used as an option [PDRL07]. According to [PDRL07], the simultaneous use of batteries and supercapacitors can lead to a promising solution. Therefore both batteries and supercapacitors are considered in this work in addition to fuel cells. Their mathematical models are presented in the next sections.

3.3.4 Battery

Batteries are electrochemical storage components where energy which is chemically bounded is converted to electrical energy just like the fuel cells; in batteries the process is reversible. Chemical energy is converted to electrical energy and vice-versa. According to [GS07], a battery can be modeled as a large capacitor. The chemical processes in electrolyte can be represented by an internal resistance. According to [HXGL12], to ensure safe and reliable battery operation battery management (or power management systems) are important. For this purpose, monitoring of temperature, voltages, currents are required and an estimation of states like SoC is needed. Commonly used models are electrochemical models and equivalent circuit models. A comparison and evaluation of seven battery models have been presented in [HXGL12]. As electrochemical models are complex and deal with a large number of unknown parameters, only equivalent circuit models are considered in this contribution. As detailed in [HXGL12], some of the equivalent circuit models are Thevenin, Rint, and DP models. The disadvantage is that the relation between internal resistance and current is not considered. In reality, internal resistance is related to non-linear processes for which electrochemical models are required [GS07]. In [**?**], the non-linearity of battery resistance is investigated and the dependency of impedance on factors such as SoC is studied. According to [GS07], an alternative solution is to develop black box models using experimental data derived from constant current discharge tests. Fitting techniques can then be used to obtain input-output relations. Developing accurate methods to estimate states like SoC is a challenge. A comparison of different approaches to estimate battery states is given in [HXGL12]. The approach called 'Coulomb counting' is briefly described in [GS07] along with quasi-static and dynamic modeling of batteries. The quasi-static model is based on Rint model and dynamic model based on Thevenin model.

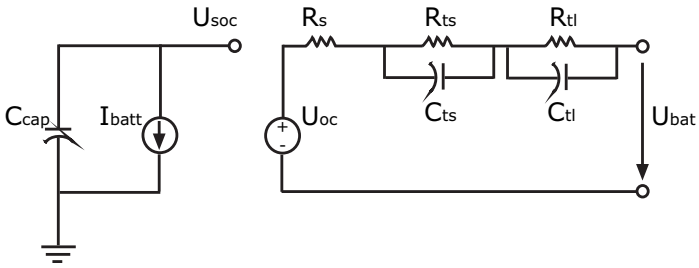

Figure 3.10: Circuit diagram of battery model

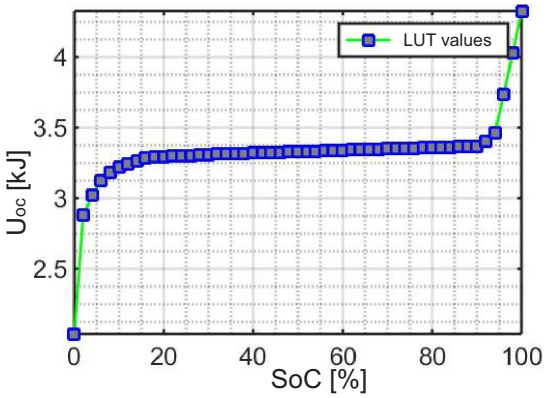

Figure 3.11: Relation between SoC and voltage

In this work, a Li-ion battery is chosen and the battery is modeled using a dynamic modeling approach according to [KDN+07, CRM06]. With the help of dynamic models, the transient behavior of the battery can be described [GS07]. Inductive and capacitive effects are taken into account and model-based determination of SoC is possible [GS07]. The circuit diagram is shown in Figure 3.10. In one circuit, the overall capacity of the battery is represented, while in the other, the internal resistance and other dynamic effects. The SoC of the battery is determined from the total capacity C_{cap} and the battery current I_{bat}. The voltage source linking the two circuits, represents the non-linear relation between battery state of charge and open circuit voltage U_{oc}. This non linear relation between SoC and U_{oc} using 33 cells, can be represented by a LUT as shown in Figure 3.12.

From the equations of voltages as derived from the second loop in the circuit as shown in Figure 3.10, namely,

$$U_s = -R_s \cdot I_{bat}, \tag{3.23}$$

$$\dot{U}_{ts} = -\frac{U_{ts}}{R_{ts} \cdot C_{ts}} - \frac{I_{bat}}{C_{ts}}, \tag{3.24}$$

$$\dot{U}_{tl} = -\frac{U_{tl}}{R_{tl} \cdot C_{tl}} - \frac{I_{bat}}{C_{tl}}, \tag{3.25}$$

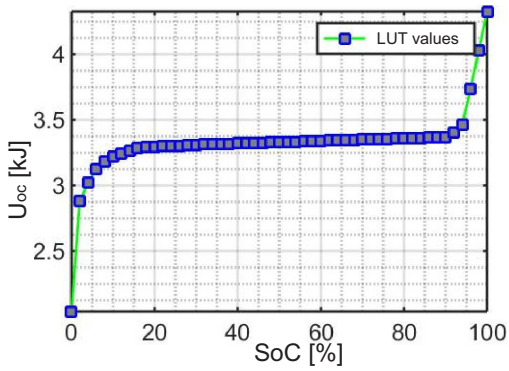

Figure 3.12: Relation between SoC and voltage

the following state space model can be generated according to [KDN+07, CRM06]

$$\dot{\mathbf{x}} = \begin{bmatrix} 0 & 0 & 0 \\ 0 & -(R_{ts}C_{ts})^{-1} & 0 \\ 0 & 0 & -(R_{tl}C_{tl})^{-1} \end{bmatrix} \mathbf{x} + \begin{bmatrix} -C_{cap}^{-1} \\ -C_{ts}^{-1} \\ -C_{tl}^{-1} \end{bmatrix} \mathbf{u}, \tag{3.26}$$

with,

$$\mathbf{x} = \begin{bmatrix} U_{soc} \\ U_{ts} \\ U_{tl} \end{bmatrix}, \ \mathbf{u} = I_{bat}, \tag{3.27}$$

$$y = U_{bat} = g(U_{soc}) + U_{ts} + U_{tl} - R_s \cdot I_{bat}, \tag{3.28}$$

where, battery current I_{bat} is the input and terminal voltage U_{bat}, is the output.

In [KDN+07], first an initial model is built with parameters based on literature. Then the U_{oc}-SoC relationship is derived from experiments on a real battery, then a refined model is built based on the U_{oc}-SoC relationship and finally the resistances and capacitances namely $R_{ts}, C_{ts}, R_{tl}, C_{tl}$, and R_s are estimated. The experimental set-up with the real battery connected to programmable load is given in [KDN+07]. After a constant resistance discharge test, the SoC over the entire test is calculated by integrating the current as

$$U_{soc} = -\frac{1}{C_{cap} \cdot \int I_{bat}} \ \Rightarrow \ \dot{U}_{soc} = -\frac{I_{bat}}{C_{cap}}, \tag{3.29}$$

where, normalized values of U_{soc} from 0 to 1 volts corresponds to SoC values between 0% to 100%. The relationship between U_{oc} and U_{soc} or SoC is given by

$$U_{oc} = g(U_{soc}) \tag{3.30}$$

and can be established with the help of a LUT [REC12] as shown in Figure 3.12.

The specifications of the real Li-ion battery (used in [KDN+07]) as available from the manufacturers is: maximum cell voltage as 4.2 V and capacity as 60 Ah. For a fully charged battery, U_{soc} should be 1 V but as 4.09 V is measured in [KDN+07] instead of the specified value by manufacturer that is, 4.2, so instead of 1 V, 0.9 V is calibrated for full charge.

Estimation of the values of $R_{ts}, C_{ts}, R_{tl}, C_{tl}$, and R_s are given in [KDN+07], where constant current discharge tests are carried out. The load is switched between 3.6 A and 0 A by the programmable sink. The battery is discharged over 9 cycles (constant current followed by rest), the begin of each cycle depending on when a specific U_{soc} value reached. The test data are analyzed for the discharge and rest phases leading to the estimation of the resistances and capacitances. In [KDN+07], this is done using curve fitting toolbox. The parameters are plotted as function of SoC. These variations of resistances and capacitances with SoC can either be implemented as LUTs or assumed as constants (averaged values over 9 discharge cycles). The numbers are assumed as constants to avoid unnecessary model complexity in this contribution.

3.3.5 Supercapacitor

Supercapacitors (also known as ultracapacitors or double layer capacitors) are capable of storing a large amount of energy as compared to conventional capacitors. Their specific power is much higher than batteries but specific energy is lower. Due to their higher power density, they can be used in hybrid powertrains to realize fast transient power demands. Here, the energy is stored as a result of charge separation. The charge separation occurs between the layers that separate the electrolyte and the electrodes. According to [FPCP09], the difference in the way energy is stored in the battery and in the supercapacitor is that, in battery, an indirect storage via an electrochemical process is used. In a supercapacitor, a direct storage of charge as a result of electrostatic process occurs. The difference in the discharge curves of battery and supercapacitor is given in [FPCP09]. In [FPCP09], experiments were conducted and model parameters were calculated for the initial model from [JA08]. The supercapacitor model considered in this work is based on the models used in [FPCP09, JA08]. As shown in Figure 3.13, the main capacitance C_{SC} is connected in parallel to a resistance R_2 which represents the self-discharge of supercapacitors. The RC network is connected to another RC network consisting of capacitance C_p and resistance R_p. The charge/discharge losses are represented by the resistance R_1 and the resistance used for protecting the supercapacitor against overcharge is represented by R_3. Considering that the switch is open,

$$I_{SC} = I_{norm}, \tag{3.31}$$

and,

$$U_{SC} = U_1 + U_p + U_2, \tag{3.32}$$

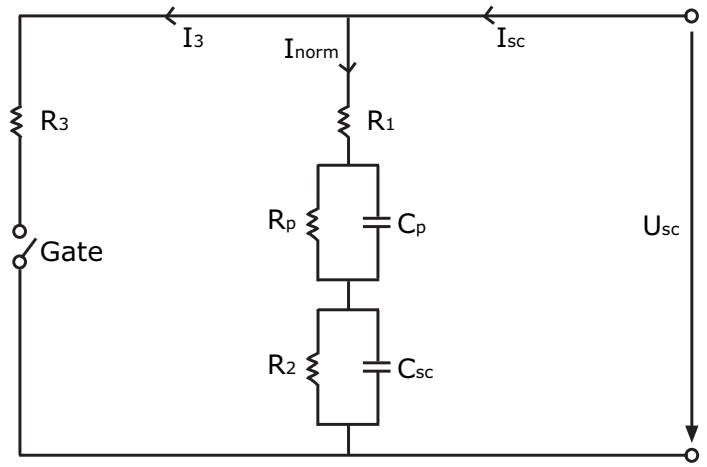

Figure 3.13: Circuit diagram of supercapacitor model

where,

$$U_1 = R_1 \cdot I_{norm}. \tag{3.33}$$

For the RC network, the following equations can be derived

$$\dot{U}_p = \frac{I_{norm}}{C_p} - \frac{U_p}{R_p \cdot C_p}, \tag{3.34}$$

$$\dot{U}_2 = \frac{I_{norm}}{C_{SC}} - \frac{U_2}{R_2 \cdot C_{SC}}. \tag{3.35}$$

From the equations, 3.32, 3.33, 3.34, and 3.35, the following state space equations can be derived

$$\dot{\mathbf{x}} = \begin{bmatrix} -(R_p C_p)^{-1} & 0 \\ 0 & -(R_2 C_{SC})^{-1} \end{bmatrix} \mathbf{x} + \begin{bmatrix} C_p^{-1} \\ C_{SC}^{-1} \end{bmatrix} \mathbf{u}, \tag{3.36}$$

where,

$$\mathbf{x} = \begin{bmatrix} U_p \\ U_2 \end{bmatrix}, \ \mathbf{u} = I_{norm}, \tag{3.37}$$

$$y = U_{SC} = R_1 \cdot I_{norm} + U_p + U_2. \tag{3.38}$$

The extraction of model parameters is done based on a real supercapacitor model [FPCP09]. The data available from manufacturers are: nominal voltage: 14 V, nominal capacity: 350 F; mass: 24 kg. In [FPCP09], constant current tests are carried out with the real supercapacitor by connecting it to a programmable load. The supercapacitor is charged at 10 A until the voltage reaches 11 V, then the current is cut off for about 10 minutes and a constant current discharge phase follows at -20

A. For the calculation of C_{SC}, the time period when the voltage rise is from 2 V to 9 V is chosen, namely $\Delta t = 225s - 46s = 209s$. So,

$$C_{SC} = \frac{\Delta Q}{\Delta U}, \tag{3.39}$$

and

$$Q = \int i(t)dt, \tag{3.40}$$

where, $\Delta t = 209s$ and $\Delta U = 9V - 2V = 7V$,

$$Q = 10\ A * 209\ s = 2090\ C, \tag{3.41}$$

and,

$$C_{SC} = \frac{2090}{7} \approx 300\ F. \tag{3.42}$$

The value of capacitance C_p is chosen as one-thirteenth of C_{SC}.

To estimate R_1, the phase right after the charge current is cut off is taken into account. This corresponds to [FPCP09] as

$$R_1 = \frac{\Delta U}{\Delta i} \approx 2m\Omega. \tag{3.43}$$

The resistance R_2 is estimated as 200Ω. To estimate R_3, the voltage drop after turning off of charging current is considered as

$$R_3 = \frac{\Delta t}{-\ln(\frac{U_1}{U_0}) \cdot C_{SC}} R_3 = 10\Omega. \tag{3.44}$$

The relationship between the capacitance C_{SC} and voltage U_{SC} can be implemented with the help of a LUT as shown in Figure 3.14. Protection against overcharge using the resistance R_3 is simulated by a relay-switch combination. If the voltage exceeds a certain value, the relay closes the switch and current

$$I_{norm} = I_{SC} - I_3, \tag{3.45}$$

flows through the circuit. Thus, the modeling of supercapacitor is complete. The input to the system is considered to be current that flows through the capacitors, and output as SoC and voltage. The model parameters are adjusted according to [FPCP09].

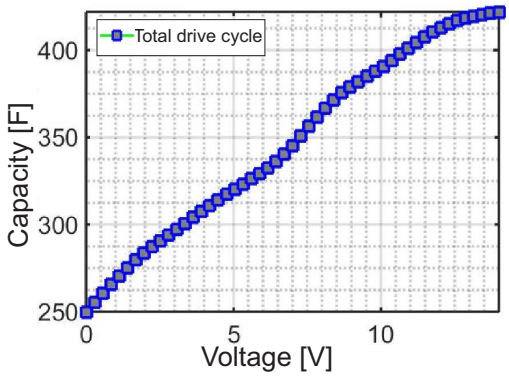

Figure 3.14: Relationship between capacitance and voltage

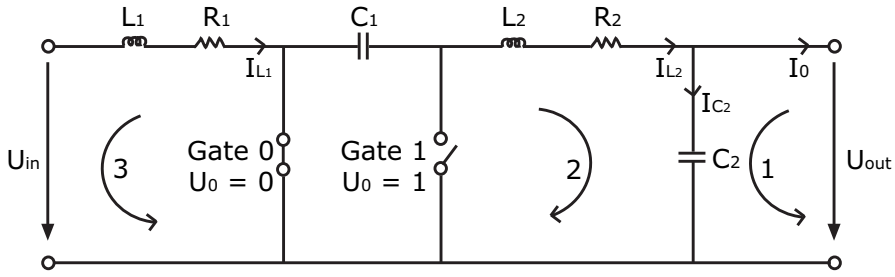

Figure 3.15: Circuit diagram of DC/DC converter

3.3.6 DC/DC converter

The purpose of the DC/DC converter in this work is to maintain a constant output voltage despite varying input voltage. It is also possible to control the output voltage in order to track a reference, but this makes the DC/DC converter more complex and expensive. The converter should be dynamic enough to respond to the changes in demanded power and make the required power available on the bus. Buck, boost and buck-boost DC/DC converters are the commonly known types. DC/DC converters can also be mono- or bi-directional. Bi-directional DC/DC converters can transfer power to and from source thus allowing the regenerated energy to be saved. Therefore, they have been considered in this work for the two storage elements: battery and supercapacitor. The DC/DC converter model chosen in this work is a CUK-DC/DC converter with buck-boost behavior and is in accordance with the model already described in [ÖWMS13]. The circuit diagram of the DC/DC converter is shown in Figure 3.15. The two states of the DC/DC converter can given as

1. *Gate* 0 is closed and *Gate* 1 open $\Rightarrow$ $u_0 = 0$; $u_1 = 1$,

2. *Gate* 0 is open und *Gate* 1 closed $\Rightarrow$ $u_0 = 1$; $u_1 = 2$.

Duty cycle is defined as

$$D = \frac{t_{on}}{t_{off}}, \tag{3.46}$$

From the two states, two equations can be derived as follows

$$\dot{U}_{C1} = \frac{I_{C_1}}{C_1} \; ; \; \dot{U}_{C2} = \frac{I_{C_2}}{C_2}, \tag{3.47}$$

and

$$U_{L1} = \dot{I}_{L1} \cdot L_1 \; ; \; U_{L2} = \dot{I}_{L_2} \cdot L_2. \tag{3.48}$$

For the first state where $u_0 = 0 \; ; \; u_1 = 1$,

$$-U_{in} + U_{L1} + U_{R1} \tag{3.49}$$

$$\Rightarrow \; \dot{I}_{L1} = -\frac{R_1 I_{L1}}{L_1} + \frac{U_{in}}{L_1}, \tag{3.50}$$

For the left loop and right loops 3 and 2,

$$U_{C1} + U_{L2} + U_{R2} + U_{C2} \tag{3.51}$$

$$\Rightarrow \; \dot{I}_{L2} = -\frac{U_{C1}}{L_2} - \frac{U_{C2}}{L_2} - \frac{R_2 I_{L2}}{L_2}. \tag{3.52}$$

$$I_{C1} = I_{C2} = I_{L2}. \tag{3.53}$$

From equations (3.47), (3.49), (3.50), (3.51), (3.52), (3.53) the following can be derived,

$$\dot{\mathbf{x}} = \underbrace{\begin{bmatrix} -\frac{R_1}{L_1} & 0 & 0 & 0 \\ 0 & -\frac{R_2}{L_2} & -\frac{1}{L_2} & -\frac{1}{L_2} \\ 0 & \frac{1}{C_1} & 0 & 0 \\ 0 & \frac{1}{C_2} & 0 & 0 \end{bmatrix}}_{\mathbf{A_1}} \mathbf{x} + \begin{bmatrix} \frac{1}{L_1} & 0 \\ 0 & 0 \\ 0 & 0 \\ 0 & -\frac{1}{C_2} \end{bmatrix} \mathbf{u}, \tag{3.54}$$

with

$$\mathbf{x} = \begin{bmatrix} I_{L1} \\ I_{L2} \\ U_{Cl} \\ U_{C2} \end{bmatrix} \; , \; \mathbf{u} = \begin{bmatrix} U_{in} \\ I_{out} \end{bmatrix} \; , \; \mathbf{y} = \mathbf{x}, \tag{3.55}$$

The input current I_{L1} is the current signal sent from power management to DC/DC converter and this is the current required to be drawn from the sources. The capacitor voltage U_{C2} is the output voltage that is the bus voltage and that needs to be held constant.

For the second state where $u_0 = 1\ ;\ u_1 = 2$,

$$\dot{\mathbf{x}} = \underbrace{\begin{bmatrix} -\frac{R_1}{L_1} & 0 & -\frac{1}{L_1} & 0 \\ 0 & -\frac{R_2}{L_2} & 0 & -\frac{1}{L_2} \\ \frac{1}{C_1} & 0 & 0 & 0 \\ 0 & \frac{1}{C_2} & 0 & 0 \end{bmatrix}}_{\mathbf{A_2}} \mathbf{x} + \begin{bmatrix} \frac{1}{L_1} & 0 \\ 0 & 0 \\ 0 & 0 \\ 0 & -\frac{1}{C_2} \end{bmatrix} \mathbf{u}, \tag{3.56}$$

with

$$\mathbf{x} = \begin{bmatrix} I_{L1} \\ I_{L2} \\ U_{Cl} \\ U_{C2} \end{bmatrix}\ ,\ \mathbf{u} = \begin{bmatrix} U_{in} \\ I_{out} \end{bmatrix}\ ,\ \mathbf{y} = \mathbf{x}, \tag{3.57}$$

According to [ÖWMS13], coupling between $\mathbf{A_1}$ and $\mathbf{A_2}$ can be expressed by the duty cycle D as follows

$$\mathbf{A_{tot}} = \mathbf{A_2} + D \cdot (\mathbf{A_1} - \mathbf{A_2}) \tag{3.58}$$

For the coupled system, the following non-linear state-space equations can be derived

$$\dot{\mathbf{x}} = \underbrace{\begin{bmatrix} -\frac{R_1}{L_1} & 0 & -\frac{1}{L_1} & 0 \\ 0 & -\frac{R_2}{L_2} & 0 & -\frac{1}{L_2} \\ \frac{1}{C_1} & 0 & 0 & 0 \\ 0 & \frac{1}{C_2} & 0 & 0 \end{bmatrix}}_{\mathbf{A_{lin}}} \mathbf{x} + \underbrace{\begin{bmatrix} 0 & 0 & \frac{D}{L_1} & 0 \\ 0 & 0 & -\frac{1}{L_2} & 0 \\ -\frac{D}{C_1} & \frac{D}{C_1} & 0 & 0 \\ 0 & 0 & 0 & 0 \end{bmatrix}}_{\mathbf{A_{nonlin}}} \mathbf{x} + \begin{bmatrix} \frac{1}{L_1} & 0 \\ 0 & 0 \\ 0 & 0 \\ 0 & -\frac{1}{C_2} \end{bmatrix} \mathbf{u}, \tag{3.59}$$

with

$$\mathbf{x} = \begin{bmatrix} I_{L1} \\ I_{L2} \\ U_{Cl} \\ U_{C2} \end{bmatrix}\ ,\ \mathbf{u} = \begin{bmatrix} U_{in} \\ I_{out} \end{bmatrix}\ ,\ \mathbf{y} = \mathbf{x}. \tag{3.60}$$

Thus the state space form of DC/DC converter model has a linear system matrix A_{lin} and a non-linear system matrix A_{nonlin} which is dependent on the duty cycle. According to [UA07], the DC/DC converter can be internally controlled by a PI-controller with bus voltage as the reference input, and externally, it can be controlled

by the power management controller that sends the required current output signal to the converter. The switching losses of the DC/DC converter can be calculated based on a LUT which is based on the validated results from [Bru15, Bru14]. From this LUT, the energy conversion efficiency $\mu_{DC/DC}$ can be calculated. Therefore from,

$$P_{out} = P_{DC/DC} \cdot \mu_{DC/DC} \; = \; I_{out} \cdot U_{C2} \cdot \mu_{DC/DC} \tag{3.61}$$

the output power of the converter P_{out} can be determined.

3.3.6.1 Simplification of the DC/DC converter model

The model of DC/DC converter considered in the previous section is based on complex dynamical equations and therefore, increases the computational cost of the system. Due to the presence of three DC/DC converters, the simulation time and memory required are large. Since the optimization of power management (discussed in chapter 4) is considered as a separate offline process, therefore, a simplified version of the DC/DC converter for the optimization loop is used to ease the simulation process. The optimization algorithm involves a complicated and time-consuming procedure to optimize the controller parameters and therefore, a simplified version of the HEV model (which contains simplified DC/DC converter models) is helpful in generating solutions at lower computational cost and memory. In the simplified DC/DC converter model, only the losses are taken into account and the switching dynamics omitted. The calculation of $\mu_{DC/DC}$ based on LUT has already been mention and therefore from 3.61,

$$P_{in} \cdot \mu_{DC/DC} = P_{out} \; \Rightarrow \; I_{in} = I_{out} \cdot \frac{U_{out}}{U_{in}} \cdot \frac{1}{\mu_{DC/DC}}. \tag{3.62}$$

The main task of DC/DC converter here is to regulate the voltage level. In other words, it is sufficient to consider the power balance at the two sides of the converter [GS07]. The term I_{in} which is the input to the converter, is the required current from sources to be calculated by power management.

3.3.7 Theoretical sizing of components

3.3.7.1 Component sizing

The fuel cell, being a primary energy source, should be able to supply the total required power as demanded by the given drive cycle. For the given drive cycle, the total energy can be calculated as

$$E_{total} = 3821 \; kJ, \tag{3.63}$$

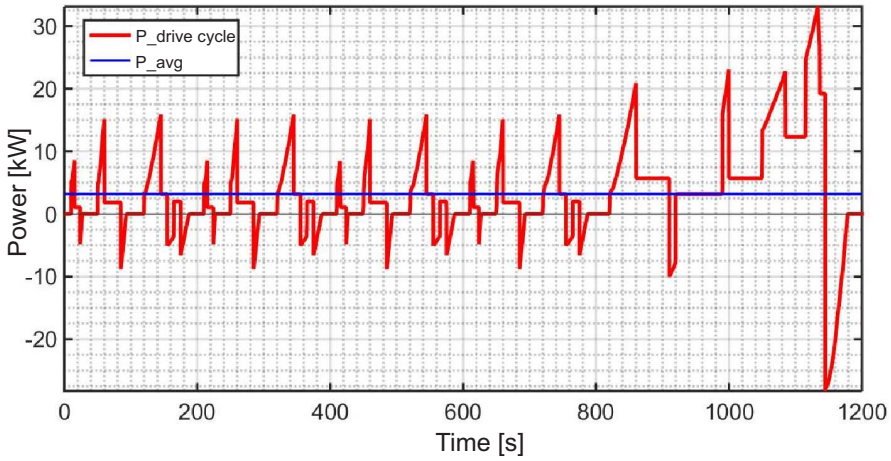

Figure 3.16: Average fuel cell power

resulting in an average power of P_{avg}, calculated over $t_{total} = 1200sec$ as follows

$$P_{avg} = \frac{E_{total}}{t_{total}} = 3.184\ kW. \tag{3.64}$$

Considering the losses of the DC/DC converter (with $\mu_{DCDC,nor} = 0.98\%$ approx.), together with the losses of fuel cell (with an optimum efficiency of $\mu_{FC,opt} = 0.92\%$), the averaged fuel cell power $P_{FC,avg}$ can be calculated as

$$P_{FC,avg} = P_{avg} \cdot \frac{1}{\mu_{DCDC,nor}} \cdot \frac{1}{\mu_{FC,opt}} = 3.515\ kW. \tag{3.65}$$

The average power and the power demand from the drive cycle can be represented in Figure 3.16. It becomes clear from the figure that the power management strategy must consider, both operating the fuel cell in its most efficient region as well as the peak loads of power demand. The sizing of the fuel cell can done by changing the factor N (Equation 3.22).

3.3.7.2 Battery sizing

For the battery to be able to supply the maximum peak of power, the maximum energy to be stored is given for the corresponding time period as

$$E(t_0 = 820s) - E(t_1 = 1144s) = 3.1MJ. \tag{3.66}$$

with a factor $k = 2$ which takes into account the losses while battery discharging and charging, the maximum energy to be stored can be considered as

$$E_{bat} = 6.2MJ. \tag{3.67}$$

The model design parameters and capacity of the battery can be adjusted according to this value. In spite of the design considered, the actual maximum power delivered by the battery will be defined by the power management strategy. The power management will keep the battery operation within limits by using the second storage element namely, the supercapacitor. It is also to be noted that the battery model is not designed based on the charging/discharging limits of a real battery. A real battery is equip with a battery management system that keeps the SoC within operation limits (15%-95%). In this work, this feature is considered to be a task of power management.

3.3.7.3 Supercapacitor sizing

The parameters chosen to model the supercapacitor in this work are from [FPCP09]. The configurations are determined by arranging the capacitors in series and parallel. The nominal voltage of the supercapacitor $V_n = 14V$ is not enough to maintain a constant bus voltage of 500 V. It can be achieved by a serial arrangement of supercapacitors as follows

$$U_{total} = \sum_{n=0}^{serial_{SC}} U_{SC,n}, \tag{3.68}$$

where, $serial_{SC}$ is the number of capacitors arranged in serial. Thus, the total capacitance is reduced as folows

$$\frac{1}{C_{total}} = \sum_{n=0}^{serial_{SC}} \frac{1}{U_{SC,n}}. \tag{3.69}$$

If $serial_{SC}$ is chosen as 36, then the maximum voltage $V_{n,total}$ will be

$$V_{n,total} = V_n \cdot serial_{SC} = 504V \tag{3.70}$$

Similarly, parallel arrangement of capacitors causes an increase in the total capacitance as follows

$$C_{total} = \sum_{n=0}^{parallel_{SC}} C_{SC,n}, \tag{3.71}$$

where $parallel_{SC}$ is the number of capacitors arranged in parallel. Thus, the storage capacity of the supercapacitor can be adjusted by changing the configuration. As during deciding the battery dimensions, here to a safety factor of $k = 2$ is considered and the maximum energy to be stored is given by

$$E_{SC} = 6.2MJ. \tag{3.72}$$

In order to achieve this, a parallel configuration of supercapacitors such that $parallel_{SC} = 4$ is necessary. Once again, this is to be taken into consideration by the power management strategy.

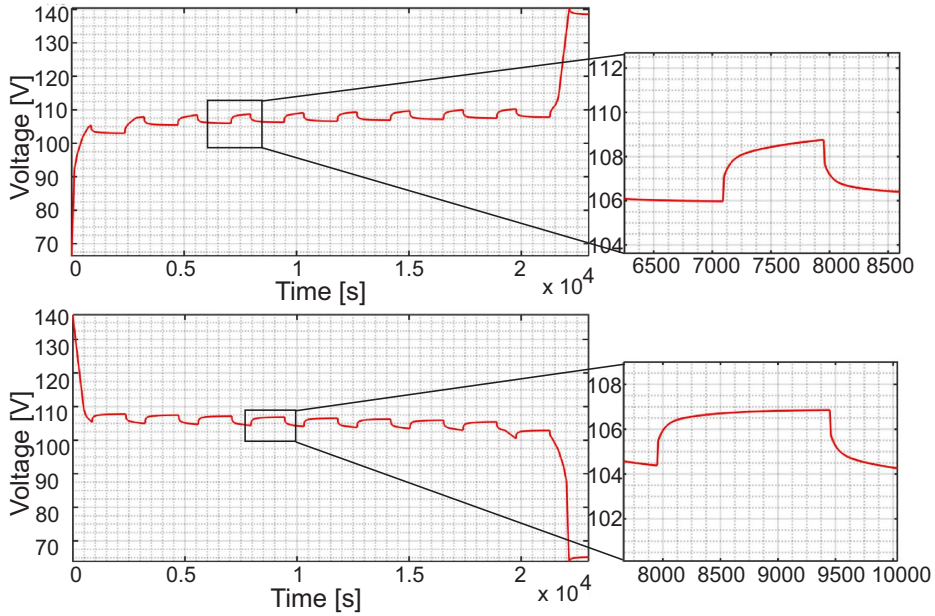

Figure 3.17: Battery voltage variation during charging and discharging [MS16b]

3.3.8 Model verification based on literature

3.3.8.1 Verification of the battery model

In order to verify the dynamic behavior of the simulated model, the results are compared to experimentally validated models of [KDN+07], [REC12], [CRM06], and [KQ11]. The battery is first fully charged, then fully discharged in a cyclic manner. A constant current of $I_{bat} = 25A$ is applied till the next SoC level ($SoC_{bat} = 10\%, 20\%, ..., 90\%$) is reached. At the next SoC level, current is turned off, then turned on again after a 25 minute pause. The voltage variation resulting from the SoC-U_{soc} relationship (Figure 3.12) is similar to that discussed in the literature. In Figure 3.17, the voltage variation while battery charging is shown. At the moment when current is turned off, the resulting voltage curve exhibits an initial peak followed by a gradual logarithmic decay. Similarly, when the current is turned on again, a short dip in voltage is followed by a gradual increase. As shown in Figure 3.17, this behavior is inverted during discharging process. In Figure 3.18, the SoC variation is shown. The SoC and energy saved in the battery increase continuously with each charge cycle. In reality, the energy supplied to the battery is not always same as the energy that the battery is capable of supplying. The supplied energy or the power required to charge the battery is dependent on the battery voltage and during the charge-discharge cycles, the a part of this energy is lost in irreversible chemical processes.

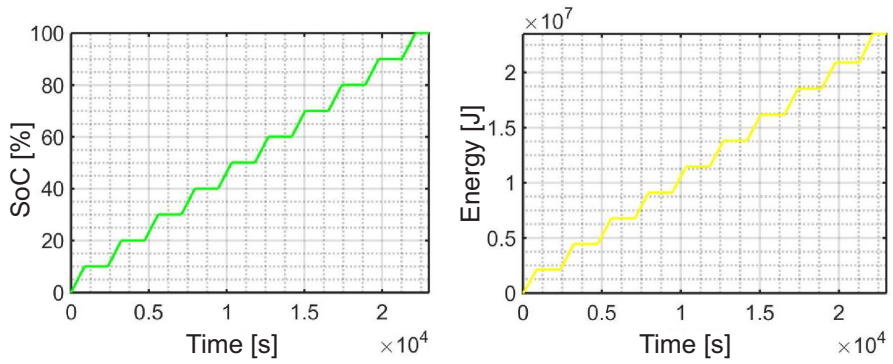

Figure 3.18: Battery SoC and energy during charging

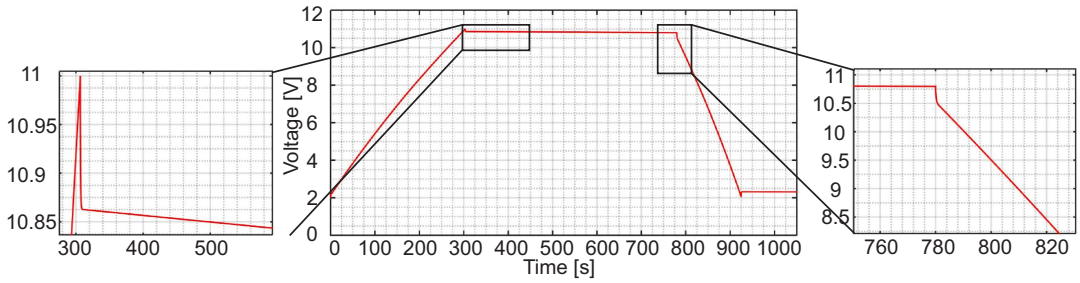

Figure 3.19: Capacitor voltage during charging and discharging [MS16b]

3.3.8.2 Verification of the supercapacitor model

In order to verify the simulation model, the tests according to [FPCP09] are carried out. First, the supercapacitor is charged with a constant current of 10 A till U_{SC} is almost equal to 11 V, then, current is turned off, and after a 8 min pause, the supercapacitor is completely discharged with -20 A. As shown in Figure 3.19, the voltage of the supercapacitor increases till the current is turned off. At the moment when current is turned off, a small peak is followed by a gradual decay of voltage. This is due to the self-discharging tendency of supercapacitors. By comparing the response of the supercapacitor while charging and discharging (Figures 3.19) with the experimentally determined results of [FPCP09] and [LZLC13], the correctness of modeling can be confirmed.

3.3.8.3 Verification of the DC/DC converter model

In order to verify the DC/DC converter model, a current (I_{out}) of 25 A is given. The task of the DC/DC converter here is to maintain constant bus voltage of 500 V. Thus, the load demand to be fulfilled by the source connected to the converter is

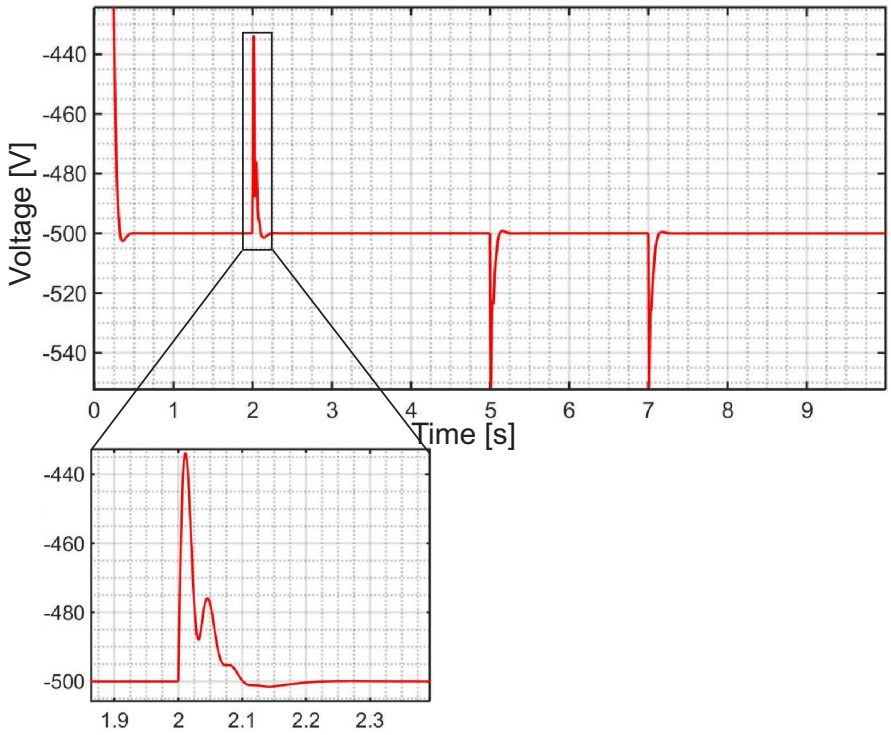

Figure 3.20: Bus voltage during charging and discharging [MS16b]

12.5 kW. The source connected to the converter during this test is a battery. After, 5 seconds, the current is turned off and a 2 second pause follows. Then, I_{out} is changed to -25 A so as to charge the battery with 12.5 kW. The result of this test can be seen in Figure 3.20. Due to the inverted bust-boost behavior, the voltage is negative. If it is multiplied by negative values of I_{out} which will be the output from the power management and reference input to the converter, then the bus voltage can be made positive. As shown in Figure 3.20, the relatively short oscillatory behavior at the switching moments die down fast due to the control action of the PI-controller in the DC/DC converter. The response to the load demand is the input current to the DC/DC current from the battery. It shows a PT2 behavior as shown in Figure 3.21. A brief oscillation at the start of simulation can also be detected, but the CUK-DC/DC converter is capable of keeping the ripples as small as possible [Ema05], so as to avoid any extreme current transients. Thus, from the above mentioned tests, in combination with the validated results from [Bru15, Bru14], the dynamics of the bi-directional DC/DC converter can be verified.

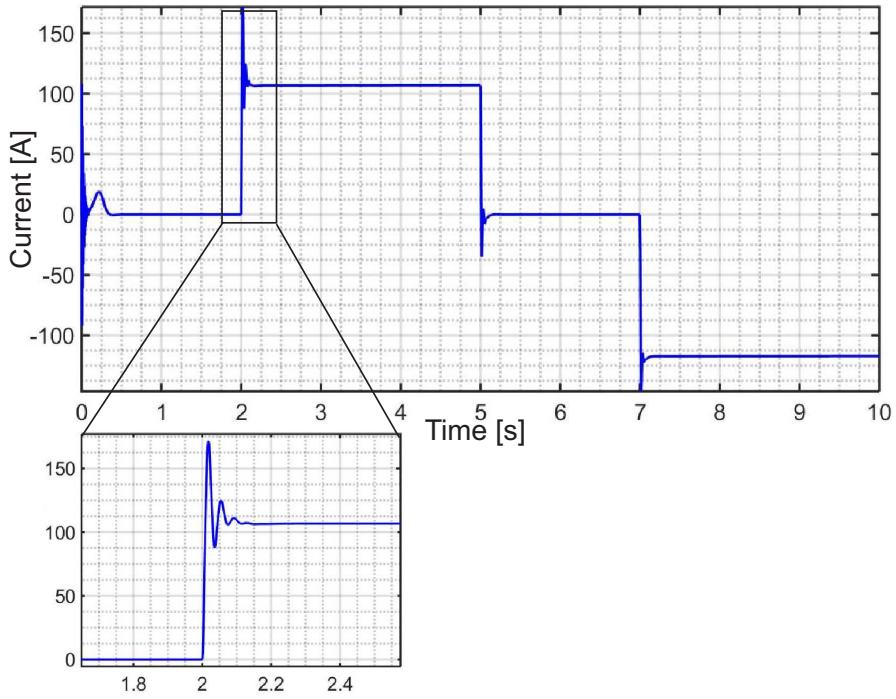

Figure 3.21: Source current during charging and discharging [MS16b]

3.3.9 Comparison of simulated powertrain dynamics with simplified and complex DC/DC converter models

In order to investigate the accuracy of the simplified model, its response is compared to that of the complex dynamic model. The DC/DC converter output for both models should be comparable. In order to test this, the parameters of the power management controller (which will be detailed in the later sections) are manually tuned. From the current variations at the sources, an oscillatory behavior at certain points of time can be noted. The battery current variation for both models is shown in Figure 3.22. Inspite of the similarity in the two response curves, it is evident that the simplified model is unable to replicate the peak amplitudes of the complex model. The fluctuations in battery current as a result of model simplification can have a negative impact on the battery life. A similar conclusion can be drawn from the current variations of fuel cell and supercapacitor current as shown in Figures 3.23, 3.24. The comparison of SoCs of battery and supercapacitor is shown Figure 3.25. The supercapacitor SoC variation for both models is quite similar. Battery SoC variation however shows a marked difference between the two models.

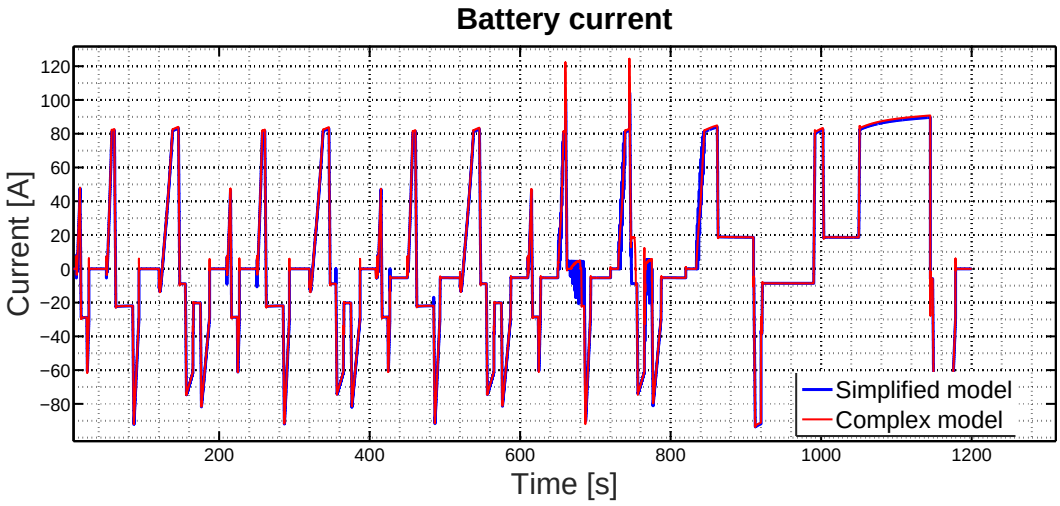

Figure 3.22: Comparison of battery current for both models

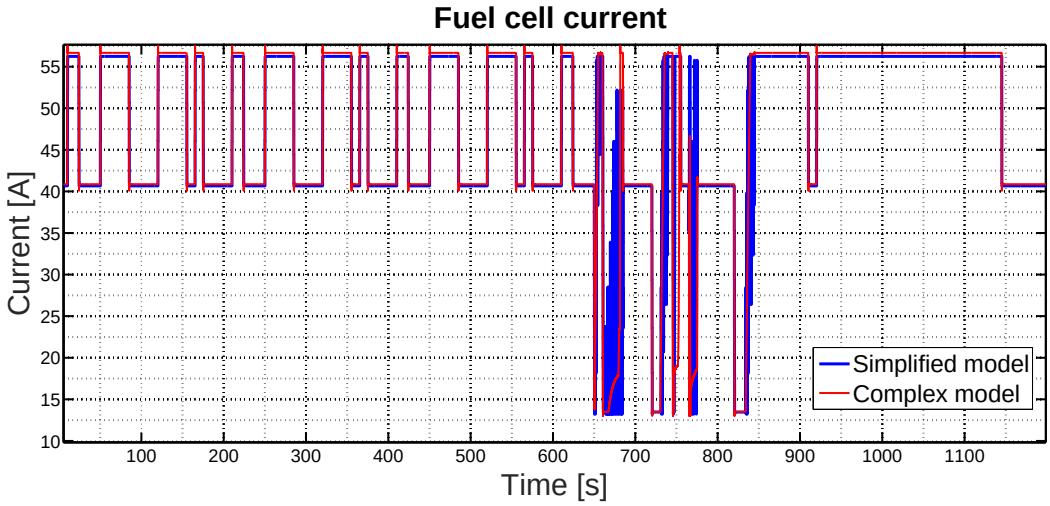

Figure 3.23: Comparison of fuel cell current for both models

3.4 Emulation of powertrain components

Although modeling and simulation are useful for gaining detailed understanding of system dynamics and behavior, experiments are important for investigating the applicability by validation of these models. According to [TDH+04], validation refers to precision at which the model represents the physical world whereas validation experiments are performed to produce data for model validation. For instance, in [VCP16], experiments are performed with the help of a 1:1 scale laboratory-based dynamic set-up; in [CV14], first, experiments are conducted on individual units in stationary conditions to evaluate their behavior at constant electric parameters, then their performance under dynamic operations with real driving cycles is evaluated.

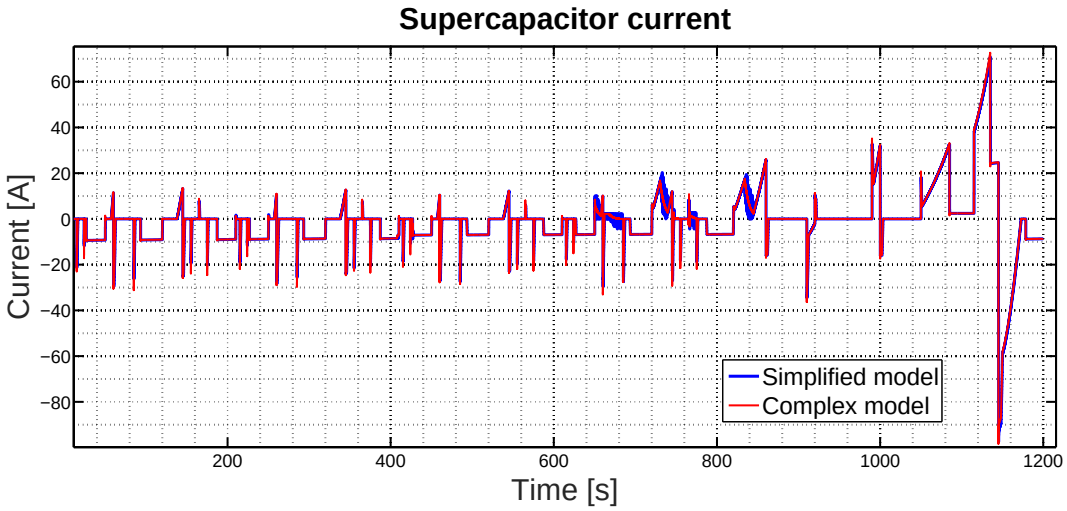

Figure 3.24: Comparison of supercapacitor current for both models

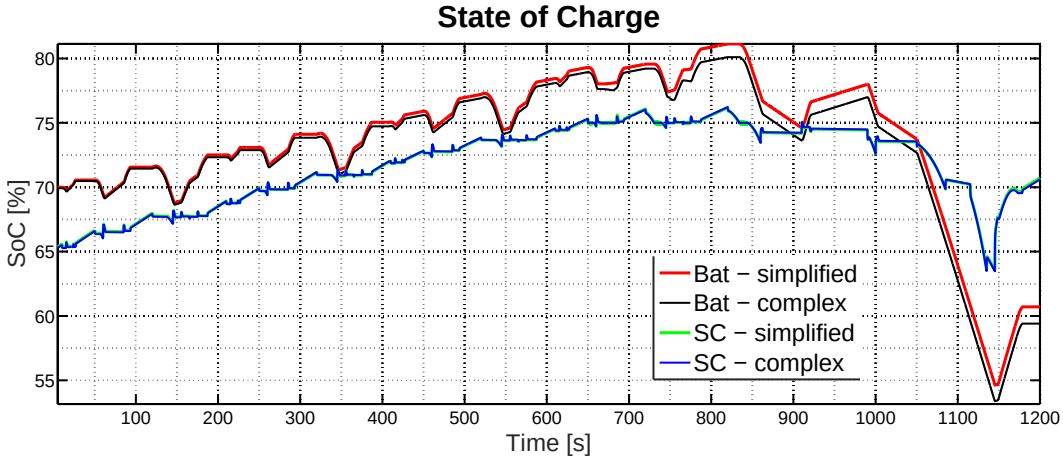

Figure 3.25: Comparison of SoC for both models

Instead of performing experiments with real powertrain components, in this work, a comparison with experimentally determined parameters from real components is considered along with a brief introduction of a concept known as emulation. To carry out power management and control of an analog subsystem integrated with a digital subsystem [CPP+03], emulation of component dynamics have been discussed in literature. According to [Mar], emulation is based on controllable powertrain components which can be used as a replacement for real components. This solves the problems posed by classical set-ups namely: high cost, deterioration/damage risks, large energy and fuel consumption, etc.

Programmable power source has been used to emulate fuel cell in [GBBM11, FPSAS08], whereas in [PABP05, GBS+09, MPV+09], a power electronic converter is used to

emulate fuel cell dynamics. Along with a programmable power source, an additional electronic load is added in [GBBM11] to emulate a supercapacitor. Power source-sink combination has also been used to emulate battery dynamics in [CPP+03, Gmb15]. According to [Gmb15], not only batteries and supercapacitors, but also bi-directional DC/DC converters can be emulated using source-sink combination. In [RC08], emulation of load is considered using voltage source inverter (VSI). The VSI emulates a three phase induction motor connected to grid. Thus along with power sources and storage components, load emulation using dynamically controllable source-sink [RC08], to ensure bi-directional power exchange can also be considered.

As stated in [CPP+03, Gmb15], the problem encountered while using real batteries for experimental purposes is that, the discharge and charge history affects the total charge level at each cycle. Various battery models have been proposed to consider these aging effects. However, in the absence of an aging model, an emulator set-up can be used to realize battery dynamics. Similarly using real fuel cells, which are expensive components, can lead to an increase in damage risks [PABP05, GBS+09]. Thus a compact and easily replaceable emulator set-up is useful when powertrain models and control strategies are to be experimentally tested. The process of testing either real powertrain components or a scaled down version of real components in combination with software models is termed as Hardware-in-the-Loop (HiL) simulation/emulation [PABP05].

3.4.1 Powertrain configuration with emulated components

At the Chair of Dynamics and Control (University of Duisburg-Essen), a fuel cell-supercapacitor based Hardware-in-the-Loop (HiL) test rig was built [ÖWMS13]. It was later modified and generalized for the emulation of different powertrains for example hybrid hydraulic powertrains and wind energy conversion systems [MÖS14, LMMS13] along with hybrid electric powertrains. In this work, a further generalization is considered by replacing all the real powertrain components by emulated components. The experimental set-up is shown in Figure 3.26 and is explained in Figure 3.27. On the left side is the model layer comprising of the configuration shown in Figure 3.3. This simulation model of HEV along with the supervisory controller are compiled into a real time interface that enables communication with the emulation layer. On the right side is the emulation layer comprising of real hardware components. Here, the simulated models of fuel cell and DC/DC converter can be considered as a single unit and the corresponding hardware component- controllable power source $q1$, can be used. Similarly, for battery and supercapacitor, source-sink combination $q2 - s2$ and source-sink combination $q3 - s3$ can be used. Corresponding to the backward simulated part, the power demand or load can be emulated by another source-sink combination $q4 - s4$.

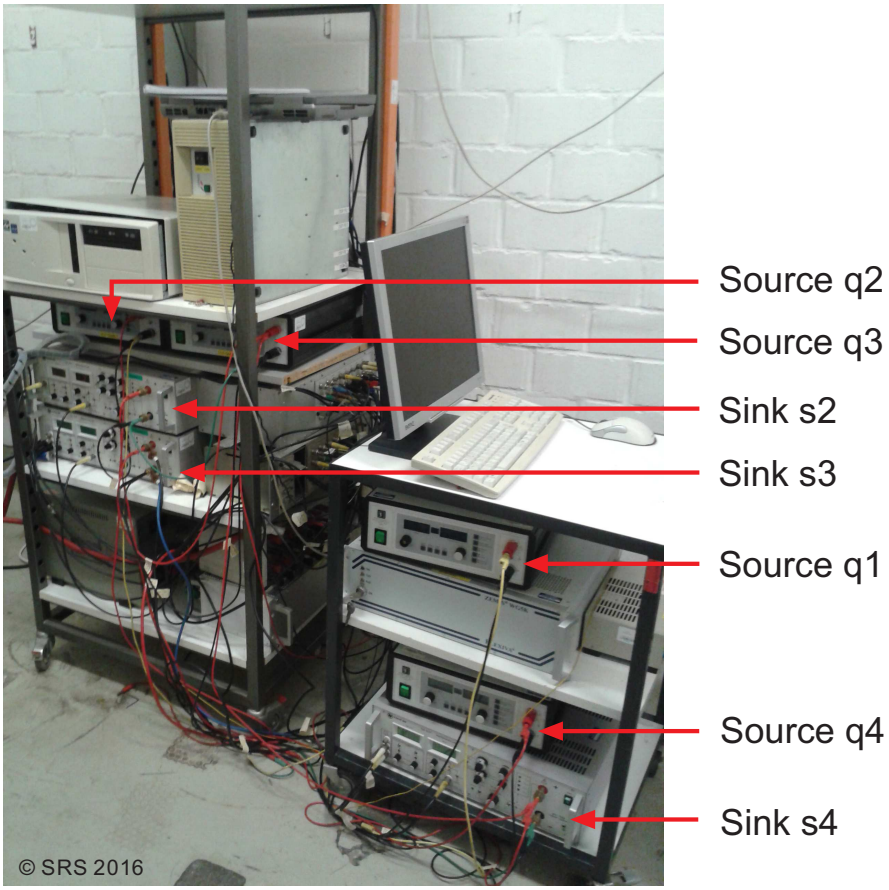

Figure 3.26: Emulation experimental set-up

3.4.2 Comparison of simulation and emulation results

In order to test the capability of the source-sink combinations in replicating powertrain dynamics, as an initial step, only the backward part of the HEV model is emulated. The simulated are emulated power demand are compared. The performed test is explained in Figure 3.28. The source-sink combination $q_4 - s_4$ is checked for emulation of both positive and negative power demand. Here, demand is the load current from the backward part of the powertrain. Its value is positive when the HEV is accelerating or driving at constant velocity and negative when the HEV is braking. During the positive half, the power source q is expected to supply the demand to the power sink s_4. A constant current value is set at q and the simulated demand is realized by s_4. This is the motor action. During the negative half, the generator action is realized by q_4 as it recuperates energy back to the s. Here, a constant current is set at the s. The result of this test is shown in Figure 3.29. It can be noted from the figure that the q_4-s_4 combination is capable of emulating the motor/generator dynamics. During the positive half of the load cycle, current is drawn by the sink s_4 (motor mode) and in the negative half of the load cycle,

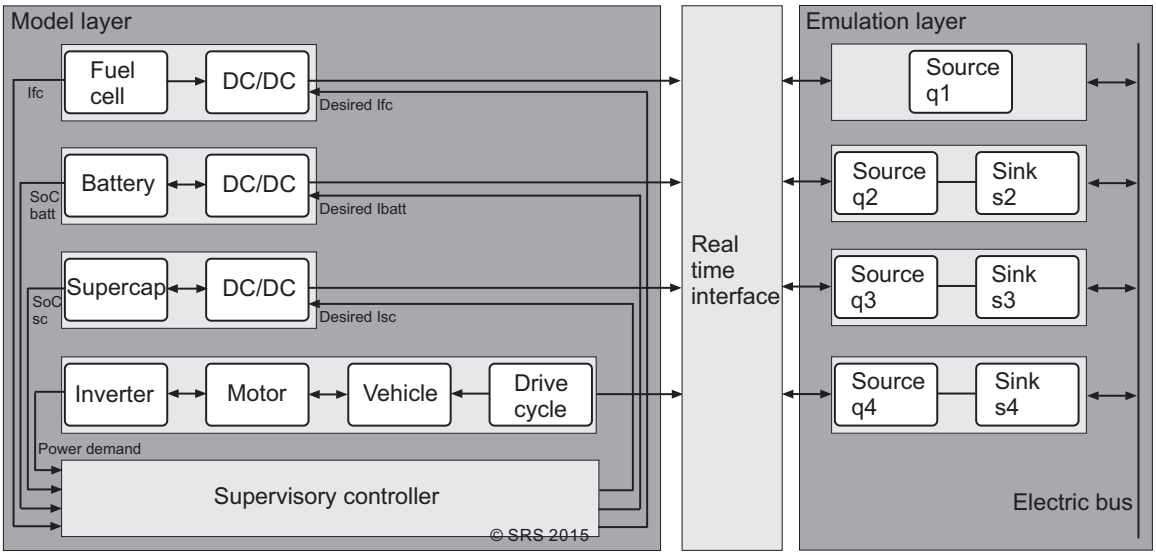

Figure 3.27: Emulation hardware configuration

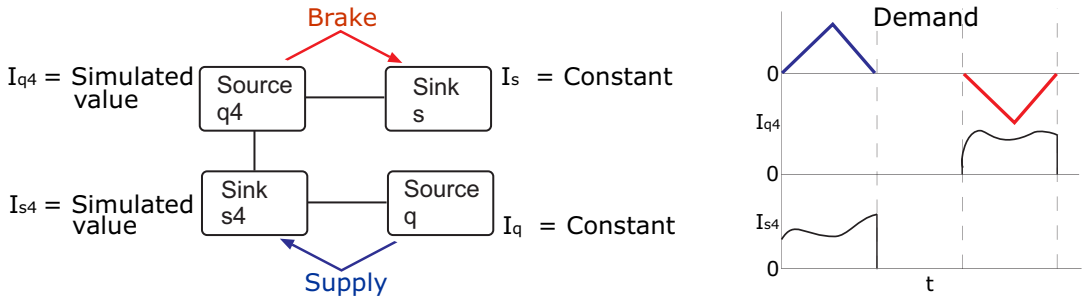

Figure 3.28: Emulation of motor/generator behavior [MS16b]

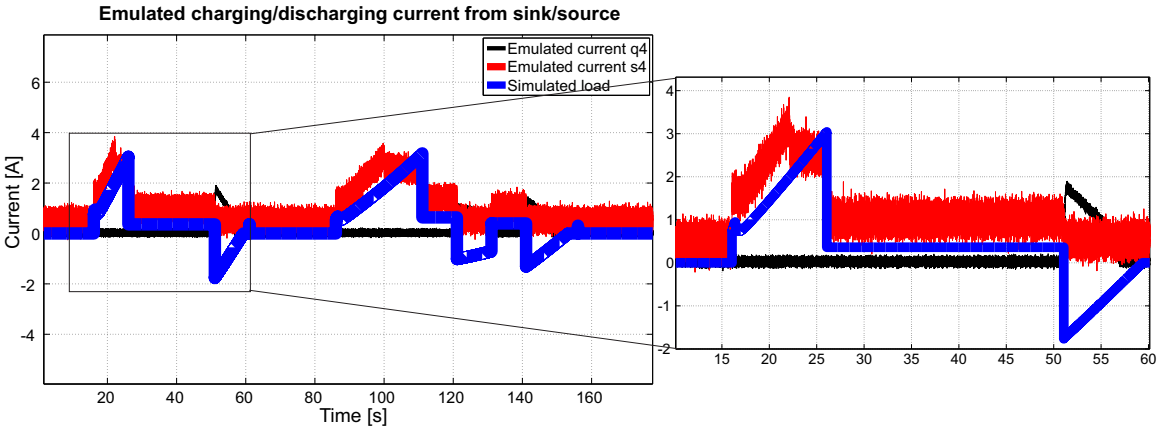

Figure 3.29: Simulated and emulated load current [MS16b]

power is supplied by the source q_4 (generator mode). This initial test is important

to check the ability of power source-sink combinations in emulating not just the motor/generator dynamics, but also battery and supercapacitor. The constant current supplied by q in the positive half will be replaced by supply from each/either of the sources as defined by power management. The constant current demanded by s in the negative half will be replaced by the demand from each/either of the storage components.

4 Power management and optimization

This chapter is published in the form of scientific papers [MS16b],[MS15a]. As the vehicle considered is a hybrid vehicle and involves multiple sources of power, a supervisory power management control strategy is needed to determine the power flows along single power flow paths in order to satisfy various objectives while satisfying the power demand at the same time [GS07]. Some of the key goals according to [BGT10] are: maximum fuel economy, minimum emissions, minimum system cost, and good driving performance. Due to increasing environmental issues and fast depletion of fossil fuels, the control of hybrid vehicles in terms of fuel consumption has become a global issue. According to [BDGB10], the power management strategy should also keep the state of charge of energy buffer/buffers used within reasonable bounds, while reducing fuel consumption. In this chapter, an introduction on different power management optimization strategies with focus on rule-based power management is given. Details of the power management control strategy developed in this work and parameter optimization strategy considered is given followed by simulation results.

4.1 Introduction

The need for the development of online power management strategies applicable to real-time hybrid powertrain systems is an important issue in the transportation sector. A power management strategy alone does not necessarily ensure optimal power distribution amongst the drive train components. Thus optimization of power management is another task which needs to be considered in terms of multiple objectives.

4.1.1 Classification and comparison of power management strategies

In order to select a suitable power management strategy, it is important to compare existing methods and related advantages and disadvantages. An evaluation of their performance and applications makes it possible to choose an appropriate power management optimization approach for this work. According to [GS07], two kinds of classification can be made: first, based on knowledge of future situations, where, non-causal controllers require knowledge of the future i.e. a drive cycle and causal controllers do not need a priori knowledge of future driving profiles; second based on optimality, like heuristic, optimal, and sub-optimal controllers. Within these three types, some can be causal and others non-causal. They are listed in [BGT10, Sal07] and in Figure 4.1.

Rule-based strategies are generally designed based on heuristics, human expertise, or mathematical models and do not require a prior knowledge of the drive cycle

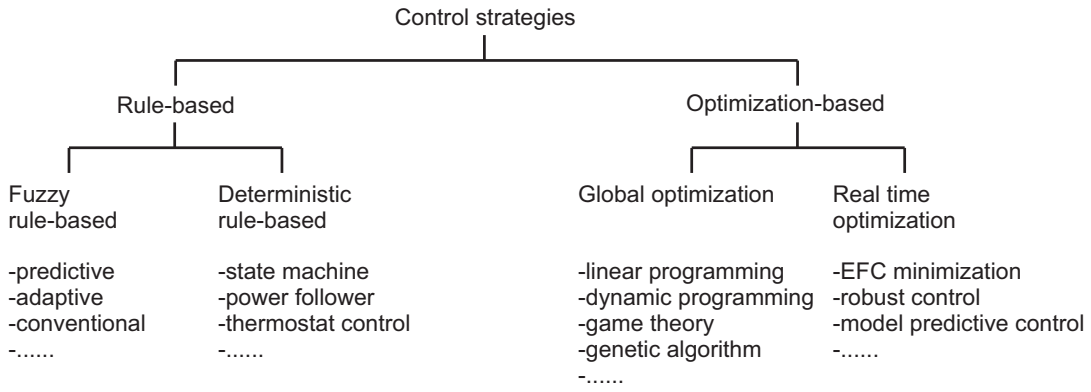

Figure 4.1: Classification of power management strategies

[BGT10]. These strategies are less complex than the other types and can be implemented online and in real-time. Their major drawback is that they are not optimal. The alternatives to rule-based strategies are detailed in [GS07] and briefly described in the following text.

Dynamic programming (DP) is a commonly used global optimization method. It can generate optimal solutions over a given time period. Dynamic programming requires griding of the state and time variables and suffers from long computation effort, due to relatively large grid density required. If the grid density is not high then it can lead to inaccurate results. Moreover, DP is non-causal and not real-time applicable. In order to reduce the computational effort, approaches based on minimization principle such as equivalent consumption minimization strategies (ECMS) are considered. Here, the optimization problem can be reduced to evaluation of an equivalence factor which is assumed to be constant for every type of driving condition in the simplest case.

For real-time applicability, knowledge about future driving conditions is necessary. The complete driving mission can be known beforehand for example, in public vehicles that drive along fixed routes or vehicles that have access to GPS navigation systems, etc. Based on this information, it is possible to estimate future driving conditions. Once future is known, DP can be applied and combined with model predictive control (MPC) which has been used in [KKDJ$^+$05].

However, instead of using MPC and DP if a single strategy such as ECMS is to be used then the problem of uncertainty about future is transferred to the correct approximation of equivalence factor. Unlike MPC that requires estimation of power demand as a function of time on a prediction horizon of particular duration, here, determination of only one parameter i.e the equivalence factor is considered. For estimation of this factor, three approaches can be considered based on the knowledge used: only past information, both past and present, and using all three-past, present, and future. In cases where only past is considered, concepts of pattern recognition

[JJPL02], and pre-calculation of offline generated values for a set of representative driving patterns [LJPML04] are used.

Optimization in hybrid vehicles often involves multi-objectives which might be in conflict with one another. The other category of global, offline optimization techniques is called genetic algorithm (GA). These optimization algorithms are based on biological evolution theory. The genes that characterize individuals are varied through typical biological processes: selection, mutation, and crossover. For solving multi-objective optimization problems, multi-objective genetic algorithms (MOGA) are considered suitable where non-dominated sorting genetic algorithm II (NSGA II) [DPAM02] has been considered in [ZCMM09, BLM$^+$10, BMFF11] for optimization in the presence of multiple and conflicting goals.

The last method, which is a relatively simpler technique, described in [GS07] as time-invariant feedback controller consists of storing the control algorithms in look-up tables (LUTs). The control variable/variables are functions of current driving conditions (like power demand, velocity) and state variables (like SoCs of storage elements). Thereby, follows the concept of combining rule-based strategies with optimal control strategies like GA and ECMS [MF08], GA and DP [SRA11], or with NSGA II [BLM$^+$10], etc. Thus, the advantages of rule-based strategies namely, relatively simpler structure and low computational effort required, can be utilized for carrying out online power management. In order to optimize rule-based strategies, they can be combined with global and multi-objective optimization algorithms. They can also be combined with prediction and real-time control strategies to provide solutions where no pre-defined drive cycle is given. From the concept of embedded-online optimization by using offline algorithms [Mar], it is clear that the embedding of optimization results from a decoupled offline process to an online power management controller is possible. As shown in [Mar], this makes it suitable for experimental applications where computational effort plays an important role.

4.1.2 Concept of power management with embedded optimization

The developed approach in this work comprises of a supervisory controller based on rules designed for a particular drive cycle. The optimization of controller parameters is carried out as a decoupled offline process, results from which are later embedded online. The optimization algorithm takes into account the fuel consumption of the primary source, the SoC deviation of two storage components, and lifetime conservation of components. This power management optimization is implemented on the considered powertrain configuration (detailed in Chapter 3) with three power sources. The developed concept is depicted in Figure 4.2.

Here, the two HEV models considered: one for the online part and other for offline part, differ in their DC/DC converter dynamics. As discussed in Chapter 3, for the sake of simplicity, the detailed dynamics of DC/DC converters are omitted in

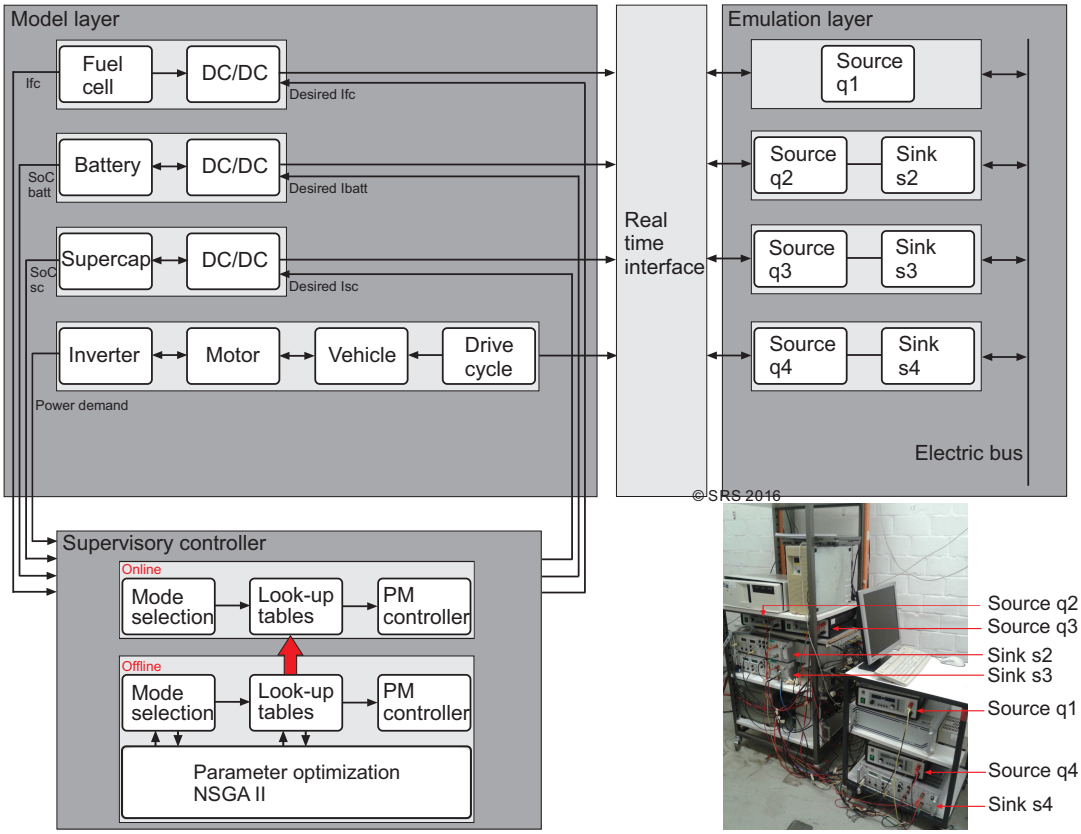

Figure 4.2: Power management optimization concept [MS16b]

the HEV model considered for the optimization loop. As shown in Figure 4.2, the values of battery and supercapacitor SoCs from the forward part of the powertrain, along with the power demand values from the backward part of the powertrain are sent to the mode selection block of the supervisory controller. This block contains IF-THEN rules based on the SoC values and demand. The rule/mode selected corresponds to certain values in the look-up table (LUT) block. These values in the look-up table are used to tune the power management (PM) controller. The controller output is in the form of desired DC/DC converter currents. The LUT block of the supervisory controller contains optimized parameters. These optimized parameters are generated as a result of a separate offline process, where, a multi-objective genetic algorithm (NSGA II) is used. The detailed working of each of the supervisory controller blocks [MS15a] [MS16b] is briefly described in the sequel.

Thus, in this new developed concept, multiple facets of HEV control can be tackled at the same time. Judicious distribution of power between the three sources to ensure proper utilization of each source is considered. This is done by a suitable choice of optimization parameters that ensures that

- the required load demand is satisfied at all times,

- the rate of change of battery and fuel cell current are limited to minimize aging effects,
- the battery current is bounded and the remaining, more dynamic peaks are taken over by the supercapacitor,
- the fuel cell is operated near its optimal range,
- the battery and supercapacitor are never fully charged or fully discharged,
- the fuel cell delivers maximum power when the SoCs of both battery and supercapacitor are too low, and
- the bus voltage is held constant to a reference value.

The goal is to integrate optimized parameters that tune the PM controller such that the above criteria are fulfilled. This approach is designed for an assumed drive cycle. If the drive cycle is changed, the designing of modes have to be done accordingly and new optimal controller parameters will be obtained. The advantage of the developed approach lies in its adaptability. Adaptability here includes the capability to modify/extend it to cases where the drive cycle is not known. The decoupling of the optimization process enables the use of sophisticated algorithms like multi-objective, global techniques. Only the results are embedded online, thereby reducing the computational effort. The controller also takes into account the advantage of battery-supercapacitor combination and allows the supercapacitor to take over the more dynamic variations in power thereby extending battery life.

4.2 Details of supervisory controller

This section describes the design and working details of the supervisory controller block in Figure 4.2. Parts from this section are based on the text and material from [MS15a][MS16b]. Further details are given in [Rau15]. The hierarchical control concept developed in this work consists of three blocks: the mode selection block, the look-up tables (LUT) block, and the power management (PM) controller block. The load is a predefined drive cycle from which three different driving modes can be defined: acceleration and constant velocity (positive load current direction), deceleration (negative load current direction), and standstill (zero load current). The sub parts of the hierarchical control concept are detailed in the following subsections.

4.2.1 Mode selection block

The mode selection block takes three inputs from the powertrain model as shown in Figure 4.3. The first input is the load current direction I_{board} for the purpose of distinguishing between the three different driving modes namely, acceleration and constant velocity, deceleration, and standstill. The second and third inputs are the battery and supercapacitor SoC (SoC_b and SoC_{sc}) to decide when the battery/supercapacitor or both battery and supercapacitor have to be charged/discharged and also when the fuel cell needs to provide maximum power. The output of the mode selection denotes a specific value. For example, when the vehicle is accelerating, and both the battery and supercapacitor SoCs have fallen below a certain pre-defined minimum value, the fuel cell is expected to provide maximum power so as to satisfy power demand and also charge the storage elements. This corresponds to the first case in the mode selection block and the corresponding value one is sent to the look-up table (LUT) block. When the vehicle velocity is positive, while charging and discharging of the battery and supercapacitor, boundary values of maximum and minimum SoC are defined as B_{max},B_{min} and SC_{max},SC_{min}. There is a possibility to determine the optimal boundary values and therefore these parameters can also be considered for the optimization process. When the vehicle is in deceleration mode, and if the fuel cell still continues to provide power then the excess power is used to charge the supercapacitor. Supercapacitor is given a priority here as according to [KS14], the dynamics of the powertrain depend mostly on the more dynamic element. In that case, the lower and upper optimal SoC limit of supercapacitor ($SoCsc_{opt}$) for the case of deceleration and standstill must be determined. If after mode standstill, the HEV needs to accelerate immediately, then the highest possible reserve should be available from the storage system. If the HEV needs to brake soon after standstill, then the upper limit of supercapacitor SoC needs to be kept in mind. The related relations are expressed by parameters according to the algorithms graphically expressed in Figure 4.3.

4.2.2 Look-up tables LUT block

This block consists of four look-up tables for the mode dependent controller parameters: fuel cell current input, power split between battery and supercapacitor, maximum battery current, and minimum battery current. There are also LUTs for mode independent parameters that is, boundaries and initial conditions. These parameters can be optimized by specifying the boundaries of variation. All parameters are listed in Tables 4.1 and 4.2. These parameters can be optimized by specifying the boundaries of variation as given in the tables. The outputs from this block are: the reference fuel cell current depending on its optimal working current value and maximum allowed value given by I_{FCin}; the power sharing between battery and supercapacitor decided by $Powersplit$; the battery current, which is limited by

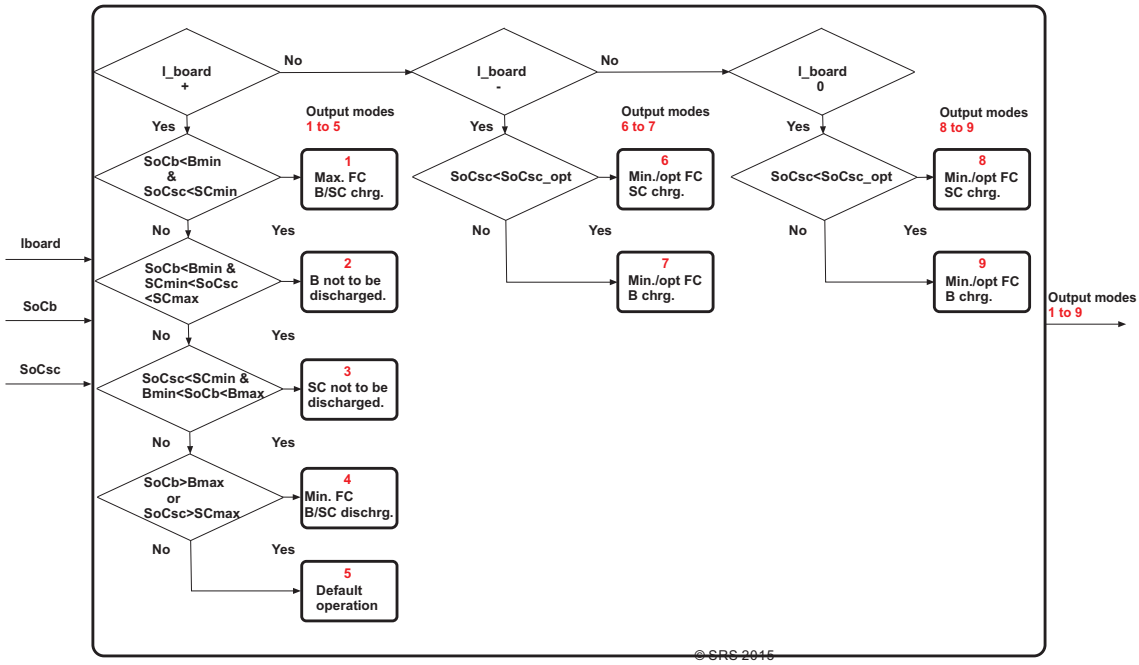

Figure 4.3: Details of mode selection block [MS16b]

$I_{Bat,max}$, $I_{Bat,min}$; and the dynamics of fuel cell and battery, which are restricted by $Ratelimit_{FC}$, $Ratelimit_{Bat}$. Thus, the aging problems faced by batteries and fuel cells are minimized by the choice of parameters. These parameters correspond to optimal fuel consumption and are pre-loaded as a result of a separate offline process. As shown in Figure 4.4, the input to the LUT block from the mode selection block is a number and it denotes a particular row in each of the four LUTs. For example, when the input is 1, the corresponding values of 1 from all the LUTs are sent to the PM controller.

Table 4.1: Mode dependent parameters

Modes		**Tasks**	I_{FCin}		$Powersplit$		I_{bmax}		I_{bmin}	
			LL	**UL**	**LL**	**UL**	**LL**	**UL**	**LL**	**UL**
1.	P > 0 **Drive**	Bat+SC:charge	8	13.5	0	1.5	-0.5	0.5	-30	-5
2.		Bat:no discharge	4	12	0	1.5	-2	0	-30	-5
3.		SC:no discharge	4	12	0	2	2	30	0	2
4.		Bat+SC:discharge	1	8	0	1.5	5	30	-0.5	0.5
5.		Standard	5	12	0.3	1.5	5	30	-30	-5
6.	P < 0	SC:charge	1	8	0	0.5	5	30	-1	0
7.	**Brake**	Bat:charge	1	8	0.5	2.5	-1	0	-30	-5
8.	P = 0	SC:charge	1	8	0	0.5	5	30	-1	0
9.	**Stop**	Bat:charge	1	8	0.5	2.5	-1	0	-30	-5

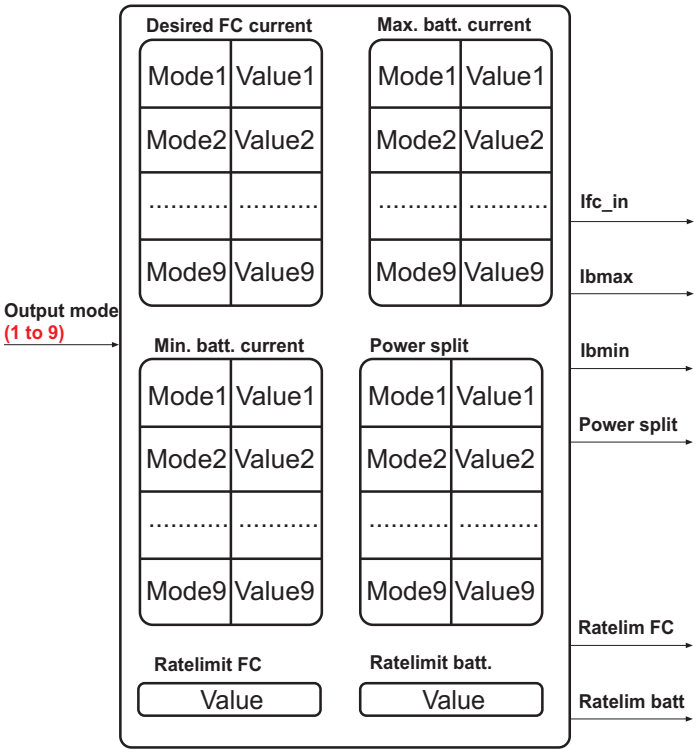

Figure 4.4: Details of look-up table block [MS16b]

4.2.3 PM controller block

Once the optimal values of I_{fcin}, $Powersplit$, $I_{Bat,max}$, $I_{Bat,min}$, $Ratelimit_{FC}$, and $Ratelimit_{Bat}$ have been pre-loaded in the LUT block, they can be used for tuning the PM controller online. As detailed in Figure 4.5, the fuel cell current I_{fcin} is restricted by a rate limiter before sending it to the DC/DC converter as I_{fc}. The rate limiter is used to limit the first derivative (rate) of the signal passing through it, such that, the output does not change faster than a specified limit [Mat16]. The load current I_{board} is divided into fuel cell current I_{fc} and the difference I_{diff}. Here, I_{diff} is multiplied by the power split value from the LUT. This pre-optimized value of power split influences the charging/discharging dynamics of battery and supercapacitor. An example of the influence of power split values on the distribution of power between battery and supercapacitor is given in Figure 4.6. Here values between 0 and 1 denote power sharing between battery and supercapacitor to satisfy the demand. Similarly, values above 1 and below 0 can be used to indicate power flow from battery to supercapacitor and vice-versa. A suitable choice of powersplit values can be made to accommodate all the possible charging and discharging options of the two storage elements. The actual value of the multiplied variables $I_{diff} * Powersplit$ is sent to a rate limiter that determines the rising and falling slopes of the current. The output of rate limiter is sent to a dynamic saturation block that determines

Table 4.2: Mode independent parameters

Parameters	**LL**	**UL**
SoC SC min [%]	35	55
SoC SC max [%]	65	78
SoC batt min[%]	35	45
SoC batt max[%]	70	90
Ratelimit FC [A/s]	0.5	10
Ratelimit batt [A/s]	1	40
SoC SC brake [%]	55	75
SoC SC stop [%]	65	78
SoC SC initial [%]	50	75
SoC batt initial [%]	55	90

the upper and lower limits based on battery minimum and maximum current values (I_{bmin} and I_{bmax}) from the LUT. Both rate limiter and dynamic saturation are time-dependent components. The output of the saturation block is the battery current I_b as shown by the green dotted region in Figure 4.6. It is sent as DC/DC converter output. This battery current subtracted from I_{diff} gives the current that needs to be supplied by the supercapacitor as shown by the blue dotted region in Figure 4.6. This is the dynamic part of current which needs to be supplied by supercapacitor which possesses much higher charging/discharging efficiency than battery. The outputs from this block, that is the desired currents to be drawn from the three sources are sent to the DC/DC converters as shown in Figure 4.2. The dynamic behavior of the DC/DC converter can be described by

$$\mathbf{x} = \begin{bmatrix} I_{L1} \\ I_{L2} \\ U_{Cl} \\ U_{C2} \end{bmatrix} \ , \ \mathbf{u} = \begin{bmatrix} U_{in} \\ I_{out} \end{bmatrix} \ , \ \mathbf{y} = \mathbf{x}, \tag{4.1}$$

where currents over inductors are denoted by I_{L1} and I_{L2} and voltages over capacitances by U_{Cl} and U_{C2}. The inputs to the system are the desired current from PM controller I_{out} and voltage from fuel cell, battery, or supercapacitor U_{in}. The capacitor voltage U_{C2} denotes the bus voltage which needs to be held constant and I_{L1} the inductor current required to be drawn from the sources. According to [UA07], the DC/DC converter can be internally controlled by a PI-controller with bus voltage as the reference input, and externally, it can be controlled by the PM controller that sends the desired current output signal to the converter.

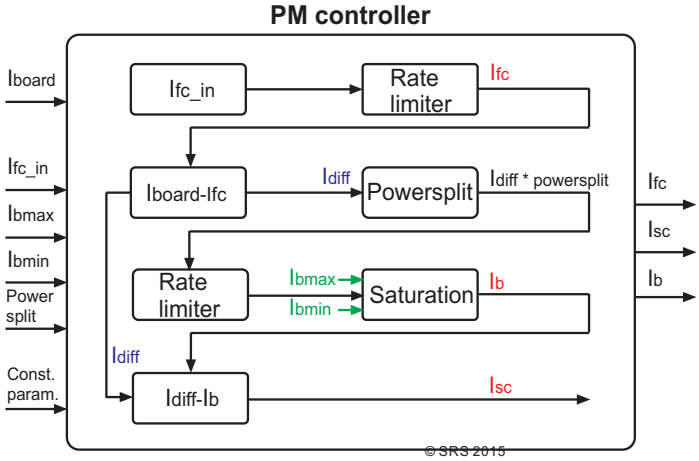

Figure 4.5: Details of PM controller block [MS16b]

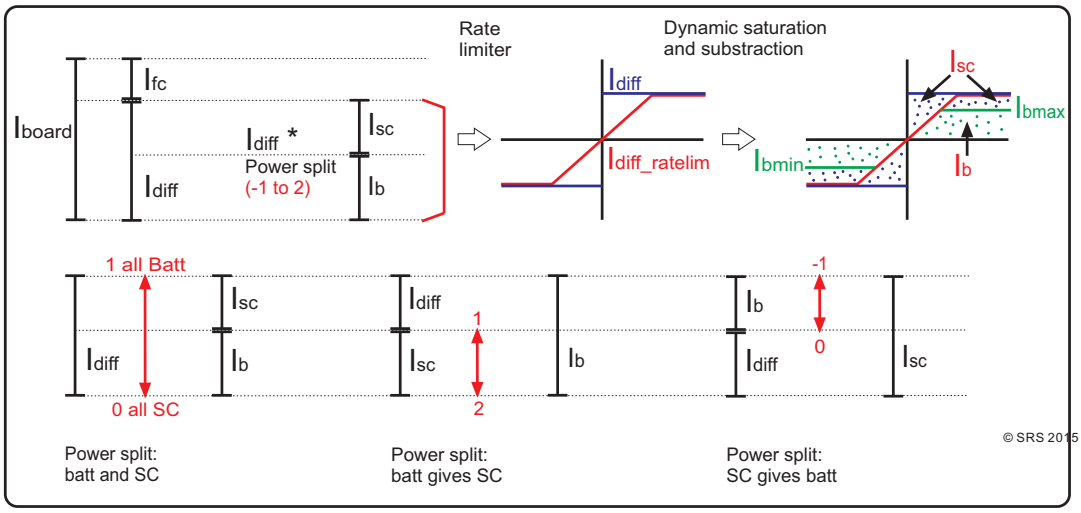

Figure 4.6: Working of PM controller block [MS16b]

4.2.4 Simulation results and discussion

The powertrain dynamics subjected to the NEDC drivecycle with developed power management control concept is discussed in this subsection. The results, based on the dynamic model, concern the verification of the power management control strategy. Here, a set of manually tuned controller parameters (power split, I_{bmin}, I_{bmax}, and I_{fcin}) are used, which are not yet optimized. The task of the three basic control rules [Mar] in controlling the power flows from three different power sources is analyzed in Figures 4.8, 4.7, and 4.10.

The power management strategy is checked for

- whether the required load demand is satisfied at all times,

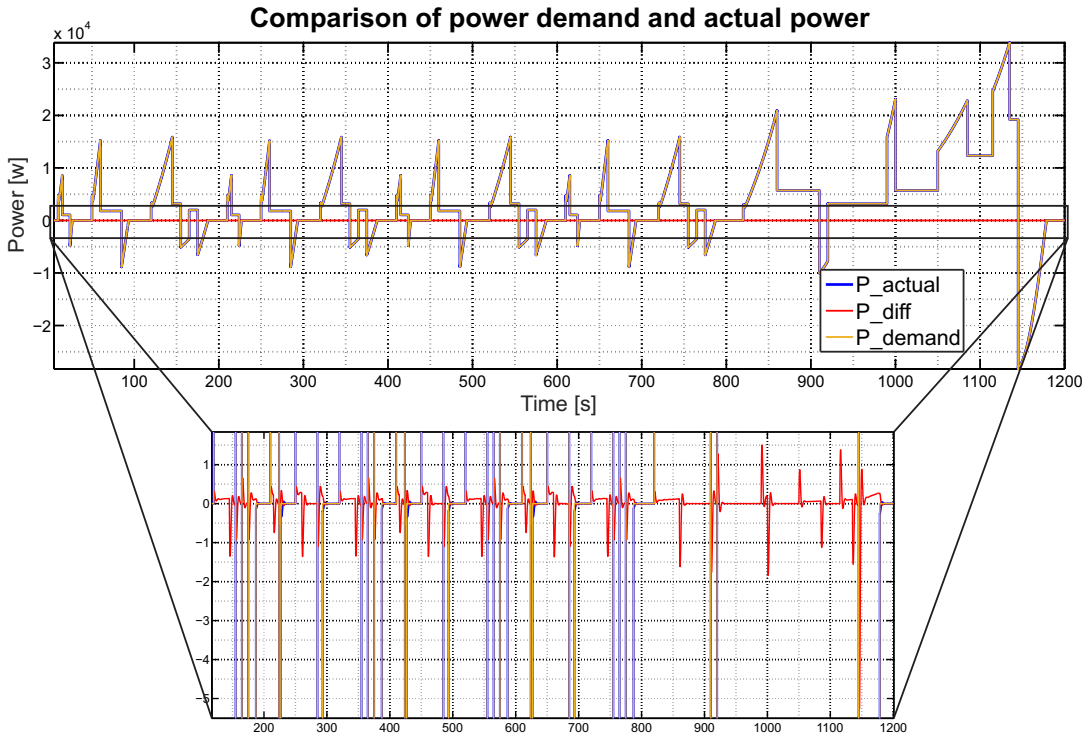

Figure 4.7: Power demand and actual power (realized by numerical simulation)

- the rate of change of battery and fuel cell current are limited,
- the battery current is bounded and the remaining, more dynamic peaks are taken over by the supercapacitor,
- the fuel cell is operated near its optimal range, and
- the battery and supercapacitor are never fully charged or fully discharged.

In Figure 4.7, the total power from the three sources is given. This illustrated power is the actual output power from the sources and it should be same as the power demand resulting from the chosen drive cycle. The error, termed as drivability error can be detected in red. It can be considered negligibly small in this work and is therefore not considered as an optimization goal. From the Figure 4.8, it is clear that, the fuel cell is operated under two position or on/off control and the power sharing between battery and supercapacitor is such that the supercapacitor takes over the more dynamic power fluctuations. The fuel cell is operated at around 4kW which is close to its efficient operating point as calculated in Equation 3.26.

As an example operation of the power management strategy, a zoomed part of Figure 4.8 for the time period $t = 670s$ to $t = 770s$ is shown in Figure 4.9 along with the switching between operation modes for the given drive cycle. As soon as

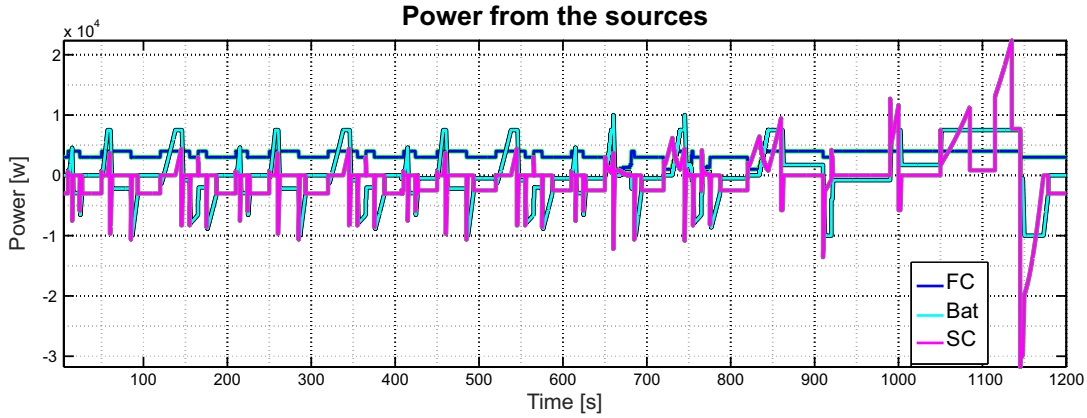

Figure 4.8: Power from the three sources (realized by numerical simulation)

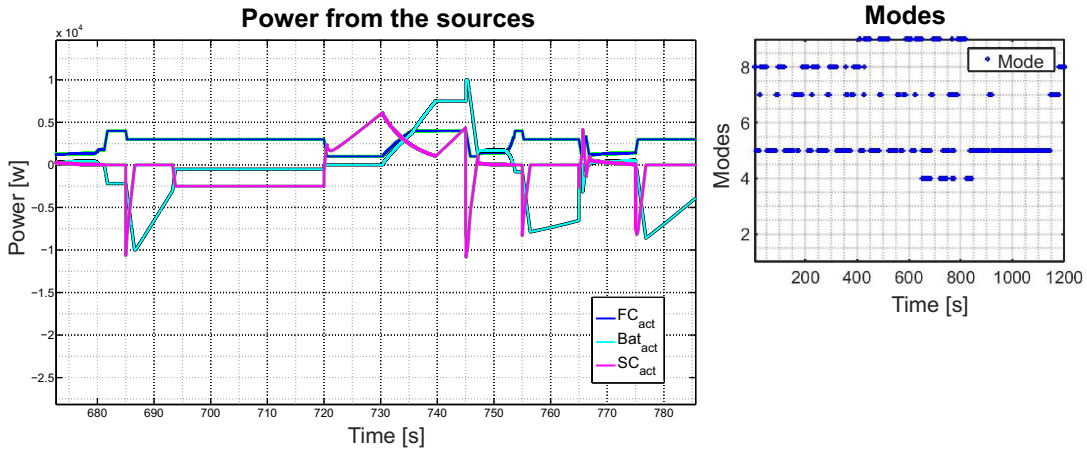

Figure 4.9: Variation between t=670s-770s (realized by numerical simulation)

the supercapacitor is charged till its maximum allowed limit, the power management strategy switches to mode 4 and discharges both battery and supercapacitor. When the supercapacitor is enough discharged, the strategy changes to the standard mode-mode 5. In Figure 4.10, the bus voltage, which should be kept constant is shown. As noted from figure, it almost constant at 500 V with occasional peaks. From the simulation results, the basic working principles of the developed power management strategy can be established. The fulfillment of the demanded power and the rate limitation of the battery and fuel cell can be concluded from the plots.

4.3 Optimization as a decoupled process

This section describes the optimization of all the parameters listed in Tables 4.1 and 4.2. Optimization problems in hybrid vehicles mainly relate to three types

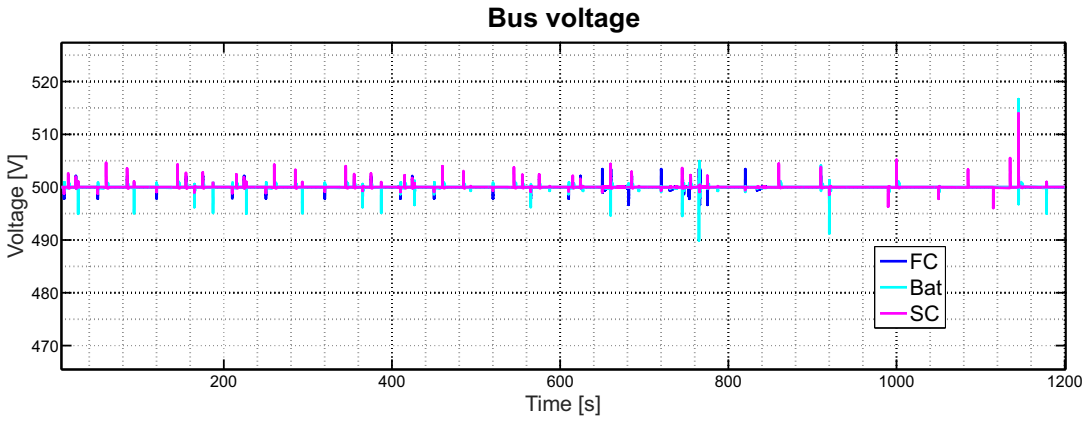

Figure 4.10: Bus voltage (realized by numerical simulation)

[GS07]: structural optimization, which finds the best possible powertrain structure; parametric optimization, where the powertrain structure is considered as fixed and the goal is to find the best set of parameters; control system optimization, which finds the best possible supervisory algorithms. In this work, a parametric optimization is considered for the topology chosen. First, the optimization is carried out at varying supercapacitor sizes for all the controller parameters along with boundary and initial conditions. Then, a reference size for the supercapacitor is chosen and the effect of optimization process is investigated. To sum up, the optimization of supervisory controller described in the previous section is carried out for 2 objectives- fuel consumption and SoC deviation, with 46 parameters- 4 mode dependent for 9 modes, 10 mode independent, and the optimization is carried out for 4 different supercapacitor sizes. The optimized results are based on pre-defined drives cycles, here for the example NEDC drive cycle is used.

In the context of supervisory control strategies, a classification can be made [GS07] namely, heuristic control strategies and optimal control strategies. The advantage of heuristic controllers is their simplicity but due to the tuning effort required to obtain optimum fuel economy, optimal control strategies such as dynamic programming, ECMS, etc. are used. Instead of using an optimal control strategy, which provides a direct optimization of control input, an offline parametric optimization based on Non-Dominated Sorting Genetic Algorithm (NSGA II) is considered. In [MKS13], NSGA II has been implemented on a hybrid hydraulic powertrain system to generate optimal sizes and control parameters corresponding to given objective functions. As described in [MKS13], the algorithm starts by randomly generating an initial population of possible solutions within the search space, keeping the boundaries of variation of each variable in consideration. The objective functions are evaluated. Each individual is assigned to a rank to generate fronts based on non dominated sorting. Next, crowding distance is assigned to the individuals to maintain diversity. In the final steps, selection and assignment of genetic operators such as crossover

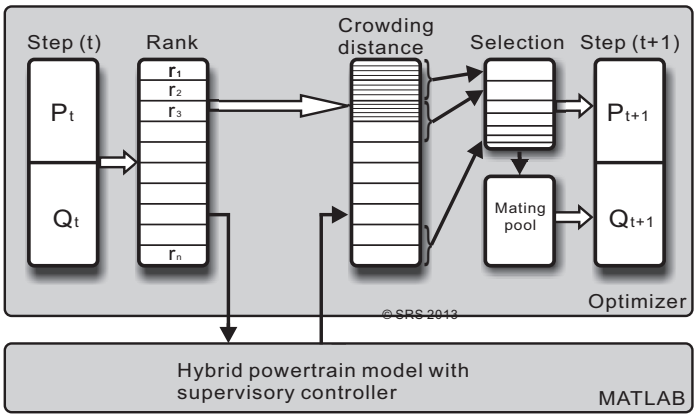

Figure 4.11: NSGA II and model interaction [MKS13]

and mutation are performed to obtain the best parameter variables. Details on adjustment of NSGA II parameter settings such as crossover probability, mutation rate, etc can be found in [Rau15]. One of the reasons for selecting this algorithm is its ability to tackle multi-objectives which might be conflicting in nature which is often the case with hybrid powertrains.

4.3.1 Optimization goals and constraints

The objective function and constraints are defined as given in [GS07]. The minimization of fuel consumption is given by

$$J = \int_0^{t_f} \dot{m}_f(t, u(t))dt \ , \ J \rightarrow min. \ , \tag{4.2}$$

where the performance index is denoted by J and fuel mass consumed over a mission of duration t_f is denoted by $\dot{m}_f$, depending on the system input $u(t)$. The fuel mass consumed $\dot{m}_f$ can also be given by the energy required by the fuel cell for the given drive cycle and represented in terms of fuel cell power P_{FC} as follows

$$J_{FC} = \int_{t_0}^{t_f} P_{FC}(t, u(t))dt \ , \ J_{FC} \rightarrow min. \ . \tag{4.3}$$

The other objective is to minimize the SoC deviation which represents the difference between the initial and final SoC values of both battery SoC_b and supercapacitor SoC_{sc}. Generally, the charge sustenance of the storage elements require small deviations from nominal value of SoC over the drive cycles. The deviation of the two SoCs, ΔSoC_b and ΔSoC_{sc} can be considered as an integral constraint [GS07] by

$$J = \phi(\Delta(SoC_b + SoC_{sc})) + \int_0^{t_f} \dot{m}_f(t, u(t))dt, \tag{4.4}$$

where the penalty term ϕ called the charge-sustaining performance index given as

$$\phi(\Delta SoC_b) = \alpha \left|(SoC_b(t_0) - SoC_b(t_f))\right|, \tag{4.5}$$
$$\phi(\Delta SoC_{sc}) = \beta \left|(SoC_{sc}(t_0) - SoC_{sc}(t_f))\right|, \tag{4.6}$$

with ΔSoC_{sc} and ΔSoC_b as the SoC deviations of supercapacitor and battery at time interval t_0 to t_f.

Some of the other relevant objective functions are

- Maximization of drivability or minimization of the error between the velocity required to be followed and the actual velocity. According to [MÖS14], if the drive cycle is considered as a reference signal, then drivability can be defined as the system's capability to fulfil it. It can be given using the integral absolute error as [MÖS14]

$$P_{driv} = f_1(\int \mid v_{ref} - v_{meas} \mid dt). \tag{4.7}$$

- Minimization of aging of fuel cell and battery. Both fuel cell and battery tend to degrade faster when subject to frequent and large magnitude changes in power. In [MÖS14], a high pass filter and a suitable function f_2 is applied to represent fuel cell aging minimization as an objective for optimization

$$P_{aging} = f_2(P_{FC,filt}(t))), \tag{4.8}$$

  where $P_{FC,filt}(t)$ is the high pass filtered fuel cell power. The main indication of battery age is its charge capacity [SOS+11]. Since the traditional cycles used to evaluate battery aging in laboratories are not same as the real driving conditions, therefore in [SOS+11], the aging effect has been characterized using severity factor σ as

$$\sigma(I, \theta, SoC) = \frac{\gamma(I, \theta, SoC)}{\Gamma} = \frac{\int_0^{EOL} \mid I(t) \mid dt}{\int_0^{EOL} \mid I_{norm}(t) \mid dt}, \tag{4.9}$$

  where $\gamma(I, \theta, SoC)$ is the battery Ah-throughput corresponding to given current I, temperature θ and SoC; Γ is the total Ah-throuput corresponding to the nominal cycle and nominal current I_{norm} and EOL is the end of life.

4.3.2 Simulation results and discussion

In this subsection, HEV dynamics corresponding to optimized controller parameters are analyzed. For the two chosen objectives, namely, minimization of fuel consumption and SoC deviation of both battery and supercapacitor, the results are analyzed in the following manner:

- To investigate the influence of component sizing, the variation of the two objective functions for different supercapacitor sizes is shown in Figure 4.12.
- A supercapacitor size is chosen and convergence of the two conflicting objectives for the chosen supercapacitor is shown in Figure 4.13.
- The preference between the two objectives is varied and its influence on SoC variation is analyzed in Figure 4.15.

To demonstrate (and to learn about) the principal behaviors, four supercapacitor sizes are chosen for comparison: reference, double of reference, half of reference, and one-fourth of reference. The optimization runs for all the supercapacitor sizes can be seen in Figure 4.12. As shown in Figure 4.12b, with double sized supercapacitor, a slight improvement in fuel consumption values is noted (Figure 4.12b2) at the cost of deterioration of ΔSoC values (Figure 4.12b1). However, this does not provide an optimal solution for the total objective function and further iteration steps of the optimization algorithm are required. As shown in Figure 4.12c, with half-sized supercapacitor, a prominent improvement in ΔSoC is noted (Figure 4.12c1). The fuel consumption is not minimized within the shown iteration steps. Finally in Figure 4.12d, with one-fourth supercapacitor, dynamic and fluctuating behavior is noted in both figures 4.12d1 and 4.12d2. Within the shown iteration steps, minimization, particularly of fuel consumption values is not possible. Thus, with such small supercapacitor sizes, the control task is difficult, the overall system might become unstable.

In Figure 4.13, conflicting solutions for the two objective functions for the reference supercapacitor can be seen. This results from the principle contradictions in the task of fuel consumption minimization and SoC sustenance. However, a convergence of the total objective function can be obtained. From Figure 4.13, it can be noted that although minimum values for ΔSoC are obtained, the values chosen for fuel consumption are not necessarily the minimum values. Lower fuel consumption values that did not satisfy minimum ΔSoC, are rejected so a compromising solution for both objectives can be obtained. In the next step, the parameters corresponding to optimized values obtained from NSGA II are integrated in the online power management control strategy. Three supercapacitor sizes: double (denoted in green), half (denoted in blue), one-fourth (denoted in black) are compared to the reference size (denoted in red) to analyze the influence on SoC and on fuel consumption. In Figure 4.14, the SoCs of battery and supercapacitor are shown along with the corresponding fuel cell output power and distinguished for small and large supercapacitors.

Smaller supercapacitors: From the battery SoC, it can be seen that, the battery is gradually charged in the beginning so as to gain reserves for following high demanding part of the drive cycle, due to the insufficient storage capacity of the supercapacitor. Then the battery is discharged till its lowest SoC value. From the

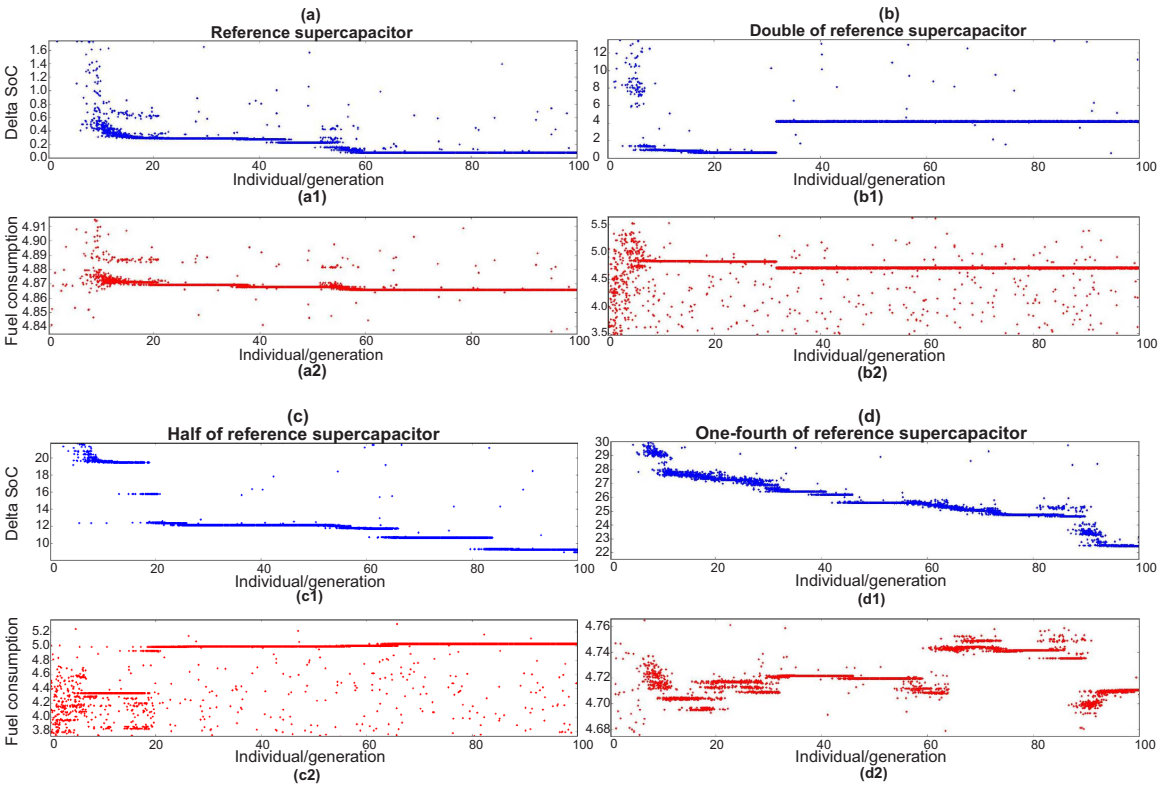

Figure 4.12: Objective function convergence for a) Reference supercapacitor b) Double of reference supercapacitor c) Half of reference supercapacitor d) One-fourth of reference supercapacitor [MS16b]

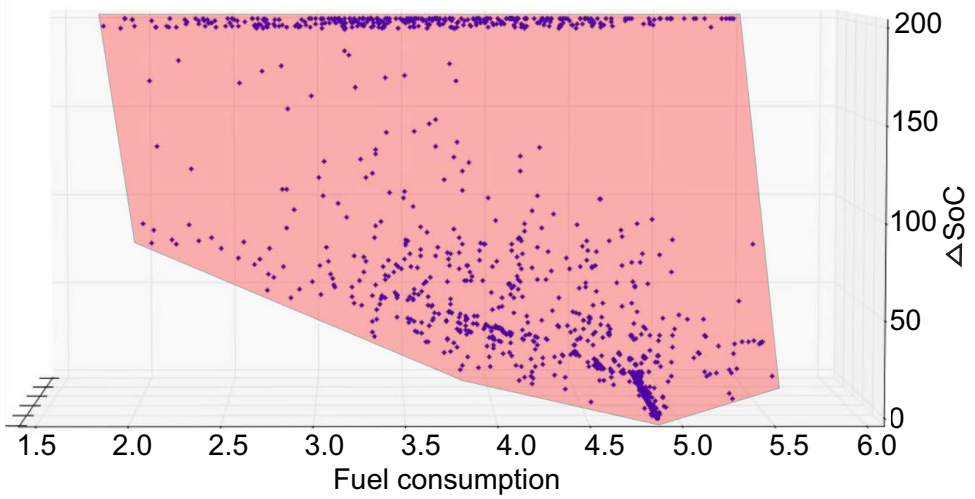

Figure 4.13: Confliction of objectives [MS16b]

supercapacitor SoC, it can be seen that smaller sizes cause more fluctuations. With the one-fourth size, the response is very dynamic. From the fuel cell output power it

can be seen that power supplied by fuel cell is increased for smaller supercapacitors than larger ones. Here also, transients are noted with the smallest supercapacitor.

Larger supercapacitors: When the supercapacitor is doubled, the battery SoC is constant meaning that the battery is not required. In this case, the large supercapacitor has sufficient storage capacity. The supercapacitor SoC curve is flatter and less fluctuating in comparison with smaller supercapacitor SoCs. From the fuel cell output power, it becomes clear that power supplied by fuel cell is also least here. Thus, with the double sized supercapacitor, most desirable performance can be achieved whereas, by using a one-fourth sized supercapacitor undesirable effects may result. These undesirable effects need to be avoided keeping the size and cost of the powertrain in mind. The reference size can be considered as a suitable option. Next, the priority between the two objectives is varied for the reference supercapacitor. For realization of different requirements, the priorities are assigned as given in following three cases:

- Case 1: priority distribution decided by NSGA II (denoted in green).
- Case 2: high priority on fuel consumption and less priority on ΔSoC (denoted in blue).
- Case 3: high priority on fuel consumption with least priority on ΔSoC (denoted in red).

These three cases can be obtained by analyzing the effects of parameter changes during different stages of optimization. In the first case, the parameters correspond to those obtained at the end of optimization. In the second and third cases, the parameters correspond to those obtained in the intermediate stages. In Figure 4.15, the SoC variations of the battery and supercapacitor can be seen along with the corresponding fuel cell power.

Case 1 is the standard case and can be used as a reference for comparison of cases 2 and 3. Case 2 (blue curve): From the battery SoC, it can be seen that, the battery SoC is mostly sustained and discharged only towards the end. The supercapacitor is charged from the fuel cell. By comparing battery ΔSoC with case 1 (green curve), it is observed that ΔSoC in case 1 is lower than in case 2. This is because in case 2, the optimization objective-fuel economy is taken into account but the second objective-battery ΔSoC is sacrificed.

Case 3 (red curve): From the battery SoC, it can be seen that the battery is more depleted than in cases 1 and 2. The supercapacitor is charged from the battery. By comparing battery ΔSoC with cases 1 and 2, it is observed that ΔSoC in both cases 1 and 2 are lower than in case 3.

Thus, when priority is assigned in the order- fuel consumption followed by supercapacitor ΔSoC followed by battery ΔSoC, the battery is more often discharged as

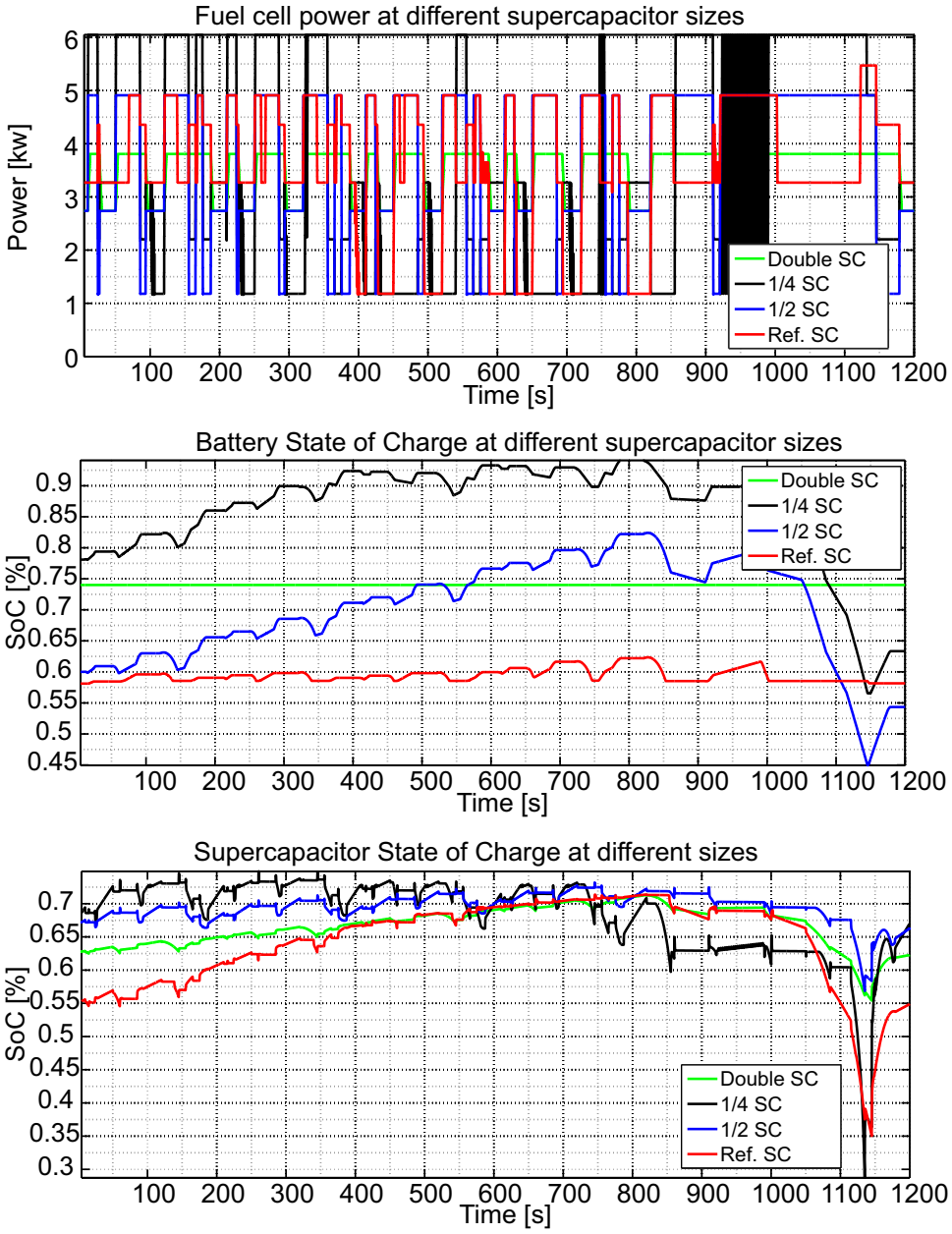

Figure 4.14: Effect of optimization parameters at different supercapacitor sizes (realized by numerical simulation) [MS16b]

shown in the above results. By changing the priority between the objectives, further possibilities can be investigated. But as the objectives are conflicting in nature, a compromise has to be made. In Figure 4.16, the total energy consumption corresponding to: non-optimal power management, optimal power management, and optimal power management at different supercapacitor sizes is shown. Total energy consumption denotes the energy of the fuel cell plus the energy of the battery and

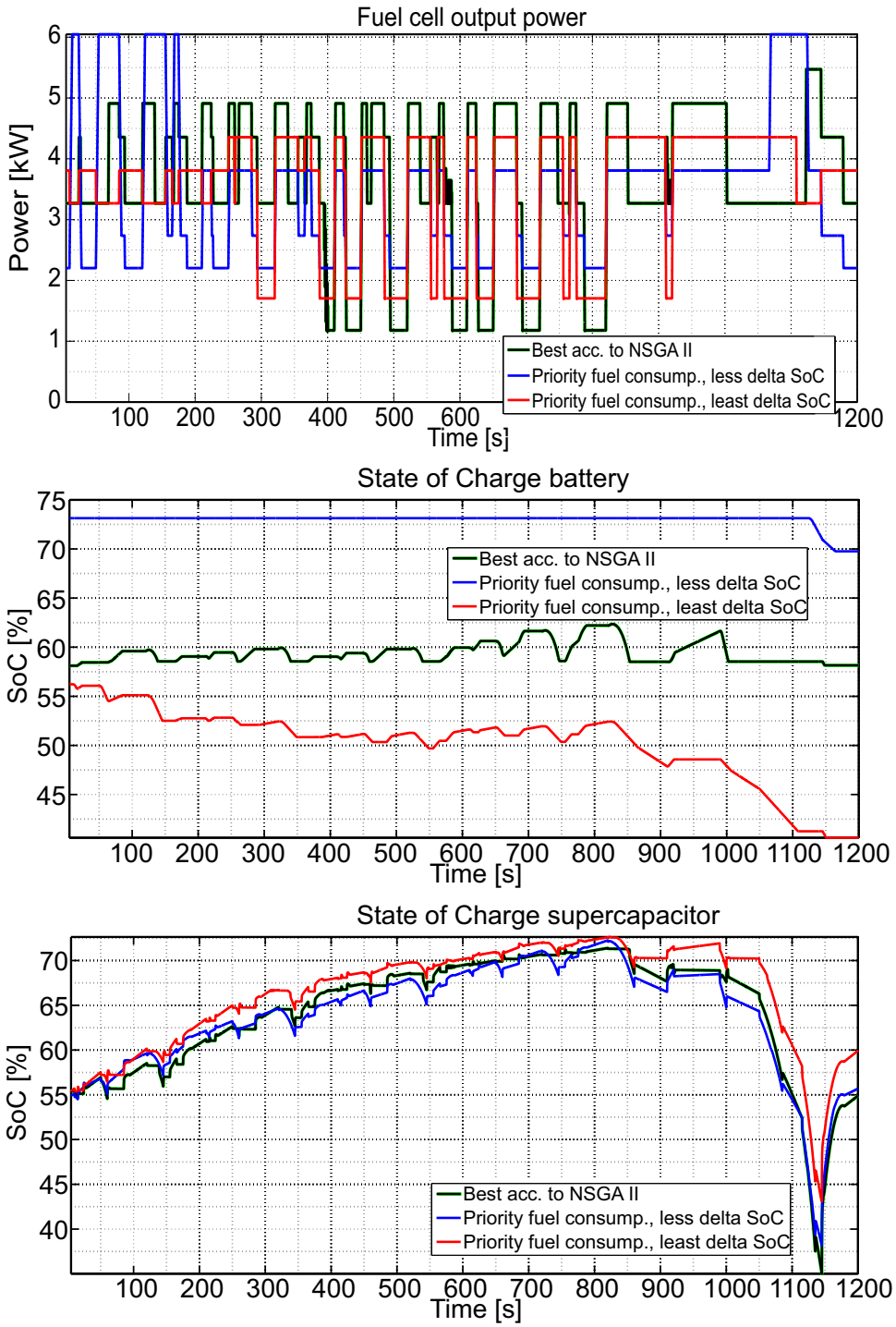

Figure 4.15: Effect of varying priorities between optimization goals (realized by numerical simulation) [MS16b]

supercapacitor, which can be added or subtracted from the total energy depending

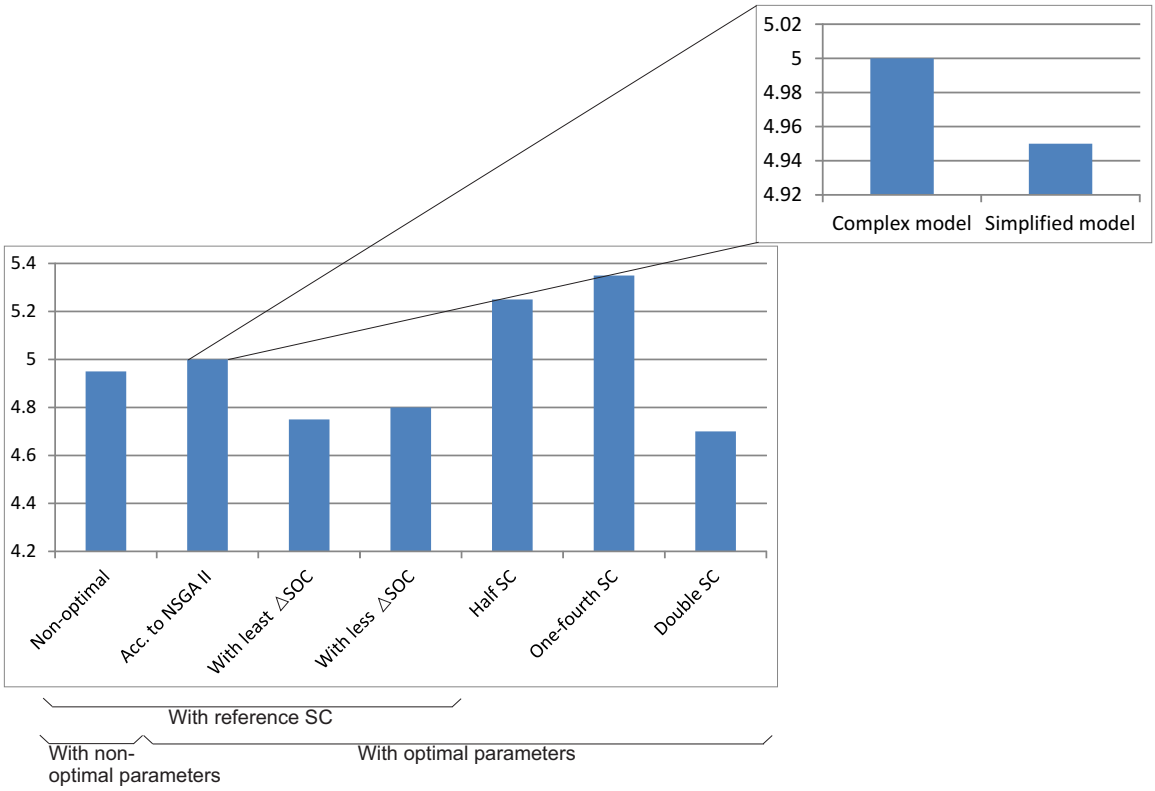

Figure 4.16: Comparison of all results in terms of energy consumption

on charge/discharge.It is clear that when the supercapacitor size is doubled, energy consumtion is the least. With smaller supercapacitors, the energy consumption is distinctively higher. It is also important to verify the results with the dynamic model. This is because, with varying load demand, particularly in the presence of frequent load fluctuations, losses occur, which cannot be accurately analyzed with the help of quasi-static model. As seen in Figure 4.16, the The fuel consumption is higher with dynamic model than with quasi-static model.

4.4 Experimental results and discussion

The developed power management optimization concept is tested with emulated hardware components as described in Chapter 3. From Figure 4.17a, the basic working principles of the power management strategy become clear using a NEDC drive cycle as example. The battery current is limited and the more dynamic fluctuations are taken over by the supercapacitor. The fuel cell is operated close to its efficient operating point as calculated in [ÖWMS13]. To validate the developed power management optimization strategy and to check the feasibility of the emulation hardware in realizing the dynamics of the powertrain, the simulated results are compared to

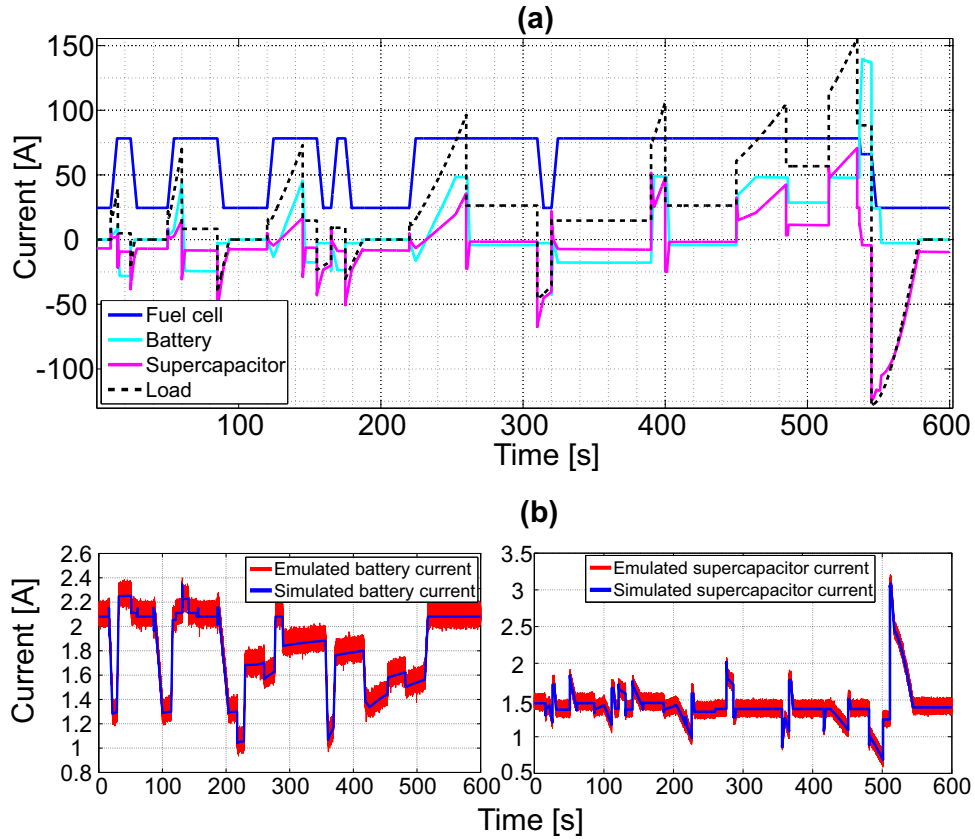

Figure 4.17: a) Simulated source and load current b) Experimentally emulated battery and supercapacitor current [MS16b]

emulation results. In Figure 4.17b the charging of battery and supercapacitor is shown. This is in accordance with the simulated battery and supercapacitor current as shown in Figure 4.17a. The curves in Figure 4.17b demonstrate an inversion of values shown in Figure 4.17a. The negative parts of load represent charging or increase in sink $s2$ and $s3$ currents and positive parts, discharging or increase in source $q2$ and $q3$ currents. Here, only emulation of charging current is shown. Similarly, emulation of supply and regenerate dynamics using s and q is explained with Figure 3.29. Here, the emulation of both positive and negative parts of the load demand by $q4 - s4$ is given. During the positive half of the load cycle, current is drawn by the sink $s4$ (motor mode) and in the negative half of the load cycle, power is supplied by the source $q4$ (generator mode). Therefore, the emulated $q4$ current, which is an absolute value, can be seen as an inversion of simulated value. From Figure 4.17, a good coincidence between model behavior and emulation can be noted. Thus the dynamics of the simulated models of components together with the supervisory controller can be validated using the emulated experimental set-up. Corresponding to the three sources, the DC/DC converter current outputs as defined by power management controller are sent to $q1$, $q2 - s2$, and $q3 - s3$. The simulated load

current from the backward modeled part is sent to $q4 - s4$.

5 Scope of developed rule-based power management controller

This chapter is published in the form of scientific papers [MS16a],[MWS15]. To investigate the adaption of the developed power management strategy with respect to unknown driving patterns, three contributions can be considered. These three different directions of contributions are relevant because all three deal with multiple power sources and implement online power management based on rules. In all three directions, the developed power management has either been tested on a variety of drive cycles or subjected to real driving data. Typical for the first direction as published in [PDRL07], a fuel cell-battery-supercapacitor hybrid electric vehicle is considered. The control strategy for power split and charge sustainment is derived based on the advantage of battery-supercapacitor combination. The power demand is addressed by the sources in the following order: fuel cell followed by supercapacitor and then battery. The power sharing between battery and supercapacitors is governed by a power split value which is one of the optimization variables. Along with power split, the other optimization parameters include both control and design parameters such as battery and supercapacitor upper and lower bounds. The optimization method chosen is a multi-objective genetic algorithm with the aim to minimize both fuel consumption and difference between final and initial battery state-of-charge (SoC). The optimization is carried out with two constraints: first with designs that limit the hydrogen fuel consumption, second with designs that preserve the total amount of energy stored in the battery i.e., the initial battery SoC is set to 70%. Different pareto optimal fronts are obtained for 4 different driving cycles from where point of minimum fuel consumption is chosen. The utilization percentages show that the optimal utilization of the three power sources vary with the drive cycle chosen. A representative for the second direction is the contribution given in [TGGL14], here an engine-battery-motor and generator PHEV is considered. The goal of the developed power management strategy is to improve fuel efficiency without deteriorating performance considering that the vehicle is steered by a human. The strategy is tested for three different drive cycles repeated over different geographic locations. Here, four operation modes are defined and each mode has its own optimization problem definition. The modes are individually offline optimized and then implemented in the online rule based controller. The control strategy selects the most appropriate mode depending on the SoC of the battery. Thus, here SoC is considered as a criteria for selecting modes. The third direction is described by contribution [CMM]. The optimal online power management developed in [CMM] is a step further in considering four sources: engine, fuel cell, battery, and supercapacitor. A fuzzy-rule-based power management is combined with machine learning algorithm to train an intelligent controller that has the capability to find the optimal combination of power sources that minimize power losses, keep the SoCs of all storage components within bounds, and minimize bus voltage fluctuation. Here, the con-

troller has 5 variables: two for SoCs of both battery and supercapacitor, one for system voltage, and two for low and high load demands. For every load demand, the machine learning algorithm searches for the best power source combination at every 10 time units, then the knowledge generated by this is used to train the fuzzy logic controller. Thus, the combination of optimal power management with training algorithms can be established.

The power management controller considered in this work [MS15a, MS16a] is developed following a similar strategy as given in [PDRL07]. The power management strategy is based on rules and the optimization method is multi-objective and offline. One of the criteria for selecting modes i.e., based on SoC is similar to [TGGL14]. The optimization of parameters specific to each mode is also carried out as a decoupled offline process. However, unlike [TGGL14], another storage unit supercapacitor is considered and unlike [PDRL07] both battery and supercapacitor SoC deviation is considered in the optimization problem definition along with fuel consumption minimization. Unlike [PDRL07], the controller parameters to be optimized includes not only the power split between battery and supercapacitor but also fuel cell current and battery current limits. Optimizing fuel cell current ensures its operation in the optimal domain and optimizing the maximum and minimum battery current prevents overcharging/discharging. The optimized design parameters includes battery and supercapacitor SoC boundaries and initial SoCs of both battery and supercapacitor. Thus the applicability of the developed power management to other drive cycles can be concluded based on [PDRL07, TGGL14]. The possibility of combining the developed optimal power management with training algorithms can be concluded based on [CMM]. Instead of finding the suitable power source combination to minimize power loss [CMM], suitable current values from the different sources can be found in an already pre-defined topology, in order to satisfy multiple objectives such as fuel consumption, SoC deviation, aging, etc. This has not been considered in [CMM].

5.0.1 Illustrative example: drive cycle prediction and optimization

The tuning of the controller parameters online is not considered in this example, therefore in Figure 5.1, the values from LUT do not go to power management controller, instead here, the loop is closed by displaying the optimal values to the human driver. The decision to follow the optimal is left on the driver. Optimal system behavior is considered in terms of evaluation of system performance using three parameters [SWS$^+$13, ÖWMS13, MÖS14]: system availability, fuel performance, and component aging of a fuel cell-supercapacitor hybrid electric vehicle [SWS$^+$13]. For validation purposes, a driving simulator environment developed at the Chair of Dynamics and Control (SRS) is connected via a real time interface to a hybrid electric vehicle experimental environment as mentioned before. The procedure followed is shown in Figure 5.1. One of the main assumptions is that the predicted velocity

is based on pre-defined drive cycles that the human driver is obliged to follow. As introduced in [SWS+13], the length of the prediction horizon can be adjusted based on the prediction performance at each time span. The other assumption is that, considering the same environment and same speed limitations set at the driving simulator, the present pattern of the driver resembles the past.

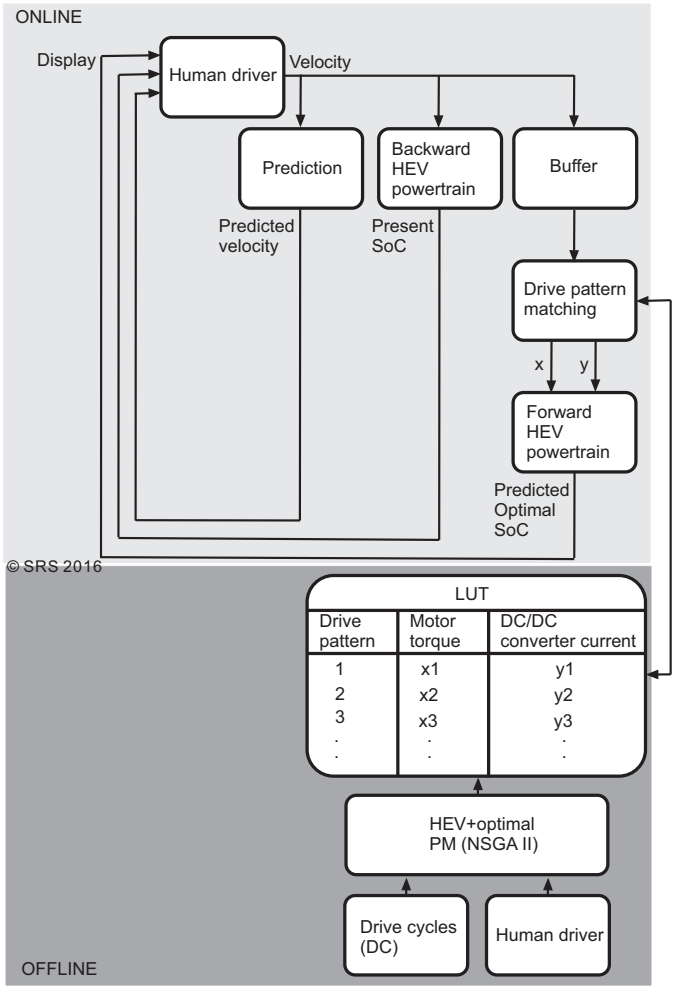

Figure 5.1: Optimization concept for HEV-driving simulator coupling [MS16a]

The velocity profile is analyzed in two steps. The first step is to generate a look-up table (LUT) offline with the help of a multi-objective optimization. Here known typical and representative velocity patterns based on a human driver's driving pattern are used for offline optimization. Optimization is with respect to predefined drive cycles. In other words, the predicted optimal is generated based on the assumption that the drive cycle is followed by the driver. The HEV powertrain model interacts with the search algorithm Non-dominated Sorting Genetic Algorithm II (NSGA II) [DPAM02] in a loop thereby generating optimal control parameters that minimize

the cost function for the predicted velocity. The optimal parameters are obtained for each representative driver velocity pattern. These parameters are motor torque and DC/DC converter current. The velocity values obtained from the driver are recorded and analyzed in a discrete manner. For example, if the optimization loop is run for every 5 seconds of the driver velocity recorded, then an optimal set of parameters are obtained for each of these velocity segments. The intervals of recording can be chosen small enough to ensure accuracy. A look-up table constructed at the end of the last optimization run provides a pattern analysis for the human driver's velocity values whereby each pattern is accompanied by its corresponding optimal parameter values.

The next step is to implement this look-up table online. Considering the same environment and same speed limitations set at the driving simulator, the velocity of the human driver is now analyzed with the help of this look-up table. A program to match the incoming velocity values with the values in the table sends the corresponding optimal motor torque and DC/DC converter current (for the predicted velocity) to the forward powertrain. Forward modeling in this case allows the realization of the vehicle behavior corresponding to optimal parameters, hence the corresponding optimal SoC is calculated. The incoming driver velocity is also sent to a backward modeled HEV in order to calculate the present SoC. Backward model in this case implies that velocity is taken as input and vehicle behavior is calculated backwards. An online prediction of the driver velocity according to the prediction algorithm in [SWS+13], [MS12] is carried out. Here, prediction is based on reference drive cycles and the assumption that the present behavioral pattern of the driver resembles the past. The predicted velocity, present SoC, and optimal SoC for predicted velocity are displayed to the human driver by a suitable interface.

5.0.1.1 Powertrain configuration and optimization goals

The HEV powertrain in range extender topology is shown in Figure 5.2. As detailed in [Mar], the charging/discharging dynamics of the supercapacitor is related to the control of mono directional DC/DC converter. Here the bus voltage is equal to supercapacitor and motor voltage. The modeling corresponding to this topology is done according to [Mar, MÖS14, ÖWMS13]. The emulator system for this powertrain topology is given in [Mar]. The primary source (fuel cell) emulation is realized by controlled power source and voltage-current controlled mono-directional DC/DC converter. The supercapacitor dynamics is realized by controlled power source-sink combination. The drivetrain is emulated by a speed controlled electric drive motor and torque controlled load motor. The charging dynamics of suercapacitor is given by [Mar]

$$U_{sc} = \frac{1}{C} \int I_{sc} dt, \tag{5.1}$$

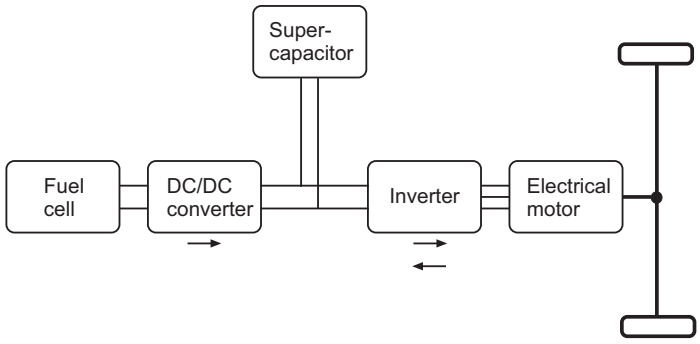

Figure 5.2: Topology of HEV powertrain according to [ÖWMS13]

where C denotes the capacity, I_{sc}, the current flow, and U_{sc} the voltage which is proportional to SoC. The power flow control is realized by DC/DC converter as

$$\begin{bmatrix} U_{bus} \\ I_{bus} \end{bmatrix} (k+1) = f(U_{bus}(k), I_{bus}(k), s_{DCDC}(k)), \tag{5.2}$$

where the bus voltage (U_{bus}) and current (I_{bus}) are defined as the output of the DC/DC converter. The control signal is given by (s_{DCDC}). The power management in [Mar] includes two control signals: current flow of DC/DC converter and vehicle speed. Here, the rotational speed of the powertrain model relates to the rotational speed of the emulator motor and the current relates to the load applied. Thus, the dynamical model of the complete powertrain is described by a discrete-time nonlinear state space model. The dynamic behavior of the motor is given by

$$x_{mot}(k+1) = \begin{bmatrix} i_{mot} \\ v_{mot} \end{bmatrix}_{(k+1)}, \tag{5.3}$$

where,

$$x_{mot}(k+1) = f(s_{mot}(k), x_{mot}(k)). \tag{5.4}$$

The motor current and speed are denoted by i_{mot} and v_{mot} respectively. The control input is denoted by s_{mot}. The dynamic behavior of the supercapacitors is given by a LTI discrete-time state space model as follows

$$x_{SC}(k+1) = A_{SC}x_{SC}(k) + B_{SC}u_{SC}(k), \tag{5.5}$$

where the state of the supercapacitor is denoted by x_{SC}. In range extender topology, the bus voltage is defined as the state of the supercapcitor model. The input is denoted by u_{SC} denoting the supercapacitor current i_{SC}. With the chosen range

extender topology [MÖS14, ÖWMS13], the DC/DC converter current flow is given by

$$i_{SC} = i_{DCDC}(s_{DCDC}) - i_{mot}, \tag{5.6}$$

where the output current of the DC/DC converter is denoted by i_{DCDC} and the control input by s_{DCDC}. Thus, two control inputs are considered here, s_{DCDC} and s_{mot}. The previously mentioned objectives according to [MÖS14, ÖWMS13] are given in the sequel where in [MÖS14], the influence of dynamic effects namely, the power flow control is considered apart from design optimization. The first objective is described by

$$P_{driv} = f_1(\int \mid v_{ref} - v_{meas} \mid dt). \tag{5.7}$$

Here, the tracking error between the measured and required velocity refers to the capability of the system to fulfill a given load cycle and is given by P_{driv}. The second objective describing the fuel efficiency

$$P_{fuel} = f_2(\dot{V}_{H_2} + \alpha\Delta(SoC(t = t_0), SoC(t = t_f)) \tag{5.8}$$

describes the supercapacitor State-of-Charge (SoC) at the beginning and end of the drivecycle as well as the fuel consumption, denoted by $SoC(t = t_0)$ and $SoC(t = t_f)$ respectively and the fuel consumption as $\dot{V}_{H_2}$.

5.0.1.2 Human driving behavior and its prediction

A data base containing known driving behaviors and related optimized power management parameters is used. Using the current driver and vehicle behavior a connection establishing the link between the human behavior, the optimized power management, and the parameters to be displayed to effect the human driver is established [SWS+13]. This concept introduced can also be used later in connection with the knowledge of current vehicle position, destination, traffic scenarios etc, and allows the evaluation of vehicle speeds for each segment of the road. A common practice is to use the data from navigation systems as applied in [AG09, HS06, SYD+04, RGRG03]. Other applications do not depend on navigation systems such as [GBC+] where the driver power request is represented by Markov model which is later used to generate an estimated future power request while in [KEK+], a given route is considered to consist of a series of route segments. Driving simulators have been used in [KII] to integrate humans into real driving conditions. Two design approaches of assistance system about enhancing driver recognition of vehicles in blind spots are developed. In order to analyze the driver-vehicle interaction, a driving simulator is applied in this contribution. In this contribution, the velocity of the human driver who is subject to produce real driving

conditions is transmitted in the form of a data stream to a simulated hybrid electric vehicle environment. A polynomial-based prediction approach as applied in [MS12] is used to generate specific features of the past trajectory measured over predefined time horizons. As detailed in [MS12], the length of the horizon is adjusted according to the prediction performance.

5.0.1.3 Interface completed by display of optimal data to driver

There are two approaches to display the calculated information. The purpose of applying two different approaches is to compare them with initial experiments and evaluate which form is better for the human driver to understand. One shows only a text of "Optimal Velocity" as shown in Figure 5.3, which informs the human driver to follow the displayed velocity. The other one as shown in Figure 5.4, showing the preliminary developed elements. The new elements are developed to illustrate the effect of the current velocity on the current SoC (indicated by the white arrow). By comparison, the effect of the future optimal velocity on the future SoC is also shown to the human driver. The optimal SoC is shown with the movable progress bar. The dark green line indicates the SoC, which is calculated from the optimization algorithm. Near to the SoC, 5 classes illustrating the driving suggestions are displayed to the driver: accelerate hard, accelerate, drive with constant velocity, brake, and brake hard. In Figure 5.4, the current SoC is lower than the optimal one. In order to reach the suggested optimal SoC, the driver needs to accelerate hard.

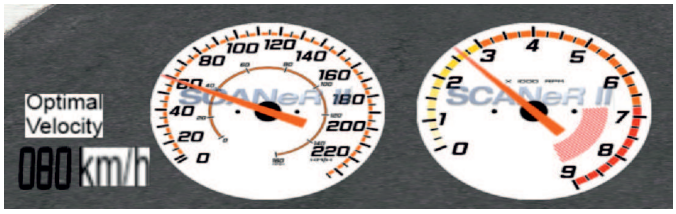

Figure 5.3: Displaying optimal velocity to the human driver [MWS15]

Figure 5.4: Displaying SOCs and velocity change suggestion to the human driver [MWS15]

5.0.1.4 Simulation results

As shown in Figure 5.1, after the initial offline procedure where optimal motor torque (x) and DC/DC converter current (y) have been determined for different driver velocities, the Look-up-Table (LUT) with the saved values is implemented online. In the online step, the driver velocity as received from the driving simulator driven by a human driver is denoted in 5.5 by the black curve using a specific speeding-up and slowing-down maneuver. The corresponding supercapacitor SoC variations are denoted in red. The vehicle model without optimal parameters shows

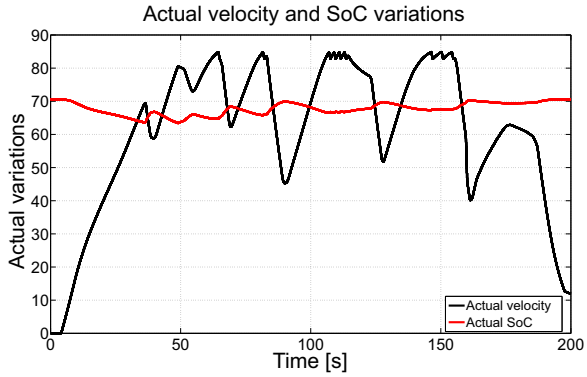

Figure 5.5: Actual velocity and SoC variations [MWS15]

a drop in SoC with each acceleration and increase in SoC as a result of regeneration with each deceleration. The SoC values were scaled for better comparison with velocity values, therefore the red curve denotes the SoC variation and not values.

As shown in Figure 5.1, a part of the driver velocity is also sent to the prediction and velocity matching blocks where the corresponding optimal values (x and y) are sent to a forward vehicle model. Considering the fact that the predicted velocity patterns are based on past data, it can be compared to the present driver velocity in figures 5.6 and 5.8.

As noted from Figure 5.6, the predicted velocity (in red) can be expected to accelerate in the beginning but is desired to be kept within limits in contrast to the rapid and frequent changes in the driver velocity denoted in black. A zoomed section of the present and future velocities from 25-60 seconds is shown in Figure 5.7. It is to be noted that inspite of the present acceleration rapidly followed by a deceleration and again acceleration, improvements can be made in terms of the objectives specified in the optimization algorithm, by gradually accelerating and then gradually decelerating (as shown in red). In Figure 5.8, a zoomed section of Figure 5.6 for the time span 90-130 seconds is shown. Unlike Figure 5.7, here a gradual decrease in velocity is expected in contrast to the present diver velocity (in black). The determining criteria behind the choice of desired future velocity are given in Equations

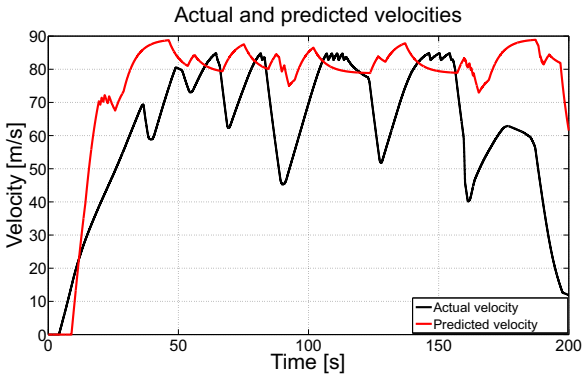

Figure 5.6: Actual and predicted velocities [MWS15]

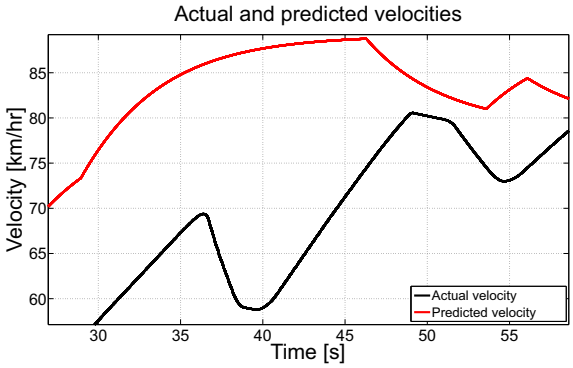

Figure 5.7: Velocities between 25-60 s zoomed [MWS15]

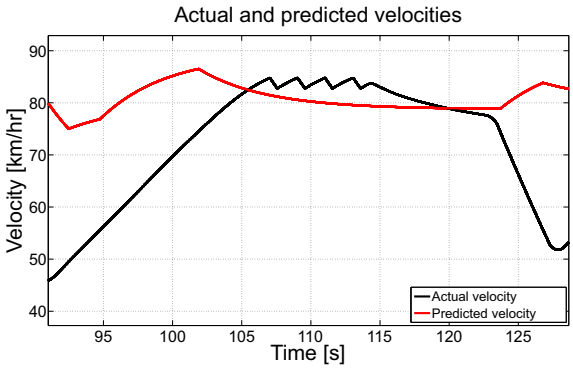

Figure 5.8: Velocities between 90-130 s zoomed [MWS15]

and 5.8. The penalizing of future SoC deviations become more clear from figures 5.9 and 5.10.

The optimal supercapacitor SoC variations corresponding to the future velocity are depicted in Figure 5.9 and the present and future optimal SoC variations are compared in Figure 5.10.

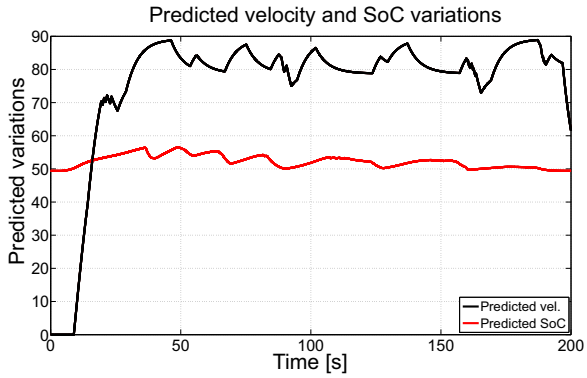

Figure 5.9: Predicted velocity and SoC variations [MWS15]

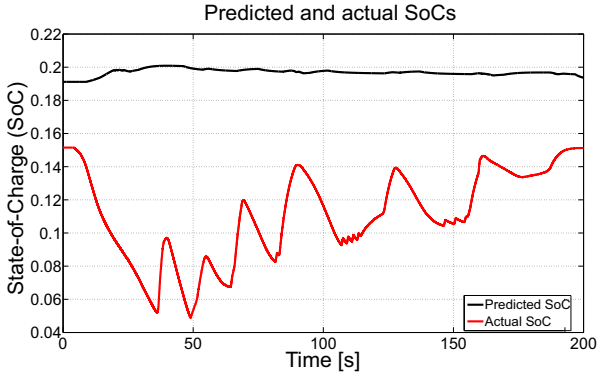

Figure 5.10: Predicted and actual SoCs [MWS15]

It is noted that the tendency to sustain charge will be better if the optimal velocity pattern is followed. Also, the SoC deviation from its initial to final value is minimized in the optimal pattern. In an enlarged section (Figure 5.11), it is shown that inspite of a decrease in the present SoC, the future SoC will gradually increase if the optimal future velocity is followed. Thus, the simulation results show the importance of following the desired pattern due to its ability to sustain the supercapacitor state of charge.

5.1 Adaptive power management for dynamic/variable driving behavior

To modify and implement the developed power management strategy, gathering driving data can be considered as a first step. According to [FYR+14], velocity, which is one of the driving data, can be used to define a driving segment. For the analysis of these segments, driving features are defined for example, average velocity and variance of velocity. As mentioned in [FYR+14], first driving profiles of

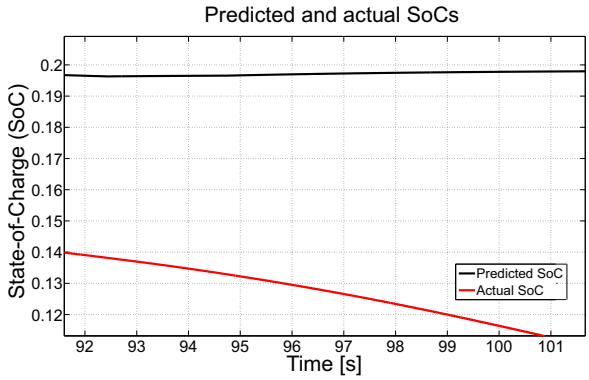

Figure 5.11: State-of-Charge variations zoomed

real human drivers can be obtained, then partitioning of these profiles into segments can be done. Next, the driving features can be extracted and segments of each of the driving profiles marked. This marking can be utilized for driving data analysis and traffic condition recognition. For example, based on average velocity, segments can be classified as highway condition, urban condition, etc.

Adaption of power management strategy based on predicted future can either use car navigation data or use a predictor in absence of car navigation data. For the latter case, two options have been mentioned in [FYR+14]: driving condition recognition based on history of motion and driving condition prediction based on history of motion. For both the options, the procedure is to prepare optimal databases offline and match the present to previously optimized past. The two principle options according to [FYR+14] are shown in Figure 5.12 and explained in [FYR+14]. The difference between the two options is that, in the first option, optimization of the entire drive pattern is considered, whereas in the second option, segment-wise optimization is carried out. Recognition of the present based on past is considered in the first option, whereas the present is matched to the past in the second option. Moreover in the first option, updating of rules to integrate new driving patterns is required at regular intervals.

5.1.1 Driving condition recognition

In driving condition recognition, the optimal parameters are calculated for different drive cycles or patterns in offline condition. The results are stored in look-up tables. In online condition, the current driving condition is recognized and the most suitable set of optimal parameters is selected for tuning the power management controller. A repetition of the recognition process in regular time intervals is required for online application [FYR+14].

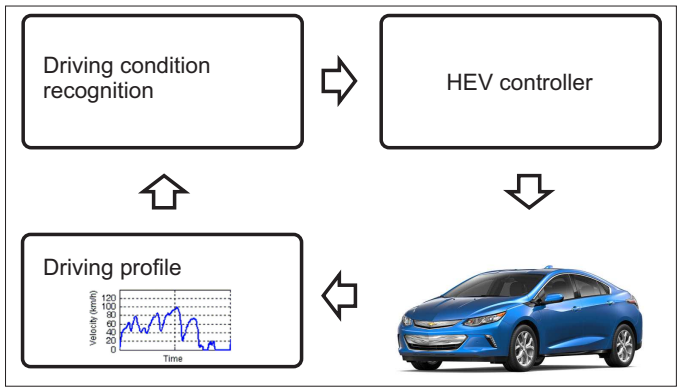

Driving condition recognition

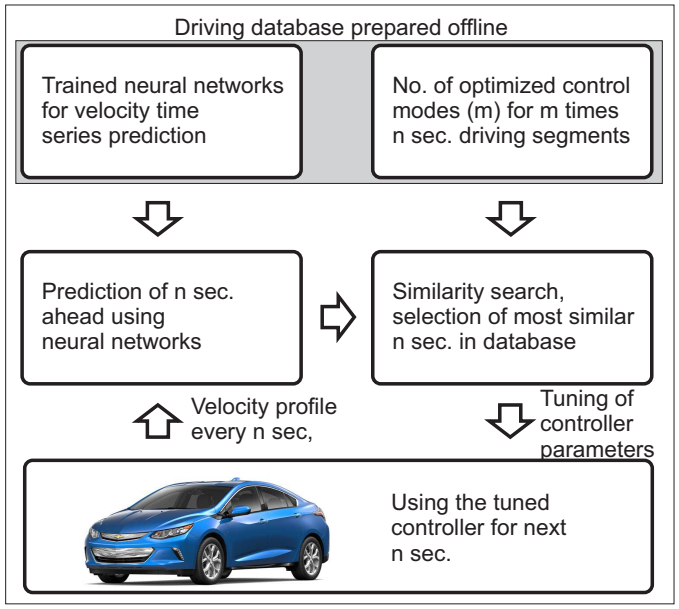

Driving condition prediction

Figure 5.12: Implementation possibilities of adaptive control (according to [FYR+14])[MS16a]

As detailed in [MS15b], an adaptive power management based on driving pattern recognition is presented in [LJPML04]. The procedure followed is capable of executing an optimal online power management, along with driver velocity classification and prediction without using complicated algorithms. Here, two separate offline processes are considered as shown in Figure 5.13: first, representative drive cycles are used to generate six driving patterns satisfying certain criteria. These patterns are classified according to power demand and stored in a look-up table for online implementation; second, where the same six representative drive cycles are analyzed for determining the optimal power split that minimizes fuel consumption. Based on

this, six control rules are formulated for a sub-optimal rule-based controller. In the online process, the driver velocity is saved and prediction based on the assumption that driving condition within a finite history will continue in near future, is done. The data in the most recent time frame from the historical data buffer can be used for characteristic parameter extraction. The classification of the driver velocity into six patterns is carried out based on the look-up table values from the first offline process. The corresponding control rule can also be determined based on the data from the second offline process as shown in Figure 5.13.

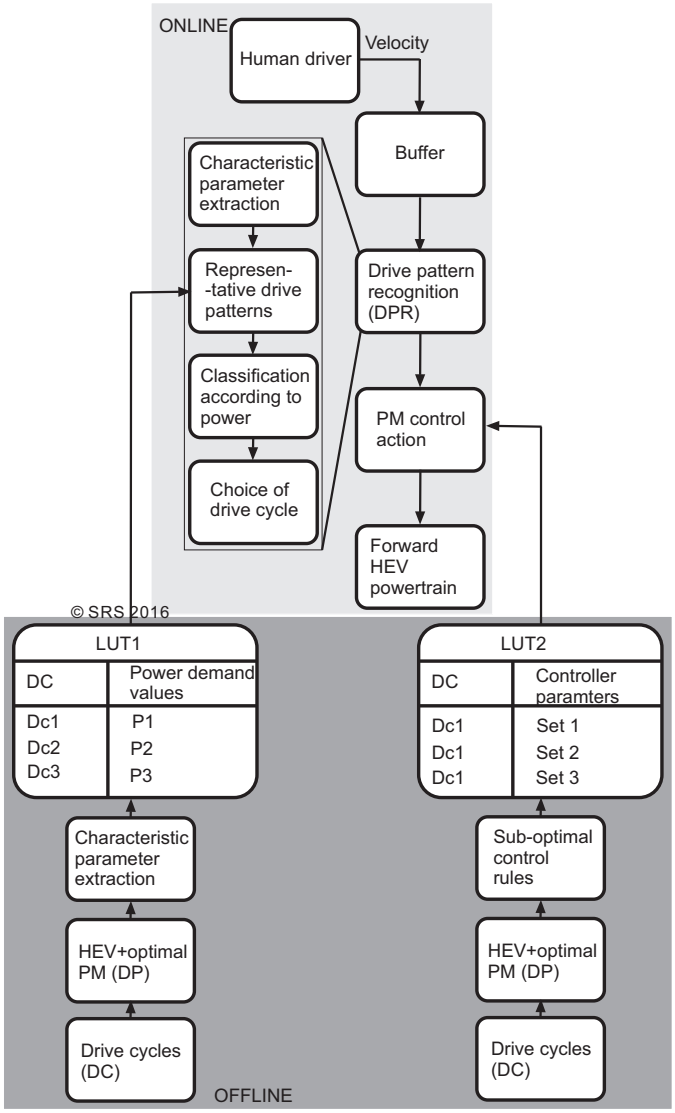

Figure 5.13: Driving condition recognition [MS16a]

The characteristic parameters chosen in [LJPML04] are the averaged positive power demand $P_{dem_{mean}}$ and standard deviation of positive power demand during driving

$P_{dem_{std}}$. The generation of representative drive patterns (RDPs) is based on mathematical operations as shown in Figure 5.14. The method used in [LJPML04] is briefly described in the sequel. Let V_0 denote the initial vehicle speed and $V_1 i (i = 1, 2, 3, ...)$, the speeds after ΔT. Let P_0 and $P_1 i (i = 1, 2, 3, ...)$ denote the power demands for V_0 and $V_1 i$ respectively. When the vehicle is accelerating or driving at constant velocity, the engine and motor speeds are calculated for a backward model and their maximum power value P_{max} are determined. If a power value is close to desired $P_{dem_{mean}}$, and the desired $P_{dem_{std}}$ is small then one point in region 1 is randomly selected as shown in Figure 5.14. If desired $P_{dem_{std}}$ is large, one point in region 2 is selected.

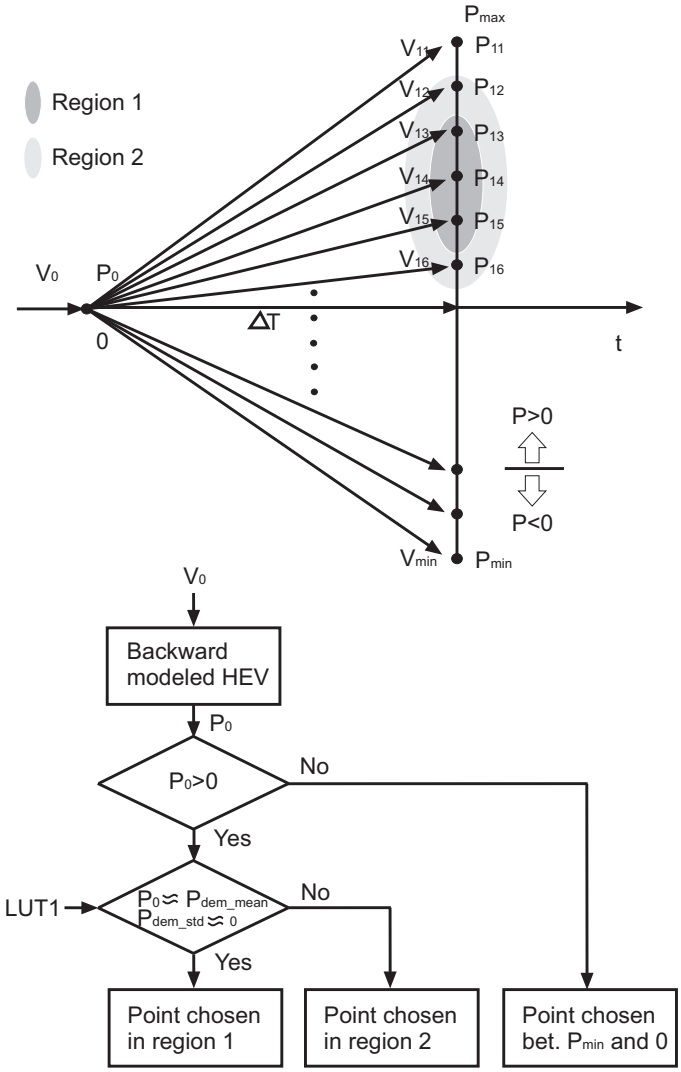

Figure 5.14: Creation of representative drive patterns (according to [LJPML04]) [MS16a]

Thus, the new power demand (after ΔT) can be assigned between points 0 and P_{max}. When the vehicle is decelerating, one point between P_{min} and 0 is randomly

chosen. In [LJPML04], six RDPs were created following the above procedure and classified into low, medium, and high power demand RDPs. The DPR algorithm in [LJPML04] decides which RDP fits the current driving pattern best. Considering T as the sampling time for measuring driver input velocity and pT as the duration of historical driving pattern which is sent to a buffer for the DPR process, fT as the duration of RDP, and NT as the duration of control horizon, the online steps are as follows

- extraction of characteristic parameters in historical window pT,
- creation and classification of current pattern in window fT, and
- according to classified pattern, choosing of corresponding control action for next NT seconds.

The historical values of driver power demand are stored in a buffer of size pT seconds. The DPR process takes the stored power demand values in the buffer at every NT seconds and finds the characteristic parameters which are then classified and control action generated for next NT seconds.

From [LJPML04], it can be concluded that rule-based power management can be modified to accommodate several rules, each corresponding to a particular drive cycle. A driving pattern recognition algorithm can be developed to match the incoming driver velocity patterns to the drive cycle patterns and select the most appropriate set of control rules. The assumptions in [LJPML04] are that

- the driver driving pattern does not change too fast, in other words, the historical pattern is likely to follow in future;
- the sets of control rules are different enough thereby ensuring a significant improvement in performance by selecting one; and
- the control horizon NT is much shorter than the duration fT used to predict the best RDP which makes the strategy similar to other predictive or receding horizon control algorithms.

5.1.2 Modified concept

The two concepts from [LJPML04] that is, offline optimization of each rule set and tuning of power management controller online can be applied to the power management control strategy developed in this work [MS15a, MS16a]. In the offline step, different drive cycles can be used for generating different sets of rules as designed in the mode selection block (Figure 4.3). For each of these unique combinations of rules, different optimal values of control parameters can be obtained to be stored in

the look-up table block. In Figure 5.15, LUT2 is considered for storing of values corresponding to optimal controller parameters and LUT1 for classified drive patterns according to power. This is shown in the offline block of Figure 5.15.

In the online step, a modification can be considered by a third look-up table (LUT3) which is a part of both online and offline processes. In the first offline step, LUT3 can be loaded with pre-defined drive cycles and corresponding controller parameters. In the first online step, LUT3 should be able to accommodate current driver velocities and store them as new patterns. In second offline step, it can be used to generate new optimal controller parameter based on new rules and hence update LUT1 and LUT2. The new driving patterns and corresponding controller parameters can now be used for tuning PM controller (Figure 3.3) in the second online step. This process can be repeated till the controller is trained for all possible circumstances. Thus, an optimally tuned intelligent power management controller can be developed that is capable of optimal distribution of power in real driving scenarios where the driver velocity is unknown. The disadvantage of this strategy is the increasing dimensionality of LUT3. In other words, if the driver changes the driving behavior frequently, the storing capacity of LUT3 will need to be considered.

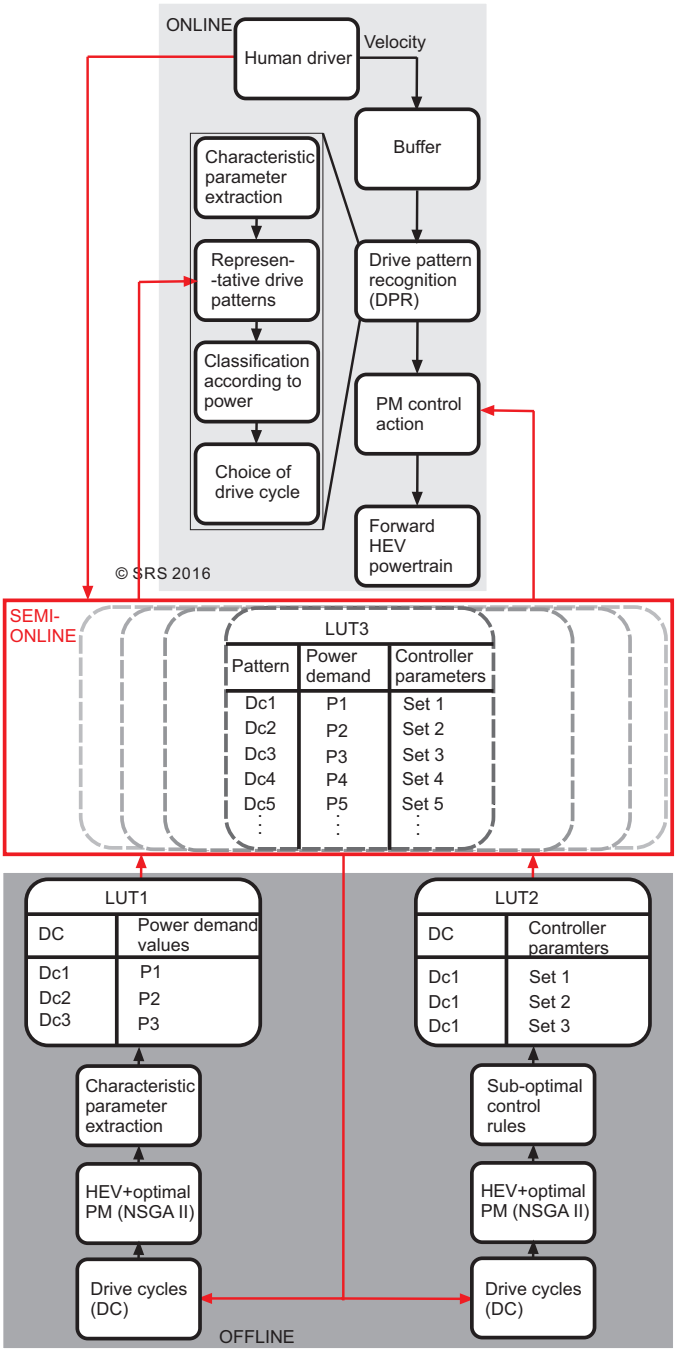

Figure 5.15: Driving condition recognition (modified from [LJPML04]) [MS16a]

6 Summary, Conclusion, and Outlook

This work focuses on the development of a suitable power management and optimization strategy for implementation in real driving scenarios. The existing strategies lack the ability to provide optimal solutions in terms of multiple objectives online. Along with online optimization, adaption of optimized control rules to real driving data is also an issue. Thus, the existing strategies and their deficits are evaluated, leading to the development of a rule-based power management concept which is tuned online with offline-generated optimal parameters. The power management strategy is implemented on a three-source HEV powertrain and validated on an emulation test-rig. A possibility to adapt the developed concept to real (unknown dynamic) driving patterns is also given.

6.1 Conclusion

The literature review presented in this work, emphasizes the role of rule-based power management and optimization strategies. To overcome the deficits of existing strategies, namely integration of multiple objectives along with adaptability to real driving patterns, an optimized power management controller for a three-source HEV is developed and validated on an emulation test-rig.

The newly introduced power management concept is capable of determining the optimal power distribution between the three sources online, such that, the dynamic part of the load is supplied by the supercapacitor and battery current is limited. The rate limitation of battery and fuel current prevents over-charging/discharging of these components, whereas, utilizing the higher charging/discharging efficiency of the supecapacitor ensures that the peak load demands are also satisfied. The decoupling of optimization process from the online part enables the use of offline-implementable, multi-objective algorithms. From the simulation results, it can be concluded that: multiple, even conflicting optimization objectives can be integrated in this control strategy; by changing the priority between the objectives, further options can be investigated; and by a suitable selection of parameters, all three sources can be operated within desired working ranges while satisfying the load demand at the same time. From the experimental results, the advantages of the concept introduced can be demonstrated by observing the the system dynamics from the hardware set-up.

Due to the modular structure of the power management optimization concept an extension of the concept can be easily realized by integrating more LUTs with sets of optimized parameters. Real (unknown dynamic) drive cycles can be used to generate these parameters offline to be embedded online. Two adaption possibilities are considered based on literature: driving condition prediction and driving condition

recognition. For driving condition prediction, an example application is given where the emulation hardware set-up is connected to a driving simulator operated by real human driver. Here, optimal predicted velocity is based on known or assumed drive cycles. The optimal controller is not integrated online, only the optimal values are displayed to the driver. For driving condition recognition, a concept is presented to integrate the optimal controller online. Here, a possibility to accomodate current driving patterns along with the existing patterns is considered. Thus, from the discussed example and concept it can be concluded that, the application of developed power management optimization concept to cases where the driver velocity pattern is unknown is possible.

6.2 Contributions

The main contributions of this work include

- Embedding of offline parameters in online rule-based controller: due to the decoupling of online and offline parts of the modular power management optimization concept, it is possible to carry out optimization with respect to multiple, even conflicting objectives.
- Rate limitation of battery and fuel cell current: overcharging and over discharging of battery is minimized by utilizing the supercapacitor to supply dynamic loads. This is done by a suitable choice of parameters that are preloaded from the offline optimization process.
- Validation using emulation test-rig: real powertrain components are replaced by controllable power sources and sinks that are capable of replicating powertrain dynamics. This is done by considering storage components like batteries and supercapacitors as source-sink combinations where, charging implies supply to sink and discharging, supply from source. Motor/generator dynamics are also emulated by source-sink combination.
- Adaption to real drive patterns: due to the modular structure of developed concept, integration of optimized parameter-sets for real (unknown) drive cycles is possible. A new concept for updating the control rules with respect to recent drive patterns is proposed.

6.3 Outlook

Due to the novelty of the proposed concept, several aspects can be considered for future work. The adaptation of the controller can be tested with real driver velocities (as collected from driving simulator test-rig) and the corresponding realization

of power train dynamics noted (by using the HEV emulator test-rig). In this work, a display option is considered for the optimal parameters, however, by adding more look-up tables an intelligent controller can be realized. The developed power management concept can also be extended to cases where battery aging minimization is an objective. In combination with an aging model, the integration of battery lifetime as an optimization goal can be considered.

Bibliography

[AG09] Ambühl, D. ; Guzzella, L.: Predictive reference signal generator for hybrid electric vehicles. In: *IEEE Transactions on Vehicular Technology* 58 (2009), pp. 4730–4740

[AK12] Aharon, I. ; Kuperman, A.: Topological overview of powertrains for battery-powered vehicles with range extenders. In: *IEEE Transactions on Power Electronics* 26 (2012), pp. 868–876

[BDGB10] Bernard, J. ; Delprat, S. ; Guerra, T. M. ; Büchi, F. N.: Fuel efficient power management strategy for fuel cell hybrid powertrains. In: *Control engineering practice* 18 (2010), pp. 408–417

[BE04] Baisden, A.C. ; Emadi, A.: ADVISOR-based model of a battery and an ultra-capacitor energy source for hybrid electric vehicles. In: *IEEE Transactions on Vehicular Technology* 53 (2004), pp. 199–205

[BGR00] Brahma, A. ; Guezennec, Y. ; Rizzoni, G.: Optimal energy management in series hybrid electric vehicles. In: *In Proceedings of the American Control Conference (ACC), Chicago, IL* (2000)

[BGT10] Bayindir, K. ; Gozukucuk, M.A. ; Teke, A: A comprehensive overview of hybrid electric vehicle: powertrain configurations, powertrain control techniques and electronic control units. In: *Energy Conversion and Management* 52 (2010), pp. 1305–1313

[BLGP09] Bin, Y. ; Li, Y. ; Gong, Q. ; Peng, Z.: Multi-information integrated trip specific optimal power management for plug-in hybrid electric vehicles. In: *In Proceedings of the American Control Conference (ACC), St. Louis, MO* (2009)

[BLM+10] Buerger, S. ; Lohmann, B. ; Merz, M. ; Vogel-Heuser, B. ; Hallmannsegger, M.: Multi-objective parameter optimization of a series hybrid electric vehicle using evolutionary algorithms. In: *In Proceedings of the IEEE Vehicle Power and Propulsion Conference (VPPC), Lille, France* (2010)

[BMFF07] Bashash, S. ; Moura, S.J. ; Forman, J.C. ; Fathy, H.K.: Power management and design optimization of fuel cell/battery hybrid vehicles. In: *Journal of Power Sources, Elsevier* 165 (2007), pp. 819–832

[BMFF11] Bashash, S. ; Moura, S.J. ; Forman, J.C. ; Fathy, H.K.: Plug-in hybrid electric vehicle charge pattern optimization for energy cost and battery longevity. In: *Journal of power sources, Elsevier* 196 (2011), pp. 541–549

[BMS15] Beganovic, N. ; Moulik, B. ; Söffker, D.: Li-O battery aging process: A smart review with respect to the integration of aging into system's power management. In: *In Proceedings of the ASME Dynamic Systems and Control (DSC) Conference, Columbus, Ohio* (2015)

[Bru14] Brusa: Validierungsbericht DC/DC-Wandler BDC546-B06/Brusa Elektronik AG.Forschungsbericht. (2014)

[Bru15] Brusa: Brusa Elektronik AG. In: *http://www.brusa.eu/* (last visted: 10.11.2015)

[CB11] Cassebaum, O. ; Biiker, B.: Predictive supervisory control strategy for parallel HEVs using former velocity trajectories. In: *In Proceedings of the IEEE Vehicle Power and Propulsion Conference (VPPC), Chicago, IL* (2011)

[CE12] Cao, J. ; Emadi, A.: A new battery/ultracapacitor hybrid energy storage system for electric, hybrid, and plug-in hybrid electric vehicles. In: *IEEE Transactions on Power Electronics* 27 (2012), pp. 122–132

[CMM] Chen, Z. ; Masrur, M. ; Murphey, Y.L.: Intelligent vehicle power management using machine learning and fuzzy logic. In: *In Proceedings of the IEEE International Conference on Fuzzy Systems, Hong Kong*

[Con06] Conte, F.V.: Battery and battery management for hybrid electric vehicles: a review. In: *e & i Elektrotechnik und Informationstechnik* 123 (2006), pp. 424–431

[CPP+03] Chou, P.H. ; Park, C. ; Park, J. ; Pham, K. ; Liu, J.: B#: a battery emulator and power profiling instrument. In: *In Proceedings of the international symposium on Low power electronics and design, Seoul* (2003)

[CRM06] Chen, M. ; Rincon-Mora, G.A.: Accurate electrical battery model capable of predicting runtime and I-V performance. In: *IEEE Transactions on Energy Conversion* 21 (2006), pp. 504–511

[CV14] Capasso, C. ; Veneri, O.: Experimental analysis on the performance of lithium based batteries for road full electric and hybrid vehicles. In: *Applied Energy* 136 (2014), pp. 921–930

[Dai15] Daimler: Technology and nnovation-Drive technologies-Fuel cell. In: *http://www.daimler.com/* (last visited: 10.11.2015)

[DCC+10] Debert, M. ; Colin, G. ; Chamaillard, Y. ; Guzzella, L. ; Ketfi-Cherif, A. ; Bellicaud, B.: Predictive energy management for hybrid electric vehicles-Prediction horizon and battery capacity sensitivity. In: *In Proceedings of the IFAC Symposium Advances in Automotive Control, Munich, Germany* (2010)

[DPAM02] Deb, K. ; Pratap, A. ; Agarwal, S. ; Meyarivan, T.: A fast and elitist multiobjective genetic algorithm: NSGA-II. In: *IEEE Transactions on Evolutionary Computation* 6 (2002), pp. 182–197

[EBV14] Eddahech, A. ; Briäat, O. ; Vinassa, J.M.: Determination of lithium-ion battery state-of-health based on constant-voltage charge phase. In: *Journal of power sources, Elsevier* 258 (2014), pp. 218–227

[EHr00] Eker, J. ; Hagander, P. ; Årzén, K.E.: A feedback scheduler for real-time controller tasks. In: *Control Engineering Practice* 12 (2000), pp. 1369–1378

[Ema05] Emadi, A.: *Handbook of automotive power electronics and motor drives.* CRC Press, 2005

[ERWL05] Emadi, A. ; Rajashekara, K. ; Williamson, S. S. ; Lukic, S. M.: Topological overview of hybrid electric and fuel cell vehicular power system architectures and configurations. In: *IEEE Transactions on Vehicular Technology* 54 (2005), pp. 763–770

[FPCP09] Fărcaş, C. ; Petreuş, D. ; Ciocan, I. ; Palaghită, N.: Modeling and simulation of supercapacitors. In: *In Proceedings of 15th International Symposium for Design and Technology of Electronics Packages, Gyula* (2009)

[FPSAS08] Ferreira, A. ; Pomilio, J.A. ; Spiazzi, G. ; Araujo Silva, L. de: Energy management fuzzy logic supervisory for electric vehicle power supplies system. In: *IEEE Transactions on Power Electronics* 23 (2008), pp. 107–115

[FYR+14] Fotouhi, A. ; Yusof, R. ; Rahmani, R. ; Mekhilef, S. ; Shateri, N.: A review on the applications of driving data and traffic information for vehicles' energy conservation. In: *Renewable and Sustainable Energy* 37 (2014), pp. 822–833

[GBBM11] Gao, F. ; Blunier, B. ; Bouquain, D. ; Miraoui, A.: Model based DC power source emulator for electrical and hybrid electrical vehicles drive train tests. In: *In Proceedings of the IEEE Vehicle Power and Propulsion Conference (VPPC), Chicago* (2011)

[GBC+] Giulio, R. ; Bernardini, D. ; Cairano, S.D. ; Bemporad, A. ; Kolmanovsky, I.V.: A stochastic model predictive control approach for series hybrid electric vehicle power management. In: *In Proceedings of the American Control Conference (ACC), Maryland, USA*

[GBS+09] Gao, F. ; Blunier, B. ; Simoes, M. ; Miraoui, A. ; El-Moudni, A.: PEM fuel cell stack hardware-in-the-loop emulation using DC/DC converter design. In: *In Proceedings of Electrical Power and Energy Conference (EPEC), Montreal, Canada* (2009)

[Glo15a] Global, Toyota: Innovation-Environmental Technology-Fuel cell. In: *http://www.toyota-global.com/* (last visited: 10.11.2015)

[Glo15b] Global, Toyota: Innovation-Environmental Technology-Hybrid. In: *http://www.toyota-global.com/* (last visited: 10.11.2015)

[Gmb15] GmbH, Höcher & H.: Battery emulation with NL Source-Sink,H&H Customer Application 12. In: *http://www.hoecherl-hackl.com* (last visited: 11.25.15)

[GS07] Guzzella, L. ; Sciarretta, A.: *Vehicle propulsion systems: Introduction to modeling and optimization.* Springer-Verlag Berlin Heidelberg, 2007

[HEMF10] Hofmann, M. ; Eckardt, B. ; März, M. ; Frey, L.: Effizienzoptimierung integrierter elektrischer Antriebssysteme fuer Hybrid- und Elektrofahrzeuge. In: *In Proceedings of the EMA Elektromobilausstellung - Fachtagung - Wettbewerbe, Aschaffenburg, Germany* (2010)

[HS06] Hajimiri, M.H. ; Salmasi, F.R.: A fuzzy energy management strategy for series hybrid electric vehicle with predictive control and durability extension of the battery. In: *In Proceedings of the IEEE Conference on Electric and Hybrid Vehicles (ICEHV), Pune, India* (2006)

[HS07] Hofman, T. ; Steinbuch, M.: Rule-based energy management strategies for hybrid vehicles. In: *International Journal of Electric and Hybrid Vehicles* 1 (2007), pp. 71–94

[HXGL12] He, H. ; Xiong, R. ; Guo, H. ; Li, S.: Comparison study on the battery models used for the energy management of batteries in electric vehicles. In: *Energy Conversion and Management* 64 (2012), pp. 113–121

[IYD+04] Ichikawa, S. ; Yokoi, Y. ; Doki, S. ; Okuma, S. ; Naitou, T. ; Shiimado, T. ; Miki, N.: Novel energy management system for hybrid electric vehicles utilizing car navigation over a commuting route. In: *Intelligent Vehicles Symposium,IEEE* 124 (2004), pp. 161–166

[JA08] Johansson, P. ; Andersson, B.: Comparison of simulation programs for supercapacitor modelling. In: *Master of Science Thesis. Chalmers University of Technology, Sweden.* (2008)

[JDW09] Jain, M. ; Desai, C. ; Williamson, S.S.: Genetic algorithm based optimal powertrain component sizing and control strategy design for a fuel cell hybrid electric bus. In: *In Proceedings of the IEEE Vehicle Power and Propulsion Conference (VPPC), Dearborn, MI* (2009)

[JJPL02] Jeon, S.I. ; Jo, S.T. ; Park, Y.I. ; Lee, J.M.: Multi-mode driving control of a parallel hybrid electric vehicle using driving pattern recognition. In: *Journal of dynamic systems, measurement, and control* 124 (2002), pp. 141–149

[JKS97] Jalil, N. ; Kheir, N.A. ; Salman, M.: A rule-based energy management strategy for a series hybrid vehicle. In: *In Proceedings of the American Control Conference (ACC), Albuquerque, NM* (1997)

[KBK10] Khoucha, F. ; Benbouzid, M.E.H. ; Kheloui, A.: An optimal fuzzy logic power sharing strategy for parallel hybrid electric vehicles. In: *In Proceedings of the IEEE Vehicle Power and Propulsion Conference (VPPC), Lille, France* (2010)

[KDN+07] Knauff, M. C. ; Dafis, C. J. ; Niebur, D. ; Kwatny, H. G. ; Nwankpa, C. O.: Simulink model for hybrid power system test-bed. In: *In Proceedings of IEEE Electric Ship Technologies Symposium, Arlington, VA* (2007), Mai

[KEK+] Katsargyri ; Evangelia, G. ; Kolmanovsky, I.V. ; Michelini, J. ; Kuang, M.L. ; Phillips, A.M. ; Rinehart, M. ; Dahleh, M.A.: Optimally controlling hybrid electric vehicles using path forecasting. In: *In Proceedings of the American Control Conference (ACC), Missouri, USA*

[KII] Kuwana, J. ; Itoh, M. ; Inagaki, T.: Dynamic side-view mirror: Assisting situation awareness in blind spots. In: *In Proceedings of the IEEE Intelligent Vehicles Symposium (IV)), Gold Coast, Australia*

[KKDJ+05] Koot, M. ; Kessels, J.T. ; De Jager, B. ; Heemels, W.P.M.H. ; Bosch, P.P.J. Van d. ; Steinbuch, M.: Energy management strategies for vehicular electric power systems. In: *IEEE Transactions on Vehicular Technology* 54 (2005), pp. 771–782

[KL10] Khaligh, A. ; Li, Z.: Battery, ultracapacitor, fuel cell, and hybrid energy storage systems for electric, hybrid electric, fuel cell, and plug-in hybrid electric vehicles: state of the art. In: *IEEE Transactions on Vehicular Technology* 59 (2010), pp. 2806–2814

[KMS09] Kim, T.S. ; Manzie, C. ; Sharma, R.: Model predictive control of velocity and torque split in a parallel hybrid vehicle. In: *In Proceedings of the IEEE International Conference on Systems, Man, and Cybernetics, San Antonio, Texas* (2009)

[KQ11] Kim, T. ; Qiao, A.: A hybrid battery model capable of capturing dynamic circuit characteristics and nonlinear capacity effects. In: *IEEE Transactions on Energy Conversion* 26 (2011), pp. 1172–1180

[KR99] Kitoh, K. ; Remoto, H.: 100 Wh large size Li-ion batteries and safety tests. In: *Journal of Power Sources* 2 (1999), pp. 887890

[KS14] Karbaschian, M.A. ; Söffker, D.: Review and comparison of power management approaches for hybrid vehicles with focus on hydraulic drives. In: *Energies* 7 (2014), pp. 3512–3536

[KVNS00] Kolmanovsky, I. ; Van Nieuwstadt, M. ; Sun, J.: Optimization of complex powertrain systems for fuel economy and emissions. In: *Nonlinear Analysis: Real World Applications* 1 (2000), pp. 205–221

[LCB+08] Lukic, S.M. ; Cao, J. ; Bansal, R.C. ; Rodriguez, F. ; Emadi, A.: Energy storage systems for automotive applications. In: *IEEE Transactions on Industrial electronics* 55 (2008), pp. 2258–2267

[LCL+12] Li, Q. ; Chen, W. ; Li, Y. ; Liu, S. ; Huang, J.: Energy management strategy for fuel cell/battery/ultracapacitor hybrid vehicle based on fuzzy logic. In: *Journal of Electrical Power and Energy Systems* 43 (2012), pp. 514–525

[LFL+04] Lin, C. ; Filipi, Z. ; Louca, L. ; Peng, H. ; Assanis, D. ; Stein, J.: Modeling and control of a medium-duty hybrid electric truck. In: *International Journal of Vehicle Design* 11 (2004), pp. 349–370

[LJPML04] Lin, C.C. ; Jeon, S. ; Peng, H. ; Moo Lee, J.: Driving pattern recognition for control of hybrid electric trucks. In: *Vehicle System Dynamics* 42 (2004), pp. 41–58

[LMMS13] Liu, Y. ; Marx, M. ; Moulik, B. ; Söffker, D.: Experiment-based simulation and optimization of wind powertrain systems based on electric power flow emulation. In: *In Proceedings of the first Conference for Wind Power Drives, Aachen* (2013)

[LSWZ11] Li, S.G. ; Sharkh, S.M. ; Walsh, F.C. ; Zhang, C.N.: Energy and battery management of a plug-in series hybrid electric vehicle using fuzzy logic. In: *IEEE Transactions on Vehicular Technology* 60 (2011), pp. 3571–3585

[LWR+06] Lukic, S.M. ; Wirasingha, S.G. ; Rodriguez, F. ; Cao, J. ; Emadi, A.: Power management of an ultracapacitor/battery hybrid energy storage system in an HEV. In: *In Proceedings of the IEEE Vehicle Power and Propulsion Conference (VPPC), Windsor* (2006)

[LZLC13] Liu, K. ; Zhu, C. ; Lu, R. ; Chan, C.C.: Improved study of temperature dependence equivalent circuit model for supercapacitors. In: *IEEE Transactions on Plasma Science* 41 (2013), pp. 1267–1271

[Mar] Marx, M.: Multiobjective obtimization of the power flow control of hybrid electric power train systems within simulation and experimental emulation applications. In: *Chair of dynamics and control (SRS), University of Duisburg-Essen, Dissertation, 2014*

[Mat16] MathWorks: Rate Limiter. In: *http://www.mathworks.com, last visited: 01.26.16* (last visited: 01.26.16)

[MF08] Meintz, A. ; Ferdowsi, M.: Control strategy optimization for a parallel hybrid electric vehicle. In: *In Proceedings of the IEEE Vehicle Power and Propulsion Conference (VPPC), Harbin, China* (2008)

[MKS13] Moulik, B. ; Karbaschian, M.A. ; Söffker, D.: Size and parameter adjustment of a hybrid hydraulic powertrain using a global multiobjective optimization algorithm. In: *In Proceedings of the IEEE Vehicle Power and Propulsion Conference (VPPC), Beijing, China* (2013)

[MÖS14] Marx, M. ; Özbek, M. ; Söffker, D.: Power management of a hybrid electric powertrain system - design, power flow control and optimization targets. In: *International Journal of Powertrains* 3 (2014), pp. 221241

[MPP13] Mihael, C. ; Pavković, D. ; Petrić, J.: A Control-oriented simulation model of a power-split hybrid electric vehicle. In: *Applied Energy* 101 (2013), pp. 121–133

[MPV+09] Marsala, G. ; Pucci, M. ; Vitale, G. ; Cirrincione, M. ; Miraoui, A.: A prototype of a fuel cell PEM emulator based on a buck converter. In: *Applied Energy* 86 (2009), pp. 2192–2203

[MS12] Marx, M. ; Söffker, D.: Optimization of the powerflow control of a hybrid electric powertrain including load profile prediction. In: *In Proceedings of the IEEE Vehicle Power and Propulsion Conference (VPPC), Seoul, Korea* (2012)

[MS14] Moulik, B. ; Söffker, D.: Combined voltage-current control of DC/DC converters for power management of a multi-power source hybrid with HIL tests. In: *In Proceedings of the ASME Dynamic Systems and Control Conference, San Antonio, Texas* (2014)

[MS15a] Moulik, B. ; Söffker, D.: Online Powermanagement with Embedded Optimization for a Multi-source Hybrid with Dynamic Power Sharing between Components. In: *In Proceedings of the ASME Dynamic Systems and Control (DSC) Conference, Ohio, USA* (2015)

[MS15b] Moulik, B. ; Söffker, D.: Optimal rule-based powermanagement for online, real-time applications with multiple sources and objectives: A review. In: *Energies - Open Access Energy Research, Engineering and Policy Journal* 8 (2015), pp. 9049–9063

[MS16a] Moulik, B. ; Söffker, D.: Adapted power management for unknown drive patterns: Development of a new concept from systematic analysis of existing approaches. In: *IEEE Transactions on Vehicular Technology, submitted* (2016)

[MS16b] Moulik, B. ; Söffker, D.: Online power management with embedded offline-optimized parameters for three-source hybrid powertrain with experimental application. In: *Energies - Open Access Energy Research, Engineering and Policy Journal, submitted* (2016)

[MSS12] Marx, M. ; Shen, X. ; Söffker, D.: A data-driven online identification and control optimization approach applied to a hybrid electric powertrain system. In: *IFAC Mathematical Modelling* 7 (2012), pp. 153–158

[Mur08] Murphey, Y.L.: *Intelligent vehicle power management: An overview.* Springer-Verlag Berlin Heidelberg, 2008

[MWS15] Moulik, B. ; Wang, J. ; Söffker, D.: Optimized powermanagement for human driver-HEV using online identification of velocity patterns. In: *In Proceedings of the IEEE Vehicle Power and Propulsion Conference (VPPC), Montreal, Canada* (2015)

[NGK10] Na, W. ; Gou, B. ; Kim, T.: Analysis and control of a bidirectional DC/DC converter for an ultracapacitor in a fuel cell generation system. In: *Journal of Electrical Engineering: Theory and Application* 1 (2010), pp. 72–78

[OAK97] Oei, D. ; Adams, J.A. ; Kinnelly, A.A.: Direct-hydrogen-fueled proton-exchange-membrane fuel cell system for transportation applications. In: *Ford Motor Co., Dearborn, MI, United States* No. DOE/CE/50389–503 (1997)

[OIQ05] Ordonez, M. ; Iqbal, M. T. ; Quaicoe, J. E.: Development of a fuel cell simulator based on an experimentally derived model. In: *In Proceedings of the IEEE Canadian Conference on Electrical and Computer Engineering, Saskatoon, Canada* (2005), Mai

[ÖWMS13] Özbek, M. ; Wang, S. ; Marx, M. ; Söffker, D.: Modeling and control of a PEM fuel cell system: a practical study based on experimental defined component behavior. In: *Journal of Process Control* 23 (2013), pp. 282–293

[PABP05] Parker-Allotey, N.A. ; Bryant, A.T. ; Palmer, P.R.: The application of fuel cell emulation in the design of an electric vehicle powertrain. In: *In Proceedings of the Power Electronics Specialists Conference, Recife* (2005)

[PBMG06] Pérez, L.V. ; Bossio, G.R. ; Moitre, D. ; Garcia, G.O.: Optimization of power management in an hybrid electric vehicle using dynamic programming. In: *Mathematics and Computers in Simulation* 73 (2006), pp. 244–254

[PCM10] Park, J. ; Chen, Z. ; Murphey, Y.L.: Intelligent vehicle power management through neural learning. In: *In Proceedings of the International Joint Conference on Neural Networks, Barcelona, Spain* (2010)

[PDG+02] Paganelli, G. ; Delprat, S. ; Guerra, T.M. ; Rimaux, J. ; Santin, J.J.: Equivalent consumption minimization strategy for parallel hybrid powertrains. In: *In Proceedings of the 55th IEEE Vehicular Technology Conference (VTS), Birmingham, USA* (2002), Mai

[PDRL07] Paladini, V. ; Donateo, T. ; Risi, A. ; Laforgia, D.: Supercapacitors fuel-cell hybrid electric vehicle optimization and control strategy development. In: *Energy Conversion and Management* 48 (2007), pp. 3001–3008

[PIGV01] Piccolo, A. ; Ippolito, L. ; Gal, V.Z. ; Vaccaro, A.: Optimisation of energy flow management in hybrid electric vehicles via genetic algorithms. In: *In Proceedings of the IEEE International Conference on Advanced Intelligent Mechatronics (IEEUASME), Como, Italy* (2001)

[PL00] Park, Y.I. ; Lee, J.: Multi-mode driving control of a parallel hybrid electric vehicle using driving pattern recognition. In: *Journal of Dynamic Systems, Measurement, and Control* 124 (2000), pp. 141–149

[PRS05] Pagerit, S. ; Rousseau, A. ; Sharer, P.: Global optimization to real time control of HEV power flow: Example of a fuel cell hybrid vehicle. In: *In Proceedings of the 20th International Electric Vehicle Symposium (EVS20), Long Beach, USA* (2005)

[Rau15] Rauhut, T.: Power-Management und Optimierung eines Multi-Quelle-Hybrid-Antriebes für Echtzeitanwendungen. In: *Master Thesis* (June 2015)

[RBBP11] Riffonneau, Y. ; Bacha, S. ; Barruel, F. ; Ploix, S.: Optimal power flow management for grid connected PV systems with batteries. In: *IEEE Transactions on Sustainable Energy* 2 (2011), pp. 309–320

[RC08] Rao, S.Y. ; Chandorkar, M.: Electrical load emulation using power electronic converters. In: *In Proceedings of the TENCON 2008-2008 IEEE Region 10 Conference, Hyderabad* (2008)

[REC12] Rahimi-Eichi, H. ; Chow, M. Y.: Adaptive parameter identification and state-of-charge estimation of lithium-ion batteries. In: *In Proceedings of IECON 2012-38th Annual Conference on IEEE Industrial Electronics Society, Montreal, Canada* (2012)

[RGRG03] Rajagopalan, A. ; Gregory, W. ; Rizzoni, G. ; Guezennec, Y.: Development of fuzzy logic and neural network control and advanced emissions modeling for parallel hybrid vehicles. In: *National Renewable Energy Laboratory: Cole-Boulevard* (2003)

[Sal07] Salmasi, F.R.: Control strategies for hybrid electric vehicles: evolution, classification, comparison, and future trends. In: *IEEE Transactions on Vehicular Technology* 56 (2007), pp. 2393–2404

[SHMS15] Sun, C. ; Hu, X. ; Moura, S.J. ; Sun, F.: Velocity predictors for predictive energy management in hybrid electric vehicles. In: *IEEE Transactions on Control Systems Technology* 23 (2015), pp. 1197–1204

[SOS+11] Serrao, L. ; Onori, S. ; Sciarretta, A. ; Guezennec, Y. ; Rizzoni, G.: Optimal energy management of hybrid electric vehicles including battery aging. In: *In Proceedings of the American Control Conference (ACC), San Francisco, CA* (2011)

[SRA11] Sorrentino, M. ; Rizzo, G. ; Arsie, I.: Analysis of a rule-based control strategy for on-board energy management of series hybrid vehicles. In: *Control Engineering Practice* 19 (2011), pp. 1433–1441

[SSD+14] Sciarretta, A. ; Serrao, L. ; Dewangan, P.C. ; Tona, P. ; Bergshoeff, E.N.D. ; Bordons, C. ; Charmpa, L. ; Elbert, Ph. ; Eriksson, L. ; Hofman, T. ; Hubacher, M. ; Isenegger, P. ; Lacandia, F. ; Laveau, A. ; Li, H. ; Marcos, D. ; Nüesch, T. ; Onori, S. ; Pisu, P. ; Rios, J. ; Silvas, E. ; Sivertsson, M. ; Tribioli, L. ; Hoeven, A.-J. van d. ; Wu, M.: A control benchmark on the energy management of a plug-in hybrid electric vehicle. In: *Control Engineering Practice* 29 (2014), pp. 287–298

[SWS+13] Söffker, D. ; Wang, J. ; Schiffer, S. ; Marx, M. ; Fu, X.: Know your options - Interfacing consequences and forecasted performance

analysis: A concept for the novel type of information system KYO-ICPA. In: *In Proceedings of the IFAC/IFIP/IFORS/IEA Symposium on Analysis, Design, and Evaluation of Human-Machine Systems, Las Vegas, USA* (2013)

[SYD+04] Shinji, I. ; Yokoi, Y. ; Doki, S. ; Okuma, S. ; Naitou, T. ; Miki, N.: Novel energy management system for hybrid electric vehicles utilizing car navigation over a commuting route. In: *IEEE Intelligent Vehicles Symposium* 3 (2004), pp. 161–166

[TDH+04] Thacker, B.H. ; Doebling, S.W. ; Hemez, F.M. ; Anderson, M.C. ; Pepin, J.E. ; Rodriguez, E.A.: Concepts of model verification and validation. In: *Los Alamos National Lab, Los Alamos, NM, United States* No. LA-14167 (2004)

[TGGL14] Torres, J.L. ; Gonzalez, R. ; Gimenez, A. ; Lopez, J.: Energy management strategy for plug-in hybrid electric vehicles, a comparative study. In: *Applied Energy* 114 (2014), pp. 816–824

[UA07] Uzunoglu, M. ; Alam, M. S.: Dynamic modeling, design and simulation of a PEM fuel cell/ultra-capacitor hybrid system for vehicular applications. In: *Energy Conversion and Management* 48 (2007), pp. 1544–1553

[VCP16] Veneri, O. ; Capasso, C. ; Patalano, S.: Experimental study on the performance of a ZEBRA battery based propulsion system for urban commercial vehicles. In: *Applied Energy* No. ISSN 0306-2619 (2016)

[VIPn+09] Valera, J.J. ; Iglesias, I. ; Peña, A. ; Martin, A. ; Sánchez, J.: Integrated modeling approach for highly electrified HEV. Virtual design and simulation methodology for advanced powertrain prototyping. In: *In Proceedings of International Battery, Hybrid and Fuel Cell Electric Vehicle Symposium (EVS 24), Stavanger, Norway* (2009), Mai

[Wik15] Wikipedia: Wikipedia the free encyclopedia. In: *https://en.wikipedia.org/wiki/* (last visited: 10.11.2015)

[WL11] Wang, R. ; Lukic, S.M.: Review of driving conditions prediction and driving style recognition based control algorithms for hybrid electric vehicles. In: *In Proceedings of the IEEE Vehicle Power and Propulsion Conference (VPPC), Chicago, IL* (2011)

[WMS15] Wang, J. ; Moulik, B. ; Söffker, D.: Towards interactive driver assistance system to realize a safe and an efficient driving. In: *In Proceedings of the IEEE Vehicle Power and Propulsion Conference (VPPC), Montreal, Canada* (2015)

[WY06a] Wang, A. ; Yang, W.: Design of energy management strategy in hybrid vehicles by evolutionary fuzzy system part i: fuzzy logic controller development. In: *The Sixth World Congress on Intelligent Control and Automation (WCICA)* 2 (2006), pp. 8324–8328

[WY06b] Wang, A. ; Yang, W.: Design of energy management strategy in hybrid vehicles by evolutionary fuzzy system part ii: tuning fuzzy controller by genetic algorithms. In: *The Sixth World Congress on Intelligent Control and Automation (WCICA)* 2 (2006), pp. 8329–8333

[ZCMM09] Zhang, B. ; Chen, Z. ; Mi, C. ; Murphey, Y.L.: Multi-objective parameter optimization of a series hybrid electric vehicle using evolutionary algorithms. In: *In Proceedings of the IEEE Vehicle Power and Propulsion Conference (VPPC), Dearborn, MI* (2009)

The thesis is based on the results and development steps presented in the following previous publications:

[MS16a] Moulik, B.; Söffker, D.: Online power management with embedded offline-optimized parameters for three-source hybrid powertrain with experimental application. In: *Energies - Open Access Energy Research, Engineering and Policy Journal*, (2016), submitted

[MS16b] Moulik, B.; Söffker, D.: Adapted power management for unknown drive patterns: Development of a new concept from systematic analysis of existing approaches. In: *IEEE Transactions on Vehicular Technology*, (2016), submitted

[MS15a] Moulik, B.; Söffker, D.: Online Powermanagement with Embedded Optimization for a Multi-source Hybrid with Dynamic Power Sharing between Components. In: *Proceedings of the ASME Dynamic Systems and Control (DSC) Conference, Ohio, USA*, (2015), pp. V003T41A001

[MS15b] Moulik, B.; Söffker, D.: Optimal rule-based powermanagement for online, real-time applications with multiple sources and objectives: A review. In: *Energies - Open Access Energy Research, Engineering and Policy Journal*, 8 (2015), pp. 9049-9063

[MWS15] Moulik, B.; Wang, J.; Söffker, D.: Optimized powermanagement for human driver-HEV using online identification of velocity patterns. In: *Proceedings of the IEEE Vehicle Power and Propulsion Conference (VPPC), Montreal, Canada*, (2015), pp. 1-5

[WMS15] Wang, J.; Moulik, B.; Söffker, D.: Towards interactive driver assistance system to realize a safe and an efficient driving. In: *Proceedings of the IEEE Vehicle Power and Propulsion Conference (VPPC), Montreal, Canada*, (2015), pp. 1-6

The thesis is based on the results and development steps presented in the following previous publications:

[BMS15] Beganovic, N.; Moulik, B.; Söffker, D.: Li-O battery aging process: A smart review with respect to the integration of aging into system's power management. In: *Proceedings of the ASME Dynamic Systems and Control (DSC) Conference, Ohio, USA*, (2015), pp. V001T13A004

[MS14] Moulik, B.; Söffker, D.: Combined voltage-current control of DC/DC converters for power management of a multi-power source hybrid with HIL tests. In: *Proceedings of the ASME Dynamic Systems and Control (DSC) Conference,San Antonio, Texas*, (2014), pp. V002T36A003

[MKS13] Moulik, B.; Karbaschian M.A.; Söffker, D.: Size and Parameter Adjustment of a Hybrid Hydraulic Powertrain Using a Global Multi-Objective Optimization Algorithm. In: *IEEE Vehicle Power and Propulsion Conference (VPPC), Beijing, China*, (2013), pp. 1-6

[MS15b] Karbaschian, M.A.; Marx, M.; Moulik, B.; Söffker, D.: Multiobjective NSGA II-based Control Optimization of Hydraulic and Electric Hybrid Propulsion Systems with Respect to their Dynamic Behavior in Time Domain. In: *Proceedings of 14nd Antriebstechnisches Kolloquium (ATK), Aachen, Germany*, (2013), pp. 641-657

[MS15b] Liu, Y.; Marx, M.; Moulik, B.; Söffker, D.: Experiment-based simulation and optimization of wind powertrain systems based on electric power flow emulation. In: *Proceedings of the first Conference for Wind Power Drives, Aachen*, (2013)

In the context of the research projects at the Chair of Dynamics and Control, the following student theses have been supervised by Bedatri Moulik and Univ.-Prof. Dr.-Ing. Dirk Söffker. Development steps and results of the research projects and the student theses are related to each other and hence are also part of this thesis.

[Rau15] Rauhut, T., Power-Management und Optimierung eines Multi- Quelle-Hybrid-Antriebes für Echtzeitanwendungen, Master Thesis, June 2015